NGNP-NHS 50-CC **May 2008**
Revision 0

NGNP and Hydrogen Production Preconceptual Design Study

Contamination Control

APPROVALS

Function	Printed Name and Signature	Date
Author	Name: Richard F. Turner Company: Technology Insights	May 1, 2008
Reviewer	Name: Fred A. Silady Company: Technology Insights	May 1, 2008
Reviewer	Name: Michael Correia Company: Pebble Bed Modular Reactor (Pty) Ltd.	May 1, 2008
Reviewer	Name: Charles L. Kling Company: Westinghouse Electric Company LLC	May 4, 2008
Approval	Name: Ed Brabazon Company: Shaw Group	May 7, 2008

Westinghouse Electric Company LLC
Nuclear Power Plants
Post Office Box 355
Pittsburgh, PA 15230-0355

LIST OF CONTRIBUTORS

Name and Company	Date
Richard Turner, Fred Silady - Technology Insights Hanno van der Merwe, Pieter Goede, Gert de Beer and Michael Correia - Pebble Bed Modular Reactor (Pty) Ltd. Bert Winters, Erik de Geus, Marek Stempniewicz, Cor Timmermans, Ralph Hania and Lida Magielsen - Nuclear Research and Consultancy Group Charles L. Kling – Westinghouse Electric Company LLC	May 2008

BACKGROUND INTELLECTUAL PROPERTY CONTENT

Section	Title	Description
NONE		NONE

REVISION HISTORY

RECORD OF CHANGES

Revision No.	Revision Made by	Description	Date
A	R. F. Turner Technology Insights	Final Draft	1 May 2008
0	S. A. Caspersson Westinghouse Electric Company LLC	Final Report	22 May 2008

DOCUMENT TRACEABILITY

Created to Support the Following Document(s)	Document Number	Revision
NONE	NONE	

TABLE OF CONTENTS

LIST OF TABLES

LIST OF FIGURES

ACRONYMS

Acronym	Definition
AMS	Activity Measurement System
AVR	Arbeitsgemeinschaft Versuchs-Reaktor
BUMS	Burn-up Measurement System
CIP	Core Inlet Pipe
COP	Core Outlet Pipe
CRD	Control Rod Drive
CUD	Core Unloading Devices
DDN	Design Data Needs
DPP	Demonstration Power Plant
EOFY	End of Fiscal Year
FHSS	Fuel Handling and Storage System
FS	Fuel Spheres
HC	Helium Circulator
HLW	High Level Waste
HPB	Helium Pressure Boundary
HPS	Helium Purification System
HPU	Hydrogen Production Unit
HTGR	High Temperature Gas-Cooled Reactor
HTR	High Temperature Reactor
HVAC	Heating Ventilation and Air Conditioning
HX	Heat Exchanger
IHX	Intermediate Heat Exchanger
INL	Idaho National Laboratory
KTA	German Nuclear Technical Committee
NCS	Nuclear Control System
NGNP	Next Generation Nuclear Plant
NRG	Nuclear Research and Consultancy Group
NHSS	Nuclear Heat Supply System
PBMR	Pebble Bed Modular Reactor
PCHX	Process Coupling Heat Exchanger
PCS	Power Conversion System
PIE	Post-irradiation Examination
PHTS	Primary Heat Transport System
RS	Reactor System
RUS	Reactor Unit System
SG	Steam Generator
SHTS	Secondary Heat Transport System
THTR	Thorium High Temperature Reactor
WBS	Work Breakdown Structure

SUMMARY AND CONCLUSIONS

This Contamination Control Evaluation is one of a series that addresses fundamental issues and tradeoffs to be evaluated during the pre-conceptual design phase of the Next Generation Nuclear Plant (NGNP). The study was carried out to quantify the effects of radioactive contaminants in the plant systems, particularly as they would contribute to worker radiation exposure and to radioactive transport to the product gas in a process heat application.

The first step of the study was to determine the expected generation of radionuclide and dust sources in the primary and secondary circuits during normal operation. The sources are primarily in the Reactor Unit System (RUS) and the Primary Heat Transport System (PHTS).

The second step was to determine the transport rates of the radionuclides from the PHTS to the Secondary Heat Transport System (SHTS), which would lead to potential contamination of a product gas.

The next step in the study was to evaluate the potential impact on plant maintenance due to the contaminants in the primary and secondary helium circuits.

A radionuclide of particular interest is tritium, which may penetrate metallic structures in heat transport components. The study included a particular focus on the sources and transport rates of tritium through the plant systems.

The primary conclusions of the study are the following:

1. The database for radionuclide sources and transport rates is adequate, and depends greatly on the experience from the High Temperature Reactor (HTR) programs carried out in the Federal Republic of Germany. Likewise, the models and computer codes for quantifying the release and transport of dust and fission products are well developed.
2. Dust accumulates with time mostly in the reactor vessel. Of the remaining dust amount, most is in the Intermediate Heat Exchangers (IHXs). Attention must be given to dust accumulation in the CRD channels to assure there is no impact on control rod insertion.
3. The metallic radionuclides, mainly Ag, Cs and Sr, become quickly attached to dust after leaving the reactor core. These radionuclides, as well as iodine, plate out primarily in the intermediate heat exchanger.
4. The radiation doses to which workers could be exposed are not great, and adequate procedures can be planned for limiting the worker doses.
5. The radionuclide that was found to be of greatest concern is tritium, particularly because of the potential for this nuclide to be transported offsite in a product. A tritium production rate of ~2 x 10^6 Becquerel per second is reached, and essentially all of this permeates to the SHTS. Other mechanisms and design features need to be addressed which have the potential to reduce this level by up to two orders of magnitude which will meet stringent drinking water standards.

INTRODUCTION

The Contamination Control study is one of a series of "Special Studies" that address fundamental issues and tradeoffs to be evaluated during the preconceptual design phase of the NGNP. The need for this study was addressed in the Westinghouse PBMR Team NGNP and Hydrogen Production Preconceptual Design Report that was issued in June 2007.

OBJECTIVES AND SCOPE

This study defines and evaluates the NGNP design features that provide for control of radionuclide contamination in systems and components. Key elements of the objectives and scope are:

- Determine the expected generation of radionuclides and dust in the primary and secondary circuits during normal operation.
- Determine transport rates and allowable limits on expected contamination of the gas in the primary and secondary helium circuits during normal operation.
- Evaluate the potential maintenance impact due to the contaminants in the primary and secondary helium circuits.
- Provide information on tritium permeation through metals.

ORGANIZATION OF THE REPORT

Section 1 of this report provides a brief description of the PBMR NGNP and the key top requirements related to contamination control. Section 2 describes the radionuclides and dust source terms generated during normal operation, including tritium and Carbon 14. Transport of the fission products and dust is described in Section 3. Section 4 takes the results of the earlier sections and provides the implications for personnel radiation exposure. Section 5 examines the transport of tritium during normal operation in terms of its potential release from the NGNP heat source into the power conversion and hydrogen production systems. Section 5 also reports on the merits of coatings on the heat exchangers to limit the tritium release. Finally, Section 6 provides recommendations from this study.

1 NGNP DESCRIPTION AND OPERATIONAL REQUIREMENTS

1.1 Description of the NGNP Installation

The plant system descriptions identify those parts of the overall NGNP that would be locations for the sources and transport of radionuclides and dust during normal operation. A more complete description of the NGNP can be found in the NGNP Preconceptual Design Report Executive Summary Report [1-1].

The process flow diagram of the NGNP installation is given in Figure 1-1. The most significant portions of the plant systems that are analyzed in the Contamination Control Study are the Nuclear Heat Supply System (NHSS), the Fuel Handling and Storage System (FHSS) and the Primary Heat Transport System (PHTS).

The NHSS consists of the Reactor Unit System (RUS) and all the support and auxiliary systems required for its operation and maintenance. The RUS consists of the following subsystems:

Core Barrel Assembly
Core Structure Ceramics
Reactor Pressure Vessel
Reactivity Control System
Reserve Shutdown System
In-Core Delivery System

A number of support and auxiliary systems are vital for the functioning of the RUS, and are described fully in the NGNP Preconceptual Design Report [Ref. 1-1]. These are:

Core Conditioning System
Reactor Cavity Cooling System
Fuel Handling and Storage System
Helium Services System
NHSS Control and Instrumentation System
NHSS Cooling Water System
NHSS Electrical System
Nuclear Heat Supply Building HVAC System
Primary Loop Initial Clean-up System.

Energy from nuclear fission is transported from the NHSS by the Primary Heat Transport System (PHTS). The PHTS includes the main coolant piping, the Helium Circulator (HC), and the Intermediate Heat Exchanger (IHX), in which the heat from the NHSS is transferred to the Secondary Heat Transport System (SHTS). The SHTS transports heat to the Process Coupling Heat Exchanger (PCHX) and the Steam Generator (SG), where the heat is either utilized directly, or in certain plant operating modes, rejected to the environment.

Dust and radionuclides are generated in the RUS and the FHSS, and circulate through the PHTS.

The IHX is separated into an "A" stage, and a "B" stage. The process helium flows from the secondary side of the IHX A to a splitting line, where it is directed partially to the PCHX and the balance to a mixing chamber that leads to the SG. Helium returning from the SG flows through the SHTS circulator to the IHX B.

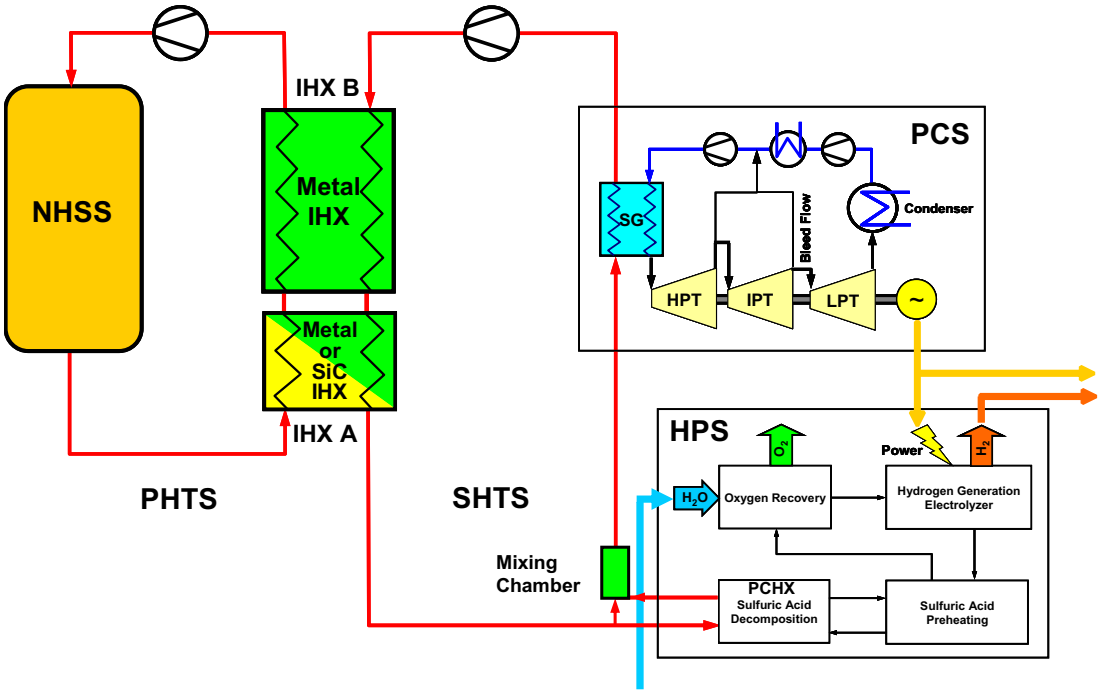

Figure 1-1 NGNP Process Flow Diagram

A more detailed description is provided of the main components of the primary circuit and the FHSS, which include the systems that generate and transport fission products, activation products and dust.

1.1.1 Nuclear Heat Supply System

The NHSS design is based on the Pebble Bed Modular Reactor (PBMR) Demonstration Power Plant (DPP) reactor design, which uses the high-temperature gas-cooled reactor technology that was originally developed in Germany. This implies the use of spherical fuel spheres (FSs), referred to as pebbles, which are in size and physical characteristics the same as the fuel developed for the German High-Temperature Reactor (HTR) programs. Also similar to the German pebble bed reactors, the PBMR design uses an online refueling scheme.

The NHSS is shown diagrammatically in Figure 1-2. The reactor vessel is of the same design and size as the PBMR Demonstration Power Plant. The design of the piping and the IHX

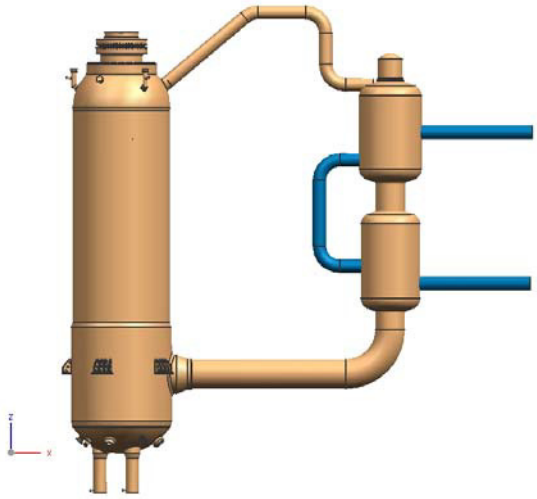

Figure 1-2 Nuclear Heat Supply System

units have been designed specifically for this process heat application. The auxiliary systems supporting the NHSS are the same designs as the PBMR-DPP.

The principal design selections of the NHSS are shown in Table 1-1.

Table 1-1 NHSS Design Selections

Parameter	NHSS Value
Inner/outer active core diameter (m)	2.0/3.7
Active core effective height (m)	11.0
Fueled region power density (w/cc)	16.9
Fuel element (solid) power density (w/cc)	9.8
Core power density (w/cc)	6.0
Core inlet/outlet coolant temperature (^{o}C)	350/950
Normal operation max. fuel temp. (^{o}C)	~1150
Off-normal max. fuel temperature (^{o}C)	~1670
Module power rating (MWt)	500
Primary He coolant inlet pressure (MPa)	9.0
Primary He flow rate (kg/s)	160
Core pressure drop (KPa)	202
Fuel composition	UO_2

Table 1-1 NHSS Design Selections

Parameter	NHSS Value
Fuel enrichment (%)	5.0 startup 9.6 equilibrium
Fuel burnup (GWd/mt U)	90

A detailed description of the NHSS is provided in Section 4: Nuclear Heat Supply System, of the Preconceptual Design Report [1-2].

1.1.2 Intermediate Heat Exchangers

The IHX design incorporates two separate high and low temperature sections, designated IHX A and IHX B. The high temperature section, IHX A, is designed for replacement one or more times within the plant lifetime, whereas IHX B is designed as a full lifetime component. A description of the functional requirements and the planned development of the IHX is provided in Section 6: Heat Transport System, of the Preconceptual Design Report [1-3]. An arrangement diagram of the IHX units is shown in Figure 1-3.

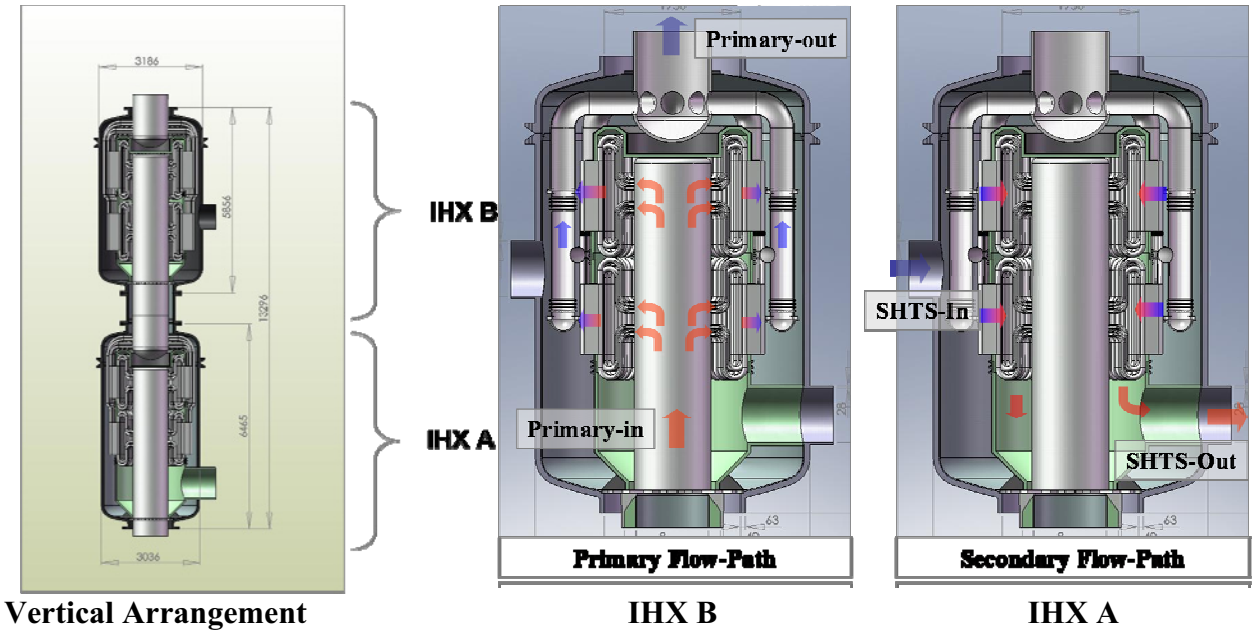

Figure 1-3 Intermediate Heat Exchanger Units

Any metallic materials have a limited lifetime for the IHX-A application, at the highest temperature of 950ºC. For this reason, the parallel development of ceramic and/or composite heat exchangers has also been recommended and identified within the Design Data Needs (DDNs). The initial IHX A is designed to be fabricated from 617 Inconel alloy, with a planned

lifetime of about 10 years. A vessel liner (not shown) is required for active cooling of the IHX A vessel. A later replacement IHX A unit may be constructed with ceramic components.

The maximum temperature in the IHX B is given as 850ºC, assumed to be a temperature at which the reference material, Inconel 617, would allow lifetime operation without replacement. Further consideration during the remainder of pre-conceptual design has led to the tentative selection of a lower temperature breakpoint, 760ºC, which would allow the use of established ASME Section III materials, based on Subsection NH for IHX B. The reference material specifically recommended for IHX B is Alloy 800H. Both the breakpoint temperature and the IHX B material are to be confirmed through future studies during conceptual design.

1.1.3 Circulator

A single circulator, top-mounted on the IHX B vessel, is employed for the PHTS. A "flapper-type", self-actuated check-valve is integrated with the circulator to limit backflow through the main loop. A description of the design of the HC is provided in Section 6: Heat Transport System, of the Preconceptual Design Report [1-3].

The electric-driven PHTS circulator operates at nominally 350ºC and 9 MPa (exit conditions) to provide for circulation of the primary coolant helium to and from the reactor. The location options considered for the circulator were on top of the lower-temperature IHX B vessel or in the PHTS piping. Placing the circulator in the IHX B vessel simplifies piping and interfaces and eliminates the need for a separate circulator pressure boundary. However, it does somewhat reduce the access to the IHX internals. A circulator location in the piping, although not selected, would provide optimum access for circulator maintenance.

1.1.4 Coolant Piping

The flow of the 950ºC helium from the reactor outlet to IHX A, and the 760^{o}C helium from IHX A to IHX B, occurs in internal concentric ducts separated by layers of insulation. The inner portion of this concentric duct arrangement, which will be at the highest temperature, will be free-floating axially. The pressure-containing internal duct that surrounds it will use bellows to accommodate thermal expansion differences between components.

A description of the design and planned development of the coolant piping is provided in Section 6: Heat Transport System, of the Preconceptual Design Report [1-3].

1.1.5 Fuel Handling and Storage System

The fuel spheres are circulated by means of a combination of gravitational flow and a pneumatic conveying process. The design of the FHSS is based partly on that of the THTR 300, which used an on-line fueling scheme with a multi-pass capability. A detailed description of the FHSS for the NGNP is provided in Section 4: Nuclear Heat Supply System, of the Preconceptual

Design Report [1-2]. An illustration describing the components of the FHSS is shown in Figure 1-4.

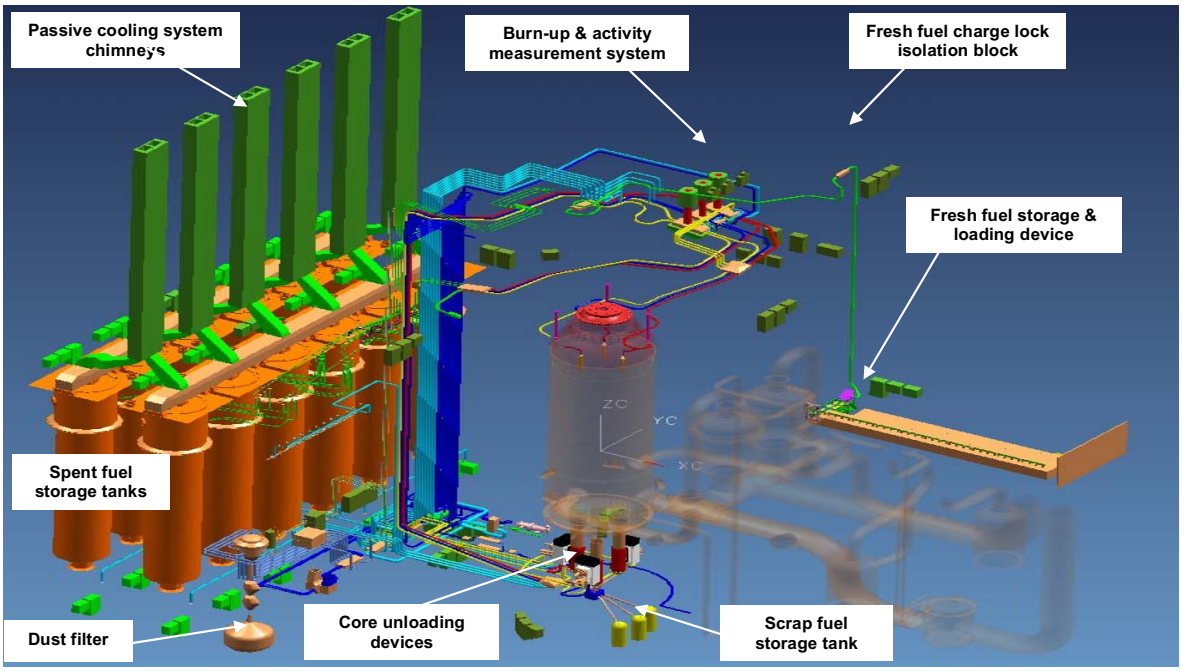

Figure 1-4 Fuel Handling and Storage System

During normal operation, the FHSS circulates the fuel and graphite spheres through the reactor core. Fuel spheres circulate through the core several times before reaching their maximum burn-up, upon which they are discharged to the spent fuel storage tanks.

The reactor core is loaded with fuel spheres or graphite spheres, depending on whether in the initial start-up mode or in the equilibrium mode. The spheres are circulated by a combination of gravitational flow and pneumatic conveying using helium gas at PHTS operating pressure, as the transporting medium. Under normal operating conditions, fuel spheres inside the conveying systems are exposed to a nominal maximum operating pressure of 9 MPa, and a temperature of 250^{o}C.

Spheres are removed via three discharge chutes at the bottom of the core by means of three Core Unloading Devices (CUDs). The CUD has a facility that can separate damaged or under-size spheres from the system. The spheres are pneumatically lifted to the top of the reactor, and after passing through the Activity Measurement System (AMS) to distinguish fuel from graphite, the burn-up is measured by means of the Burn-up Measurement System (BUMS). Spheres that do not exceed the permissible burn-up are returned to the RUS. Fuel spheres are recycled through the core nominally six times before the specified fuel burn-up is achieved.

Once the spheres have reached their maximum burn-up, the Sphere Circulation Subsystem directs/discharges fuel to the Sphere Storage Subsystem and accepts fresh fuel from

the Sphere Replenishment Subsystem to replace the discharged spent fuel. Worn and damaged fuel and graphite spheres can also be replaced if and when necessary.

An extraction point is provided for the removal of fuel or graphite spheres for Post-irradiation Examination (PIE) purposes. The extraction process does not influence the normal operation of the PHTS, and is able to take place whenever on-line circulation is active, using a discharge lock and sample sphere container.

The FHSS has the capability for separating and removing damaged spheres, sphere fragments and under-sized spheres from the circulation system. A facility is designed into the CUD where these are collected, and from where they will be removed to an High Level Waste (HLW) storage vault for long-term storage. The removal process does not influence the normal operation of the PHTS, and is able to take place whenever on-line circulation is active.

1.1.6 Helium Services System

The functions of this system are to maintain the helium pressure within the PHTS and RUS and to remove contaminants from the primary circuit. A key sub-system is the Helium Purification System (HPS), which assures the required degree of helium purity. This is done by bleeding off a partial flow of helium from the PHTS and SHTS. The extraction points are from the highest pressure points, i.e. the PHTS and SHTS circulator discharges. This flow is tapped off constantly during operation of the plant. The HPS removes chemical gaseous contaminants from the primary coolant within the PHTS by the use of catalysts, absorbers and the control of temperatures of helium extracted from the PHTS and SHTS.

The major components of the HPS are:

- Filters –for removal of dust
- Heater – raises temperature for subsequent reactions
- Catalytic Converter – converts CO to CO_2 and H2 to H_2O
- Water Cooler and Chiller - lowers to 5 °C water
- Water Separator – removes condensate
- Low Temperature Recuperator – recovers energy
- Cryogenic/Liquid Nitrogen Cooler – lowers gas temperature for traps
- Molecular Sieve – removes CO_2 and H_2O
- Activated Carbon Filter –removes CH_4
- Adsorber Bed– acts as delay bed for decay of radionuclides
- Blower – provides necessary flow rate

The HPS is designed for a flow rate of 80 kg/hr. The filter efficiency is 100% for dust greater than >0.5 μm, and 0% for dust <0.5 μm.

1.2 Operational Requirements

The operational requirements for contamination control for the NGNP are based on limits set in the US Code of Federal Regulations 10CFR20 [1-4]. The potential radiation exposure to the public during normal plan operation and to plant workers is defined in this regulation. The nuclear plant owner typically applies additional criteria on the exposure of workers during plant operation and maintenance.

1.2.1 Exposure to the Public

The total effective dose equivalent to individual members of the public from the licensed operation shall not exceed 0.1 rem (1 mSv) in a year, exclusive of the dose contributions from background radiation.

1.2.2 Exposure of Workers

The occupational dose to individual adults shall require an annual limit of an effective dose equivalent to the whole body of 5 rems (0.05 Sv), or a deep-dose equivalent to any individual organ or tissue, other than the lens of the eye, being equal to 50 rems (0.5 Sv).

The annual limit to the lens of the eye is 15 rems (0.15 Sv). Further, a shallow-dose equivalent of 50 rem (0.5 Sv) to the skin of body is an annual limit.

1.2.3 Release of Tritium in Plant Effluents

Because of the potential for tritium to enter water systems outside of the reactor plant, specific limits on tritium are required for liquid and gaseous discharges. The limit in the US for drinking water is 740 Bq/L. International standards have been moving lower, and a frequent limit selected by plant operators is 100 Bq/L. That conservative value is proposed for this study.

1.3 References

[1-1] *NGNP-ESR-RPT-001, NGNP and Hydrogen Production Preconceptual Design Report: Executive Summary Report, Rev. 1, June 2007.*

[1-2] *NGNP-04-RPT-001, NGNP and Hydrogen Production Preconceptual Design Report Section 4: Nuclear Heat Supply System, Rev. 0, May 2007.*

[1-3] *NGNP-06-RPT-0901, NGNP and Hydrogen Production Preconceptual Design Report Section 6: Heat Transport System, Rev. 0, May 2007.*

[1-4] *U.S. Code of Federal Regulations 10CFR20,Standards for Protection Against Radiation, October 2007.*

2 RADIONUCLIDES AND DUST SOURCE TERMS

This section contains the quantitative values for the expected source inventories of radionuclides and dust within the PHTS and the secondary circuits of the NGNP. The values are best estimates for normal operating conditions. The transport of the radionuclides and dust to the plant systems is evaluated in Section 3.0.

2.1 Plant Tritium Source Term

2.1.1 ^{3}H Production Reactions

Tritium production in the NGNP will be governed by the following five ^{3}H production reactions which take place in a PHTS:

- ^{3}He (n, p) ^{3}H in the helium coolant passing through the RUS
- ^{6}Li (n, α) ^{3}H in the fuel spheres and the reflectors
- Ternary fission in the fuel spheres
- ^{10}B (n, 2α) ^{3}H in the control rods
- ^{10}B (n, α) ^{7}Li (n, nα) ^{3}H in the control rods.

2.1.2 ^{3}H Production in the Reactor Unit System (RUS)

When calculating the production of ^{3}H that may reach the helium coolant, the latter two sources can be neglected, because ^{3}H produced in the control rods is mostly retained within the rods due to the low amounts of ^{3}H produced and the sorption capacity of the graphite in the rods and the reflector graphite around the rods. ^{3}H produced through ternary fission in the fuel kernels can also be neglected due to the very high retention capability of the TRISO kernels for tritium. The dominant ^{3}H sources in the NHSS, that may reach the helium coolant, are the neutron activation reactions with the ^{3}He contents of the coolant gas and the Li contamination of the fuel and reflector graphite.

The tritium production rate, due to activation, is quantified in this section. This was calculated as

$$\frac{dN_{3H}(t)}{dt} = N_{3He}(t).\sigma_{3He}.\Phi_{He} + \sigma_{6Li}.N_{FS(6Li)}(t).\Phi_{FS} + N_{FSnew(6Li)}(0).\sigma_{6Li}.\Phi_{FSnew} \quad [1]$$

Where $N_{3He}(t).\sigma_{3He}.\Phi_{He}$ represents the activation of ^{3}He in the PHTS, $N_{FS(6Li)}(t).\sigma_{6Li}.\Phi_{FS}$ the activation of ^{6}Li in the fuel spheres and $N_{FSnew(6Li)}(0).\sigma_{6Li}.\Phi_{FSnew}$ the activation of ^{6}Li in fresh fuel spheres.

The ^{3}He and ^{6}Li decrease through transmutation at a rate presented by

$$N_{3He}(t) = N_{3He}(0).e^{-\sigma_{3He}.\Phi_{He}.t} \quad [2]$$

$$N_{FS(6Li)}(t) = N_{FS(6Li)}(0).\mathrm{e}^{-\sigma_{6Li}.\Phi_{CR}.t} \quad [3]$$

The ^{3}He is replaced at a rate $L\ N_{3He}$, with L the leak rate of He, while the ^{6}Li introduced through new fuel spheres is represented by F. With these parameters and equations [2] and [3], equation [1] can be rewritten, to equation [4] for the production of tritium from ^{3}He and ^{6}Li activation, once the activation of the new ^{3}He and ^{6}Li has reached equilibrium.

$$\frac{dN_{3H}(t)}{dt} = N_{3He}(0).\sigma_{3He}.\Phi_{He}\ e^{-\sigma_{3He}.\Phi_{He}t} + L\ N_{3He} + N_{FS(6Li)}(0)\ \sigma_{6Li}.\Phi_{FS}\ e^{-\sigma_{6Li}.\Phi_{FS}t} + F \quad [4]$$

The following parameters were used:

i. The average He mass-weighted RUS plus PHTS neutron flux was used to obtain an effective flux for the ^{3}He(n,p)^{3}H production calculation. As the neutron flux distribution throughout the PHTS has not been calculated, the average neutron flux in the PBMR DPP has been adjusted with the power ratio of 500/400 for the NGNP core and riser channels, while an estimated downscaling factor of 10 has been used to estimate flux in the core barrel-reactor vessel annulus region, and a factor of 100 to estimate the flux in the reactor upper and lower volumes.
ii. The helium masses were provided as per Table 2-1.
iii. The ^{3}He content was taken as 1x10^{-7}, as for He extracted from terrestrial sources.
iv. The scaled average core neutron flux above was used for the ^{6}Li(n,α)^{3}H production calculation.
v. The ^{6}Li content of Fuel Spheres (FS) was taken from PBMR DPP specifications.
vi. The leak rate from the helium pressure boundary was taken as 0.12 % /d.
vii. The number of fuel spheres in the core is 451,516 as for PBMR DPP.
viii. Loading rate of fresh fuel is 610 FS/d, calculated from PBMR DPP.

Table 2-1 He Inventory

Section	**Volume**		**Mass**	
Reactor upper volume	80.46	m^3	548.25	kg
Reactor lower volume	57.60	m^3	392.66	kg
Core barrel-reactor vessel annulus	56.06	m^3	381.90	kg
Riser channel	13.64	m^3	92.43	kg
Upper core plenum	12.09	m^3	81.54	kg
Pebble bed core	32.65	m^3	130.30	kg
Lower core plenum	11.20	m^3	38.18	kg
Total for sections above	**263.70**	**m^3**	**1665.26**	**kg**
He in control rod centre cooling and dowel slots, side reflector-core barrel annulus, etc.	130.60	m^3	877.74	kg
Total in PBMR NGNP RUS	**394.30**	**m^3**	**2543.0**	**kg**
PHTS outside neutron field	97.70	m^3	920.0	kg

Section	Volume		Mass	
PHTS (including reactor, core conditioning system, piping, circulator and IHXs)	492	m3	3463	kg

The calculated ^{3}H production rate as a function of operating time is presented in Figure 2-1.

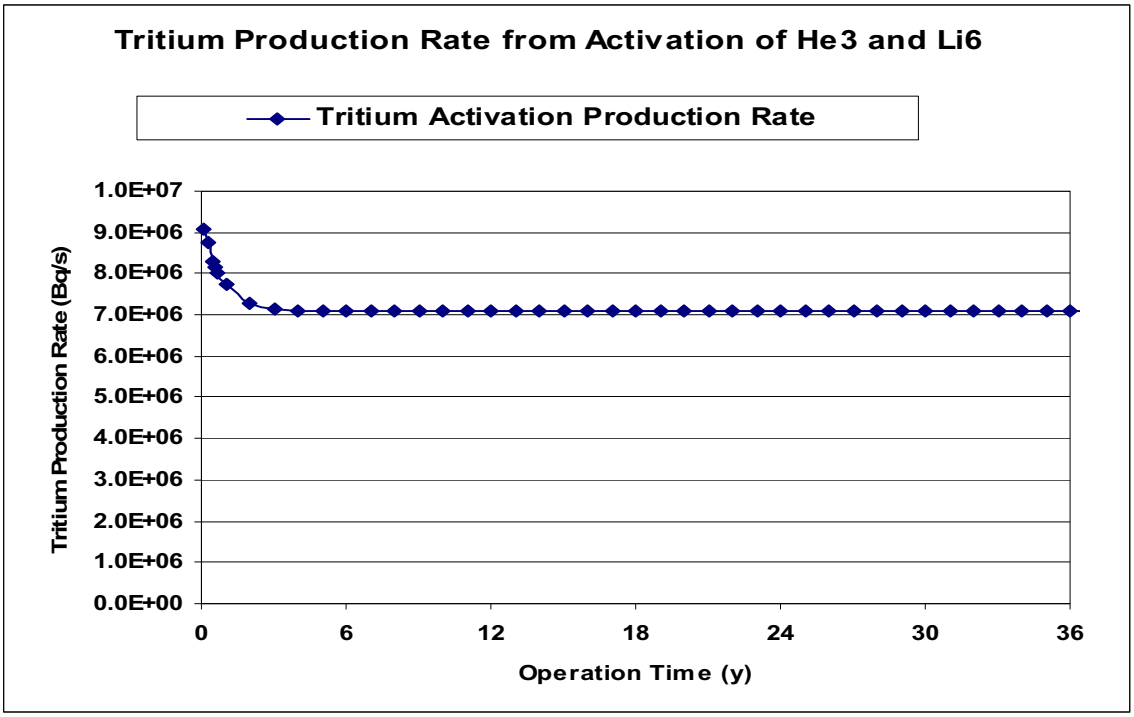

Figure 2-1 Calculated Tritium Activity to Helium Coolant for Various Operating Times

The initial high activity may be an overestimate due to the assumption that the tritium production rate from new ^{3}He and ^{6}Li introduced is equal to the introduction rate, while in fact this equality is only reached at equilibrium.

Calculation of the ^{3}H concentrations in the helium coolant and the graphite needs a more sophisticated approach, considering conservative assumptions with regards to the sorption/desorption of ^{3}He-produced ^{3}H in the coolant and the diffusion/retention of ^{6}Li-produced ^{3}H in the graphite. Due to the complex crystal structure of the graphite, these processes are also rather complex, both in terms of the different activation energies for adsorption onto and desorption from the crystal surfaces and the crystal interiors, as well as the diffusive behavior through the pores and the crystal structures.

For this study only the tritium in the outer layers of the graphite needs consideration as these may end up as abraded graphite dust in the PHTS. Due to the complexities described above, extrapolation from experimental data seems more acceptable for these layers. The fuel sphere-graphite may be a major source of graphite dust. Experimental data for the ^{3}H specific

activity of this, as obtained from the German AVR [2-2] is indicated in Figure 2-2. The specific activity increases slowly with decreasing depth to a value around $6x10^6$ Bq/g at a depth of around 3mm. It then rises fast, probably because of a net absorption of ^3H from the coolant. The graph does not extend to zero depth and needs extrapolation. It is recommended that the tritium behavior in the NGNP fuel and reflector graphite be studied in greater detail as a future project.

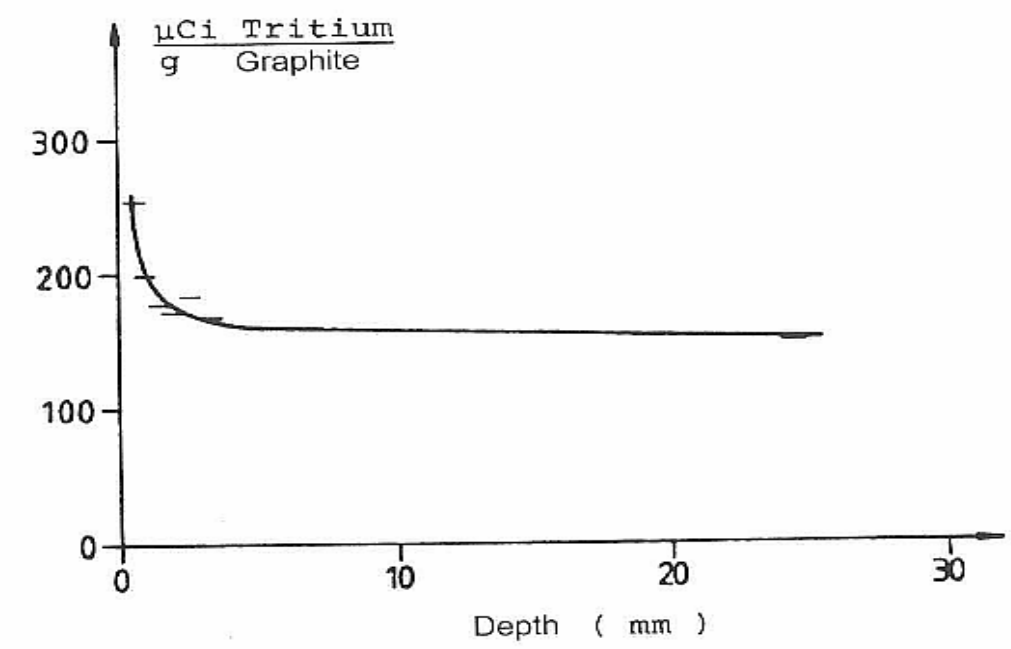

Figure 2-2 Tritium Activity Profile of an AVR Graphite Sphere after Six Years of Operation

2.1.3 Discussion of the ^3H Results

The ^3H calculation process should be seen as an iterative process with the presented results as preliminary and applicable to the first iteration. The main reason for this is the uncertainties in many of the parameters as presented in the assumptions in Section 2.1.2 and in the helium masses presented in Table 2-1. A detailed neutron flux distribution throughout the reactor pressure vessel is not presently available for the NGNP. The assumptions and parameters should be discussed individually with the design engineers and adapted where required. The permeation rate through the heat exchangers is also not considered in the source calculation. A later recalculation is recommended with adapted parameters. Further, the presented ^3H specific activity of graphite dust is an estimate only related to fuel sphere graphite. While this may be the major source of dust, dust from the reflector graphite may also need to be considered.

2.2 Plant Gaseous Carbon-14 Source Term

2.2.1 ^{14}C Production Reactions and Sinks

During normal operation the predominant source of ^{14}C production is by the neutron activation of nitrogen through the $^{14}N(n,p)^{14}C$ reaction. Some elemental ^{14}C may be present in dust generated due to abrasion of the fuel. This value can be extrapolated from PBMR data but will not be part of this section dealing only with the gaseous ^{14}C source term.

The ^{14}C gaseous inventory in the PHTS (CH_4, CO) and the emission rates (CO_2, CO, CH_4) from the Helium Purification System (HPS) and PHTS are calculated as a function of time by mathematically balancing the following source rates:

- neutron activation of nitrogen in the coolant gas considering the time dependent build-up of nitrogen (balance between nitrogen ingress rate and leakage rate);
- neutron activation of nitrogen sorbed in fuel spheres and released during subsequent selective corrosion;

and the following sink rates:

- leakage rate from the PHTS (CO, CH_4);
- CO filtration rate of the HPS, taking into account that CH_4 is not extracted.

Permeation to a secondary circuit is presently not considered for the PBMR and little is known about it. It is assumed that such permeation is negligible but this needs to be confirmed.

Some elemental ^{14}C may be present in dust generated due to abrasion of the fuel. This value will be extrapolated from PBMR data.

2.2.2 ^{14}C Gases in the PHTS

The ^{14}C gaseous source model below follows the AVR and PBMR DPP concept. The differential equation balancing the ^{14}C production and removal rates has been prepared with its analytical solution and has been fed into an Excel spreadsheet. The solution at various times provides the time-dependent ^{14}C concentrations in the helium coolant circuit. The time-dependent leak-rate out of the helium pressure boundary is also calculated as an emission rate from the plant, while the transfer rate to the HPS has been used to calculate the gaseous ^{14}C waste production rate assuming all gaseous ^{14}C to be released to the atmosphere during HPS regeneration operations.

The following parameters or assumed parameters were used but require verification:

i. As nitrogen is assumed to be homogeneously mixed with the helium, the average He mass-weighted RUS plus PHTS neutron flux was used to obtain an effective

flux for the $^{14}N(n,p)^{14}C$ production calculation. As the neutron flux distribution throughout the PHTS has not been calculated, the average neutron flux in the PBMR DPP has been adjusted with the power ratio of 500/400 for the NGNP core and riser channels while an estimated downscaling factor of 10 has been used to estimate flux in the core barrel-reactor vessel annulus region and 100 to estimate the flux in the reactor upper and lower volumes.

ii. The helium masses were provided as per Table 2-1.
iii. The assumed residual mass of N_2 from first evacuation and after each 6-year assumed maintenance is 5 kg.
iv. N_2 from FS migrating into the primary coolant is 40 ppm (mass N2 per mass C).
v. Mass of carbon per fuel sphere is 189 g.
vi. N_2 ingress rate from FHSS (extrapolated from PBMR DPP) is $1.0x10^{-5}$ m^3/hr.
vii. Residence time of FS in the core (extrapolated from PBMR DPP) is 740.32 d.
viii. Number of FS in core are 451,516 as for PBMR DPP.
ix. Loading rate of fresh fuel spheres (extrapolated from PBMR DPP) is 610 FS/d.
x. Mass of water reacting per fuel sphere until the end of residence time in the core is 40 mg.
xi. Ratio of C atoms in the fuel sphere to the number of C atoms at the inner surface is 630.
xii. CO and CH_4 concentration in the He coolant is 2.2 and 12 ppm (volume) (used to determine filter efficiency).
xiii. Leak rate from HPB taken as 0.12 % /d.
xiv. Extraction to HPS taken as 125 kg/hr at 100 % availability.

The calculated ^{14}C activity of the helium coolant for various operating times is presented in Figure 2-3. The calculated ^{14}C emission rate due to leakage from the PHTS is indicated in Figure 2-4.

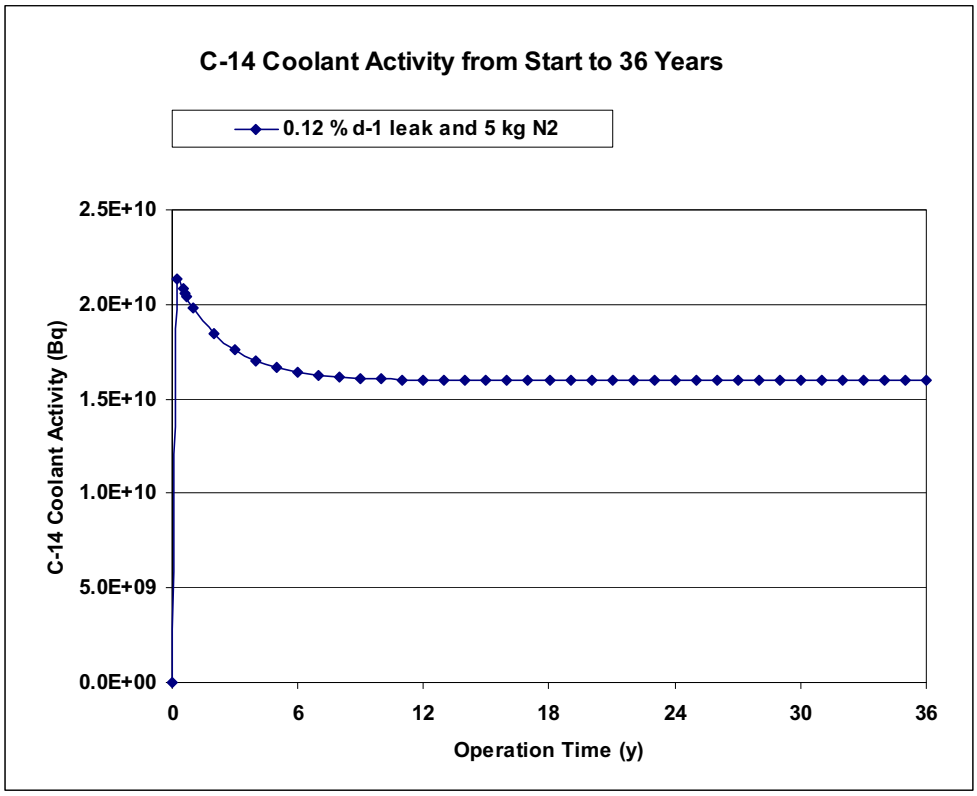

Figure 2-3 Calculated ^{14}C Activity of Helium Coolant for Various Operating Times

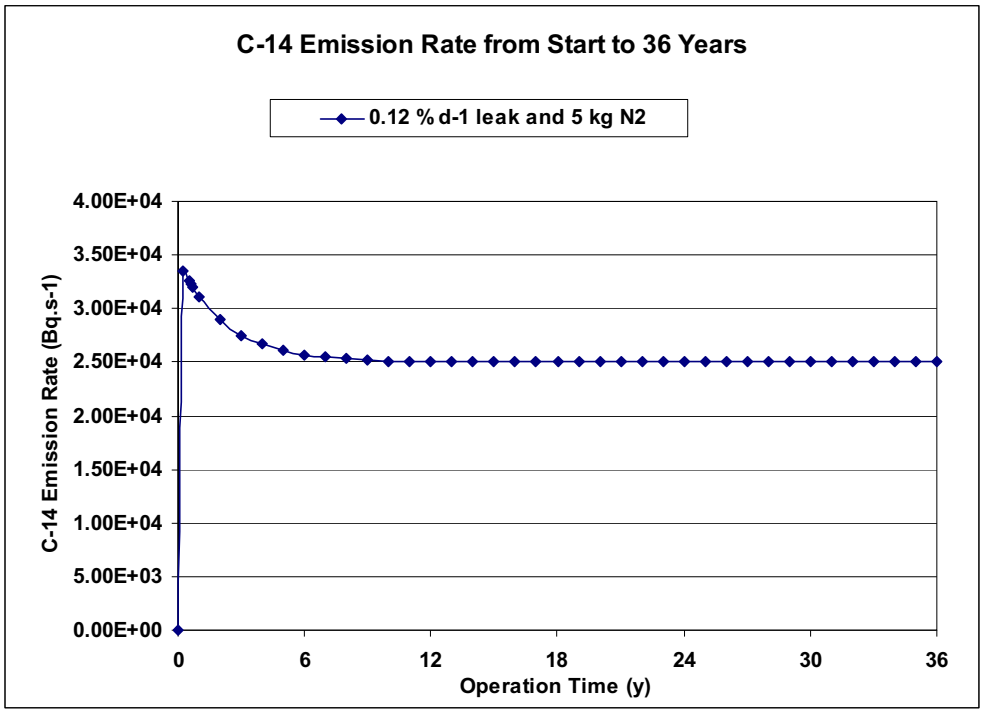

Figure 2-4 Calculated ^{14}C Emission Rate for Various Operating Times

2.2.3 ^{14}C in the Graphite Dust

Some elemental ^{14}C may be present in dust generated due to abrasion of the fuel spheres. An expected specific activity of $4.4x10^{3}$ Bq/g is extrapolated from PBMR data.

2.2.4 Discussion of the ^{14}C Results

The ^{14}C calculation process should be seen as an iterative process with the presented results as preliminary and applicable to the first iteration. The main reason for this is the uncertainties in many of the parameters as presented in the assumptions in Section 2.2.2 and in the helium masses presented in Table 2-1. A detailed neutron flux distribution throughout the reactor pressure vessel is not presently available for the NGNP. The assumptions and parameters should be re-evaluated for the final design of the NGNP.

2.3 Fission Product Source Terms

This section documents the calculated best estimate fission product release results for the 500MWt NGNP core, under normal operating conditions. The NGNP core is based on the 400MWt DPP reactor design, but with parameters, such as the core inlet and outlet temperatures and mass flow rate, adjusted to yield 500MWt thermal power.

2.3.1 Methodology and Models

The transient release behavior of long-lived metallic fission products can be predicted by using diffusion models. An intact TRISO particle coating presents an effective barrier against fission product release at normal operation temperatures (except for silver). Therefore the most important input data for coated particle performance during normal operation will be the fraction of failed/defective particles and the fraction of heavy metal contamination in the fuel element graphite, in combination with the transport data of kernel material and fuel element graphite. In addition to diffusion, other release mechanisms during normal operation are the recoil effect and the knockout effect. Both present a geometrical problem and are not dependent on temperature making them significantly more important at lower temperatures.

The releases of metallic fission and activation products from the equilibrium core were calculated with the computer code GETTER through the FIPREX software. FIPREX creates all GETTER input files from the available core geometry and parameters and determines the final core releases. The steady state releases of the noble gases, krypton and xenon, and the halogens, bromine and iodine, from the equilibrium core, were calculated with the computer code NOBLEG.

The computer code GETTER was developed to handle experimental and operational conditions. It was applied to design and support several German High Temperature Reactor projects. GETTER turned out to be a very versatile tool to evaluate different transport problems. GETTER includes subroutines which calculate the burn-up and the power history of a fuel sphere in the core, and the temperature distribution in the spheres, on the basis of given neutron cross-sections and gas temperatures.

The computer code FIPREX was developed by PBMR to automate GETTER calculations in order to perform more detailed reactor analyses calculations. FIPREX acts as a wrapper program preparing input files and post-processing GETTER output files.

Gaseous fission product release is a direct indicator of fuel performance. Its main sources are the heavy metal contamination in the fuel graphite and defective/failed coated particles. Standard particles within the specification limits are not expected to contribute to the release of gaseous fission products under normal operating conditions. Through in pile measurements of irradiation experiments and the regular monitoring of the coolant gas activities of the Arbeitsgemeinschaft Versuchs-Reaktor (AVR) and the Thorium High Temperature Reactor (THTR), the release of noble gases from spherical fuel elements has been extensively investigated. The transport mechanisms of the noble gases produced by the finely distributed uranium contamination of the matrix material were verified by the results from irradiation experiments in the R2 test reactor at Studsvik.

The gas release from artificially failed particles was studied in detail with irradiation experiments at Jülich. More refined model data of the transport characteristics of production-induced defects of TRISO particles with UO_2 kernels was drawn from the German reference irradiation tests HFR-K6 in the HFR, Petten [2-1]. All experimental findings confirm that the transport behavior of the halogens at elevated temperatures is similar to that of the noble gases.

The regular measurements of the coolant gas activities of the AVR and the THTR have been evaluated on the basis of the above transport models, verifying their reliability and applicability under real pebble bed reactor conditions. These evaluations did not only serve to test the underlying design methods, but also to identify potential failure mechanisms and to supervise the quality of the fuel elements.

The steady state releases of the noble gases, krypton and xenon, and the halogens, bromine and iodine, from the equilibrium core, were calculated with the computer code NOBLEG. The software is based on Booth's equivalent sphere model and is applied in the gaseous fission product release calculation model.

The complete calculation model that includes the approach used and methods applied is available in the calculation model reports. The number of GETTER runs was limited to 2000 runs per FIPREX run in order to limit software failures. Five FIPREX runs were combined into each result.

2.3.2 Assumptions

All assumptions are consistent with those described in [2-1]. The main assumptions are described below:

1. The calculation models are developed from original German calculation models.
2. All parameters and correlations used in the calculation models are based on German reference fuel.
3. PBMR fuel design, manufacture and qualification are aimed at achieving equivalence to the German reference fuel.
4. It is assumed that steady state conditions always apply. No temperature, power or coolant flow transients were calculated.
5. Heat transfer in the pebble bed is calculated with technical safety rules from the German nuclear technical committee (KTA), in particular part 2 of KTA 3102.
6. Heat conductivity in the fuel spheres is calculated by the Brabandt/Theymann relation which is dependent only on fast neutron fluence and surface temperature.
7. Under normal operating conditions it is assumed that no coated particles fail due to irradiation and temperature effects other than already included in the coated particle failure fraction.
8. Expected failure fraction values for PBMR fuel are based on the expected value for the number of failed coated particles obtained from burn-leach tests performed during production of state-of-the-art German fuel and expected (average) values for failure of coated particles during irradiation and during heating tests. The expected release values are calculated with a constant failed particle fraction of 1.44×10^{-5}.
9. The effective uranium contamination in the matrix material is a fraction of 2.0×10^{-6} of the total uranium content in a fuel sphere.

2.3.3 Verification and Validation

All software has been reverse engineered and numerical and analytical solutions mathematically verified. Specific subroutines have been compared with other software products and benchmarked against some irradiation test results. Complete lifecycle V&V plans are available that include integral effects testing against existing and planned irradiation tests and eventual evaluation of plant performance.

2.3.4 Fission Product Source Term Results

The expected gaseous fission product release and metallic fission product release values for the NGNP core are given in Table 2-2 and Table 2-3, respectively.

Table 2-2 NGNP Expected Gaseous Fission Product Release Data

Nuclide	Half-life (hours)	Activity Released from the Core (Bq)
Kr-83M	1.86E+00	1.23E+10
Kr-85M	4.48E+00	3.92E+10
Kr-85	9.40E+04	4.36E+10
Kr-87	1.27E+00	4.85E+10
Kr-88	2.80E+00	8.97E+10
Kr-89	5.27E-02	2.23E+10
Kr-90	8.97E-03	1.07E+10
Kr-91	2.50E-03	5.34E+09
Xe-131M	2.88E+02	2.32E+09
Xe-133M	5.35E+01	6.05E+09
Xe-133	1.27E+02	2.75E+11
Xe-135M	2.55E-01	8.58E+09
Xe-135	2.04E+00	7.87E+10
Xe-137	6.38E-02	2.33E+10
Xe-138	2.37E-01	4.16E+10
Xe-139	1.10E-02	6.73E+09
Xe-140	3.78E-03	2.88E+09
Br-83	2.40E+00	1.35E+10
Br-84	5.30E-01	1.38E+10
Br-85	4.78E-02	6.14E+09
I-131	1.93E+02	1.44E+11

Nuclide	Half-life (hours)	Activity Released from the Core (Bq)
I-132	2.29E+00	5.97E+10
I-133	2.08E+01	1.54E+11
I-134	8.77E-01	8.04E+10
I-135	6.58E+00	1.08E+11
I-136	2.36E-02	6.29E+09

Table 2-3 NGNP Expected Metallic Release Data

	^{137}Cs	^{134}Cs	^{110m}Ag	^{111}Ag	^{90}Sr
Core release rate (atoms/s)	1.28×10^{13}	5.71×10^{11}	1.90×10^{13}	1.91×10^{11}	6.33×10^{9}
Core activity release rate (Bq/s)	9 330	6 110	604 000	206 000	4.83

The activity released from the core is the total steady state activity released from fuel and is either circulating or plated out on the metallic surfaces or on the dust within the HPS and the PHTS. For comparison purposes, the expected release rates for the 400 MW DPP are given in Table 2-4 and Table 2-5. Gaseous fission product releases increase by less than a factor of 10. Cesium and iodine releases increase by less than a factor of 10, but strontium and silver-111 release increases by factors of 12 and 15, respectively. The activation product silver-110m increases the most - by a factor of 23. These are primarily temperature-driven increases for the higher fuel temperatures to achieve the higher core outlet

Table 2-4 400MWt DPP Expected Gaseous Fission Product Release Data

Nuclide	Half-life (hours)	Activity Released from the Core (Bq)
Kr-83M	1.86E+00	6.54E+09
Kr-85M	4.48E+00	1.97E+10
Kr-85	9.40E+04	2.71E+10
Kr-87	1.27E+00	2.64E+10
Kr-88	2.80E+00	4.63E+10
Kr-89	5.27E-02	1.41E+10
Kr-90	8.97E-03	6.96E+09
Kr-91	2.50E-03	3.38E+09
Xe-131M	2.88E+02	1.34E+09
Xe-133M	5.35E+01	3.72E+09
Xe-133	1.27E+02	1.63E+11
Xe-135M	2.55E-01	5.91E+09
Xe-135	2.04E+00	5.57E+10

Nuclide	Half-life (hours)	Activity Released from the Core (Bq)
Xe-137	6.38E-02	1.53E+10
Xe-138	2.37E-01	2.86E+10
Xe-139	1.10E-02	4.51E+09
Xe-140	3.78E-03	2.03E+09
Br-83	2.40E+00	7.02E+09
Br-84	5.30E-01	7.87E+09
Br-85	4.78E-02	3.88E+09
I-131	1.93E+02	8.39E+10
I-132	2.29E+00	4.22E+10
I-133	2.08E+01	9.94E+10
I-134	8.77E-01	5.72E+10
I-135	6.58E+00	7.36E+10
I-136	2.36E-02	4.12E+09

Table 2-5 400MWt DPP Expected Metallic Release Data

	^{137}Cs	^{134}Cs	^{110m}Ag	^{111}Ag	^{90}Sr
Core release rate (atoms/s)	6.77×10^{12}	3.77×10^{11}	8.14×10^{11}	1.27×10^{10}	5.27×10^{8}
Core activity release rate (Bq/s)	4 940	4 030	25 900	13 700	0.402

All calculation results are based on estimated reactor input parameters and no conservatisms other than those integral to the calculation model have been used.

2.4 Dust Source Term

This section describes the mechanisms for dust formation, the dust source locations, the dust production rates and the physical characteristics of dust that would potentially contain adhered radionuclides. These data provide the source terms for subsequent analyses on the transportation, deposition and re-entrainment mechanisms. The transport of radionuclides attached to the dust sources is described in Section 3 of this report.

The quantification of the dust sources leads to predictions of specific radioactivity dose risks to workers at different locations and plant conditions. The dust source term data have been calculated for the 500MW(t) NGNP based on the previous analyses performed for the 400 MW(t) DPP.

The volatility of all of the radionuclide groups determines the contributions to the radioactivity attached to dust. The most volatile group is comprised of the noble gases, represented by krypton and xenon. This group does not attach to dust or any surface in the PHTS. The next group is the halogens, dominated by iodine nuclides, which may attach to some degree, depending on surface conditions and temperature. The metallic fission products, dominated by Ag, Cs, and Sr, form the final group that becomes the main source of radioactivity on dust.

2.4.1 Dust Production Mechanisms

In the reactor core, graphite dust originates mainly through the abrasion of the FSs within the pebble bed and while moving along the side and central reflectors. Dust is also generated in the FHSS, through the impacts of the FSs as they are transported in the FHSS piping and valves. The majority of dust generated in the FHSS is removed through filtration, but a small quantity may be transported into the PHTS.

The dust generated from the FSs may be contaminated with small amounts of radionuclides that were present in the outer layer of the FS. However, the radioactivity associated with dust comes primarily from the adsorption of species such as Cs and Ag, which become attached to the dust while circulating in the coolant stream. The sorbed radionuclides are bound within the volume of the dust particle. While the size of dust particles varies, larger particles contain the bulk of the radionuclides trapped in the graphite dust [2-1].

Besides the graphite dust, small amounts of metallic dust may be present from the construction of the reactor, from erosion of circulator blades and from rubbing of metallic components during thermal cycling. These metallic dust particles may become activated in the reactor core neutron field. The quantity of metallic dust is expected to be very small in comparison to that of the graphite dust, and can be considered as a portion of the graphite dust when calculating the transport of radionuclides.

The graphite dust provides a mechanism for the transport and deposition of radionuclides throughout the NHSS during normal operation. The primary deposition sites are at the bottom of the reactor vessel, within the HPS, within the FHSS and especially within the compact IHX. The smaller size particles may also be transported outside the NHSS due to the small amount of expected helium leakage during normal operation. The primary leakage locations are predicted to be generally downstream of the IHX.

The amount of dust, its physical characteristics and its specific activity have been quantified from the data available from the operation of the Arbeitsgemeinschaft Versuchs-Reaktor (AVR) [2-2], and the Thorium High Temperature Reactor (THTR) [2-3].

Most of the experimental data on the production and characteristics of dust was obtained in the AVR. Three series of dust experiments were carried out in the AVR specifically to determine the role of dust in the transport of radionuclides. In the first, a set of filters was placed in a cooled line located downstream of the helium circulator. In two subsequent series of

experiments, VAMPYR-I and VAMPYR-II, special probes were placed in the main coolant stream at the core exit, to draw off dust and fission product contamination.

In addition to those experiments, data on dust was obtained by wiping down the primary circuit components after decommissioning of the plant. The AVR experiments showed that the dust mass in the AVR primary circuit varied considerably with time [2-2]. Much of the dust originated from the construction of the plant, and from the initial loading of the fuel.

The data obtained from THTR were more qualitative than that from the AVR. There were no specially designed dust experiments, as had been completed in AVR. The THTR had filters for dust in the helium purification system, the fuel handling system and in the moisture monitors. Measurements were made of the specific activity of dust wiped from components that were disassembled from the primary system and the fuel handling system. The total quantity of dust generated in the THTR was inferred from the quantities removed from the filter systems.

A series of tests was performed in THTR to determine the effects of inserting the control rods directly into the pebble bed. These tests required circulation of FSs to loosen the pebble bed. The core contained 6.75×10^5 FSs, and the total number circulated was 1.4×10^6 FSs, including 2.35×10^5 FSs that were discharged from the cycle. The general conclusion for the THTR was that dust did not pose any significant problem, neither with regard to operation nor to safety [2-3]. The reported operational actions required to accommodate dust were to replace clogged filters in the line to the moisture monitor, modification of electrical penetrations in the gas blower for the fuel handling system and cleaning of the piping in the fuel handling system.

The analyses performed on the DPP have shown that the sources of important fission products in the dust leaving the core after direct abrasion, particularly Cs and Ag sources, would be very small. Most of the activity in dust would enter by adsorption of these metallic species while the dust is circulating in the primary coolant.

During the planned operation of the DPP, the sources of dust build-up are to be monitored. Extraction and characterization of dust generated in the DPP may be carried out at scheduled maintenance operations and through online sampling means. This experience will be available for the NGNP.

2.4.2 Dust Production Rate

Expected values for the dust production rate for the 500MW(t) NGNP are based on previously developed values for the 400MW(t) DPP. The dust production in the DPP was calculated from a combination of AVR experimental data and abrasion modeling of the movement of the FSs through the RUS.

The production rates for the NGNP were calculated for the two sources for graphite dust generation, the abrasion of FSs in the core and in transit through the FHSS. These sources have been calculated independent of the removal mechanisms within the PHTS. Subsequent analyses will be reported in Section 5 on the rates of removal of the dust.

All of the dust that originates from abrasion of FSs in the core enters the PHTS. Of the dust that originates in the FHSS, only a fraction enters the PHTS, because of the effectiveness of a filter located in the FHSS. A second sink for the removal of dust, the plant HPS, is highly efficient in removing dust and gaseous fission products.

Expected values for the generation rates of dust in the NGNP systems are shown in Table 2-6.

Table 2-6 NGNP Dust Generation Rates

Graphite dust source	Dust generation rate, kg/fpy
Core (pebble bed, side reflectors and bottom reflector)	28
FHSS (dust before filtering)	20

fpy = full power year

2.4.3 Size of Dust Generated

Analyses from the AVR and THTR plants showed that the dust occurred primarily in a range between 0.2 μm and 10 μm. Some random particles from wipes were found to be as large as 200 μm; however, the cumulative distribution of dust mass, as measured in AVR, was found to be 99% of less than 10 μm [2-2].

IAEA-TECDOC-978 [2-1] provides a compilation of experimental and analytical data on the graphite dust from AVR and THTR. The following conclusions can be made from analysis of the historical AVR data:

- The elementary dust particle sizes are small, with an average size of 0.8 μm.
- Dust in the primary loop of the reactor and dust deposited onto surfaces in the reactor agglomerates with time to larger dust particles.
- Agglomeration also took place on the filters during experiments.
- Radionuclides were contained within the interior of the dust particles.

From the AVR study, the data shown in Table 2-7 were used in predicting the sizes and distributions for the DPP during the design phase. Those results are judged to also be applicable for the design of the NGNP. The values are for the size as formed, and do not include the effects of agglomeration.

Table 2-7 Dust Particle Size Distribution from AVR Tests

Average Dust Particle Size (μm)	Normalized Number Distribution (%)	Normalized Volume Distribution (%)
0.202	6.09	0.03
0.353	14.43	0.42
0.493	27.01	2.12
0.632	24.77	4.09
0.873	9.79	4.27
1.218	7.90	9.34
1.598	3.74	9.99
1.953	2.37	11.57
2.322	1.56	12.82
2.718	1.04	13.69
3.078	0.45	8.51
3.458	0.85	23.15

2.4.4 Dust Deposition Locations

The deposition of dust in the PHTS occurs through inertial separation, sedimentation and thermophoresis. The quantity of dust deposited by sedimentation is generally small in comparison to the quantity of dust deposited through inertial separation and thermophoresis.

The following locations in the PHTS are identified for inertial separation, and will be evaluated in the transport analyses in Section 3:

1. The Core Outlet Pipe (COP)
2. The IHX-A, with its compact heat transfer surfaces
3. The IHX-B, also with compact heat transfer surfaces
4. The Helium Circulator (HC), located at the top of IHX-B
5. The Core Inlet Pipe (CIP)
6. The HPS filters.
7. The FHSS filters

Re-entrainment of settled dust can occur from normal operating procedures, such as changes in circulator speed, circulator trips or reactor startup.

2.4.5 Estimate of Dust Bound Activity

In the dust experiments performed in AVR VAMPYR probes, the measured activity was primarily Cs-137 and Ag-110m. The dust-bound activity values were $1x10^6$ to $1x10^8$ Bq/g of Cs-137 and $5x10^4$ to $5x10^7$ Bq/g of Ag-110m. The mean size of the dust from the AVR tests was 0.8 μm.

The value for specific activity reported from the THTR wipes was a maximum of $2x10^8$ Bq/g, and all was attributed to activation products. The primary radionuclides were Co-60, Zr-95, Hf-181 and Pa-233. Because of the short operating life of THTR, most of the FSs did not complete one cycle through the reactor core. Therefore, the contributions of dust from abrasion were small. The observed radioactivity on dust wipes would have come from activation of dust originating from the construction of the plant.

As an indicator of how strongly a metallic radionuclide could be attached to dust, measurements were made in the AVR on Cs that had penetrated the metallic surfaces of the primary ducts. Harsh decontamination steps were required to remove the Cs, which was considered representative of the metallic fission products. The affinity of Cs to graphite is equally strong, and causes much of it to remain in the fuel sphere or migrate to the graphite structures surrounding the fuel (i.e., the reflectors) after release.

The activity in the PHTS consists of circulating aerosols, gases and fine dust particles as well as those that are deposited on the surfaces. The division of activity between plate out and dust will be discussed in Section 3.

2.4.6 Dust Release During Normal Operation

The graphite dust that is too small to deposit will circulate with the helium coolant in the PHTS. There is an expected leakage of helium coolant from the PHTS during normal operation through imperfections in flange attachments, leakages through seals and penetrations to the HPB, and diffusion through the metal. This leakage of coolant carries some radionuclides in atomic vapor form.

The fission products and dust that may be released during normal operation are filtered through the Heating Ventilation and Air Conditioning (HVAC) system. The diameter of the leakage paths from the HPB for the coolant is much smaller than the circulating graphite dust (i.e., the leakage flow paths are too small for the graphite dust to pass through) and hence it is not possible for the dust to be a significant contributor to off-site doses during normal operation.

2.5 References

[2-1] *Fuel Performance and Fission Product Transport, IAEA TECDOC-978 November 1997.*

[2-2] *R. Moorman, AVR Experiments Related to Fission Product Transport, Proceedings HTR2006, October 2006.*

[2-3] *R. Baumer and I. Kalinowski, THTR Commissioning and Operating Experience, IAEA 11th Conf. on HTGR, June 1989.*

3 DUST AND FISSION PRODUCT TRANSPORT

3.1 Introduction

The plate-out of fission products transported directly to certain locations of the primary system, as well as the fission products adsorbed on dust, may affect the maintenance and inspection of the primary coolant components. Also, graphite dust in the primary system has the potential to cause erosion of the primary system components, contamination of the electromagnetic bearings in the circulators and plugging in the IHX. The transport of fission products and dust during normal operation is analyzed with the SPECTRA code.

The following sections give a brief description of the NGNP system, an introduction to the SPECTRA code, a description of the SPECTRA model of NGNP and the analysis results.

3.2 NGNP System Features Modeled

A brief description of the overall NGNP is given in Section 1.0 of this document. Dust and fission products are generated in the core and fuel handling system and will circulate through the reactor vessel, the nuclear core, the IHX and the connecting pipes. This subsection gives a brief description of the main components of the primary circuit of NGNP, to indicate the required modeling.

3.2.1 Reactor Unit System

The PBMR reactor is an annular core within a pressure vessel. The annular core around a central graphite reflector contains about 450,000 fuel spheres each with a diameter of 60 mm. Each fuel sphere contains approximately 14,000 UO_2 coated particles, imbedded in graphite.

The reactor core is surrounded by a graphite reflector. In the reflector wall there are 24 control rod channels. Around the graphite reflector there is a thermal shield made of carbon bricks. In the thermal shield wall there are 36 inlet pipes, with helium flowing upwards to the top of the core, from where it flows down, through the core.

The next material layer outward is the core barrel. The barrel is separated by annular gaps from the thermal shield (on the inside) and the RPV wall (on the outside). Helium from the reactor inlet at the top of the vessel flows down through the core barrel outer annulus into the lower plenum, from where it flows up into the riser channels (see Figure 3-1). Finally there is the RPV wall, made of 18 cm thick steel, surrounding the core and all RPV structures.

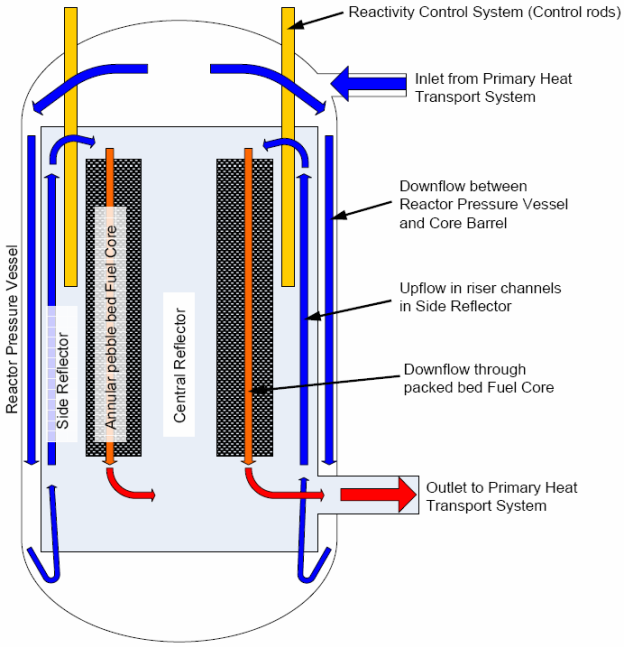

Figure 3-1 Helium Flow Path Configuration Through the Reactor Unit System

3.2.2 Intermediate Heat Exchangers

The thermal energy from the primary (nuclear) loop is transferred to the secondary (non-nuclear) system through two Intermediate Heat Exchangers (Figure 1-3). The heat exchangers are in a counter-current arrangement where IHX-A operates at high temperatures (about 700 to 950 ºC) and IHX-B at moderate temperatures (about 300 to 760 ºC). IHX-A is designed for replacement during the plant lifetime whereas IHX-B operates during the whole lifecycle.

Both IHX-A and IHX-B, which are very similar in design, are plate-fin heat exchangers operating in counter-current mode. The finned plates of IHX-B are larger than those of IHX-A, and there are more of them too: 35,230 unit cells versus 25,270 for IHX-A. Thus the maximum theoretical heat exchange is about 390 MW for IHX-B and 200MWt for IHX-A. In practice the heat exchange that can be achieved is approximately 350 MW for IHX-B and 155 MW for IHX-B.

Figure 1-3 shows the layout of IHX-A. The cores are arranged in two rows. The large pipe in the centre is the primary inlet volume. The connections on the left and right are the secondary inlet and outlet pipe respectively. Pressure assisted seals prevent secondary helium leaking from the inlet (vessel annulus) to the outlet volume (inner vessel).

3.2.3 Circulator

The electric-driven PHTS circulator operates at nominally 350ºC and 9 MPa (exit conditions) to provide for circulation of the primary coolant helium to and from the reactor. The circulator is a centrifugal compressor with titanium impellers. It is integrated with IHX-B and delivers a pressure head of about 3.7 bar.

3.2.4 Coolant Piping

Two different PHTS piping designs, depending on location in the main coolant loop, exist. The piping between the reactor vessel outlet and IHX-A and between IHX-A and IHX-B will be of a straight "rigid" design. Actual flow of the 950 ºC helium from the reactor outlet to IHX-A and the 760 ºC helium from IHX-A to IHX-B occurs in internal concentric ducts separated by layers of insulation, as shown in Figure 3-2. The inner, highest surface temperature, portion of this concentric duct arrangement will be free floating axially; the pressure containing internal duct that surrounds it will use bellows to accommodate thermal expansion.

The insulation between these ducts (not shown in the figure) provides for minimization of both heat loss and the temperature of the outer duct material. A flow of cold return PHTS helium (350 ºC), diverted from the circulator outlet, will be directed through the annulus between the outer duct and the pressure boundary pipe. Finally, the return piping from IHX B to the reactor inlet, which operates at 350ºC, will comprise a relatively simple insulated pressure boundary pipe.

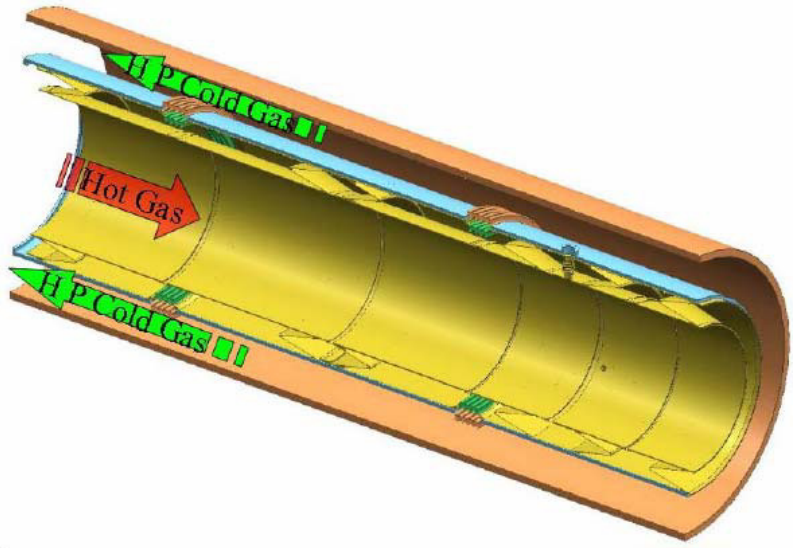

Figure 3-2 High-Temperature Duct Insulation System within the Core Outlet Pipe

3.2.5 Helium Purification System

The HPS is required in order to minimize corrosion and contamination in the PHTS, and to filter dust and radionuclides from the systems. This is done by bleeding off a partial flow of helium from the PHTS. This flow is tapped off constantly during operation of the plant. The HPS removes chemical gaseous contaminants from the primary coolant within the PHTS by the use of catalysts, adsorbers and the manipulation of helium temperature.

The performance data from the similar HPS of the Fort St. Vrain Reactor has been used as a design basis for the removal of fission products and dust for the current analyses [3-4]. In the Fort St. Vrain HPS, reactive radionuclides, such as iodine, are trapped permanently, in competition with the major fraction that is plated out in the primary circuit. Noble gases krypton and xenon are delayed in cooled adsorber beds, and their removal fraction depends on the half-life of the nuclide.

3.3 The SPECTRA Code

The SPECTRA code is an accident analysis code developed at NRG, the Netherlands. SPECTRA (Sophisticated Plant Evaluation Code for Thermal-hydraulic Response Assessment) is a computer program designed for thermal-hydraulic analyses of nuclear or conventional power plants. The models applied in the code were selected after an extensive literature review, as well as review of models available in other codes (CONTAIN, MAAP, MELCOR, RELAP, TRAC-BF1). The best available models were selected, which makes SPECTRA not only an accident analysis tool but also a library of physical models, well documented and tested, and easy to use.

The general structure of the SPECTRA code is given in Figure 3-3. The code structure is described in terms of Packages, containing Models that perform similar tasks

The modeling approach is based on the Control Volume concept. A model of a certain physical system consists of Control Volumes (usually representing a physically bounded space, like a room, containment compartment, pipe section, etc.), connected by junctions. The approach is similar to that taken in for example CONTAIN or MELCOR. Within a Control Volume, four fluid components may exist: two continuous components (atmosphere and pool), and two dispersed components (droplets and bubbles). The gas components (atmosphere and bubbles) are assumed to be mixtures of non-condensable gases and steam. Non-equilibrium is assumed between each of the four fluid components, with the inter-component heat and mass transfer modeled in a mechanistic way.

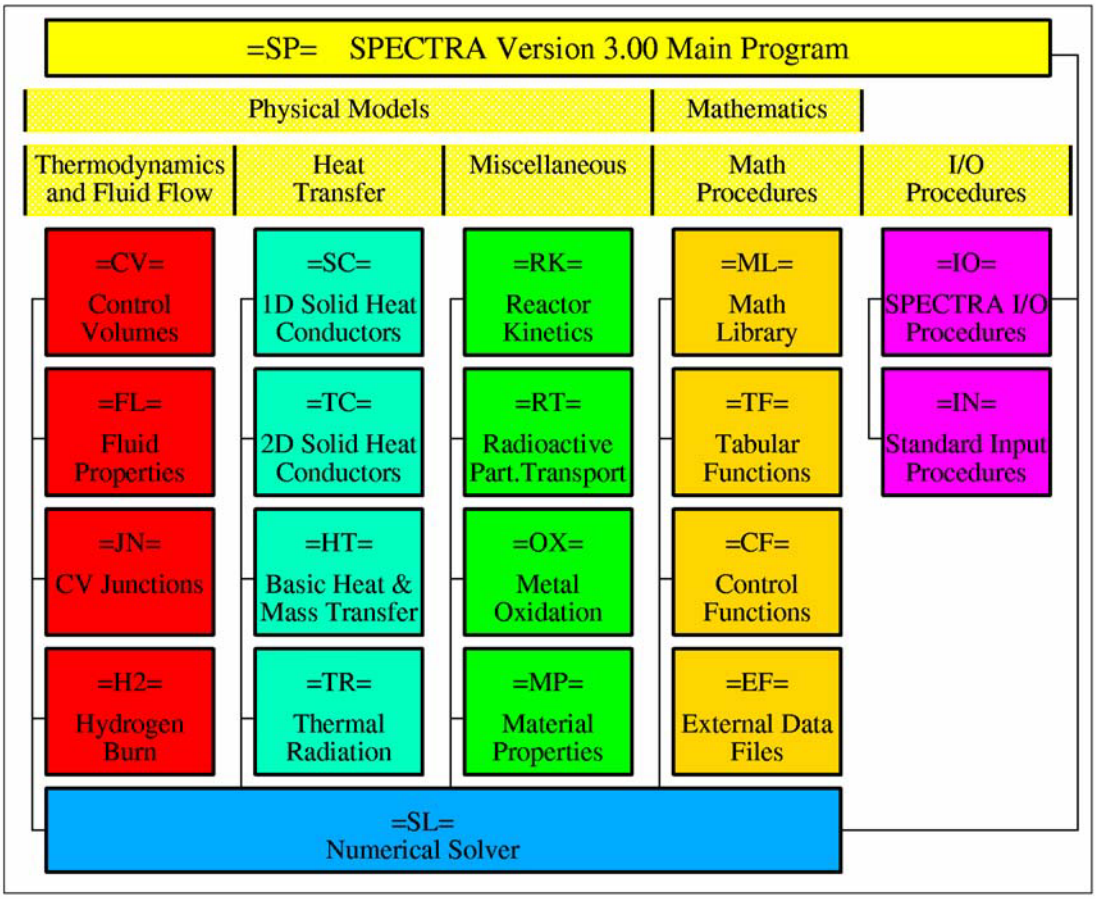

Figure 3-3 SPECTRA Code Structure

The code contains a built-in library of fluid properties, consisting of the properties of water, steam, and several non-condensable gases. All gases are treated as real gases. The steam properties were obtained using the NRC/NBC steam tables program interpolated using pre-computed tables, covering the range from 270 K to 3070 K, and from virtually 0.0 Pa to 2.1×10^{7} Pa.

A general flow solution scheme is provided to calculate inter-volume fluid flows. A one-dimensional transient momentum equation is used to calculate the flow of continuous components (atmosphere, pool). The flows of dispersed components (droplets, bubbles) are calculated using the drift flux model. Additional models include critical flow, valves, pumps/compressors and turbines.

Heat conduction is calculated by the 1-D and 2-D Solid Heat Conductor Packages, using a general transient heat conduction equation, with specific models to calculate extended surfaces: fins and spines.

The heat transfer at the boundaries of the Solid Heat Conductors is obtained from the Heat and Mass Transfer Package, which provides models for natural and forced convection,

condensation with and without non-condensable gases, nucleate boiling, critical heat flux, transition boiling, Leidenfrost transition, film boiling, heat transfer in two-phase flow, as well as non-equilibrium boiling and condensation ("flashing" and "fogging").

The heat and mass transfer models include correlations valid for wall-fluid, pool-atmosphere, atmosphere-droplets, and pool-bubbles interfaces. Models for the bubble collapse as well as the heat and mass transfer to bubbles in swarms are included.

A detailed thermal radiation model is provided, including grey enclosure models, with and without participating gas. The gas radiation model is based on the Hottel gas approach.

The point reactor kinetics model is available, with reactivity feedback from control rods, fuel temperature, moderator temperature and void fraction, as well as changes in isotope concentrations. The Isotope Transformation model is available as a part of the Reactor Kinetics Package. It allows computing core composition changes (due to fuel burnup, production of poisons, such as Xe-135, fuel reload, etc.), and their effect on reactivity as well as decay heat production.

The Radioactive Particle Transport Package deals with release of fission products, aerosol transport, deposition, and resuspension. Radioactive chains of fission products are tracked. The models for the transport and deposition of aerosols include Brownian diffusion, thermophoresis, and gravitational settling. For turbulent flow conditions, turbulent deposition models for the diffusional deposition, turbulent eddy impaction, and inertia impaction regime are included. Moreover, gravitational, Brownian, and turbulent coagulation are modeled. Two state-of-the-art dynamic resuspension models are available. Alternatively, resuspension can be modeled using a parametric model with user-defined coefficients directly obtained from resuspension experiments.

The following aerosol models are available in the SPECTRA code:

- Gravitational settling (gravitational settling velocity with Cunningham slip correction factor)
- Thermophoresis
- Brownian diffusion
- Turbulent deposition (inertial impaction, diffusion impaction, diffusional deposition)
- Inertial impaction (pipe bends, impaction on a cylinder in cross-flow)
- Resuspension (Rock'n Roll and Vainsthein resuspension models)
- Coagulation (agglomeration) of aerosol particles (Brownian, gravitational and turbulent) and coagulation of deposited particles (size of the agglomerated particles proportional to the thickness of the deposited layer)
- Inter-volume aerosol transport (slip flow with gravitational settling velocity superimposed on vertical component of the main flow velocity).

The following fission product models are included in the SPECTRA code:

- FP release models (CORSOR, CORSOR-M, user-defined functions)

- Condensation of FP vapors
- Sorption of FP on surfaces
- Sorption of FP vapors on aerosol particles

The SPECTRA code also has a hydrogen burn model for slow deflagrations, fast turbulent deflagrations and detonations. Moreover an oxidation model is available that contains models for zircaloy and steel oxidation by steam and oxygen, carbon oxidation by oxygen, as well as a general oxidation equation with user-defined coefficients. Via this equation any oxidation reaction may be modeled. Multiple reactions (for example simultaneous oxidation of zircaloy by steam and oxygen) are possible.

On top of the models mentioned above, general-purpose utilities, called tabular and control functions, are available. With these functions the user can define certain quantities in the physics packages. They can be applied for example:

- to provide boundary conditions to the analyzed problem,
- to model control systems of a reactor,
- to model safety system activations, etc.

The Numerical Solver Package is responsible for solving all packages simultaneously, using a stable implicit solution scheme. Control functions are included in the implicit solution, which allows solving stiff differential equations.

The solution scheme allows performing calculations without making practically any mass or energy error. The SPECTRA program performs a global mass and energy check at the end of each time step. In absence of the thermal radiation model, the mass and energy errors are caused only by round-off errors of double precision arithmetics, which give relative errors of order of 10^{-15}. If the thermal radiation model is active, then the energy error is governed by the accuracy with which view factors are entered (error of at most 10^{-8} is required by the input checking subroutines).

3.4 Development of NGNP Analytical Model

In this section the SPECTRA model of the primary helium circuit of NGNP (reactor unit, circulator, IHX and connecting piping) will be described. The integral nodalization of the primary helium circuit is presented in Figure 3-4. Details of the Reactor Unit System nodalization are shown in Figure 3-5 . The following sections give brief descriptions of the SPECTRA modeling of the main components of the primary helium system and the calculated steady state conditions during normal operation. More details of the SPECTRA model for NGNP are included in [3-1].

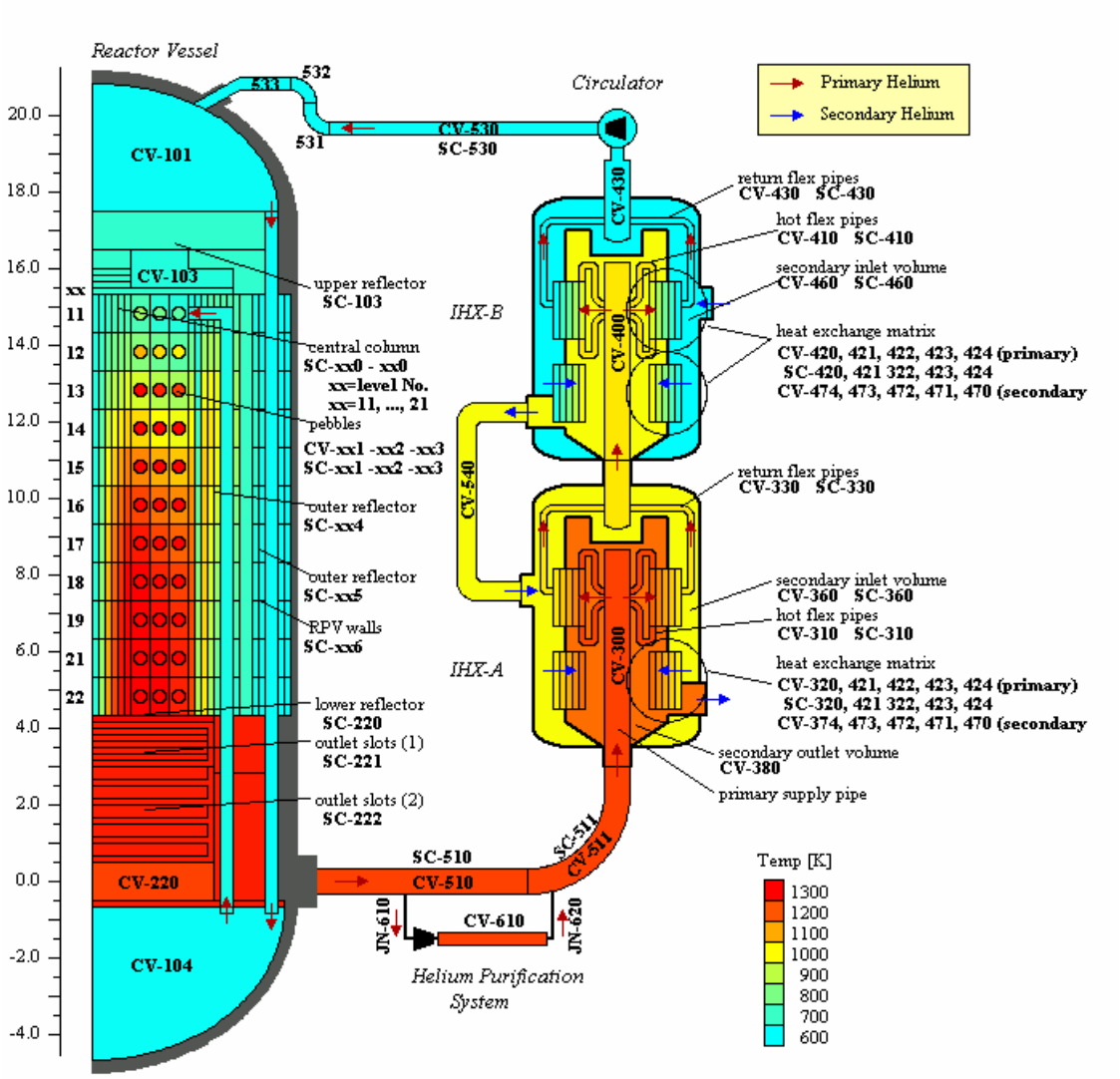

Figure 3-4 Nodalization of the Primary Heat Transport System Model

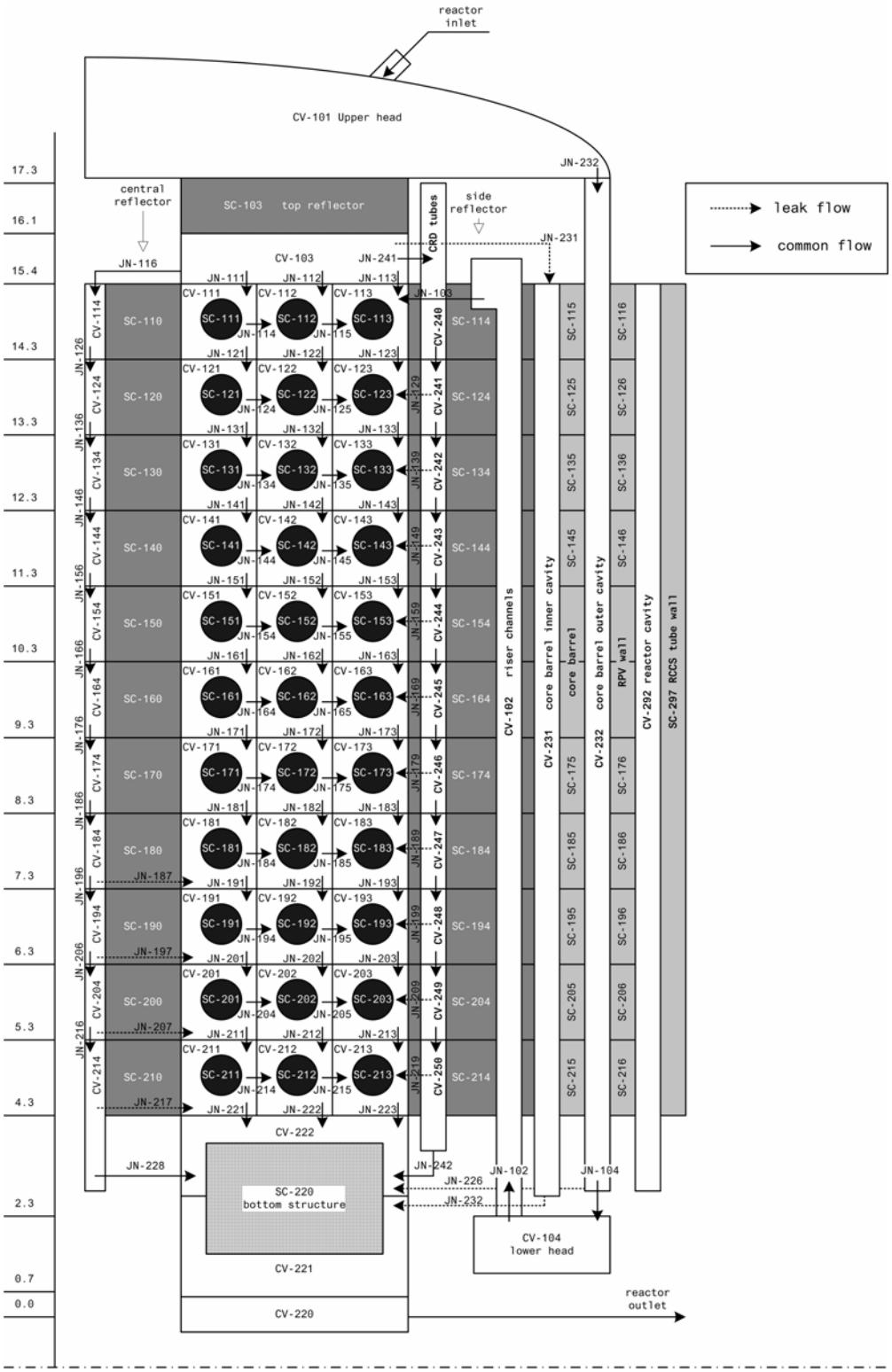

Figure 3-5 Nodalization of the Reactor Unit System Model

3.4.1 Reactor Unit System

The nodalization of the SPECTRA model of the Reactor Unit System (RUS) is shown in Figure 3-5. Different aspects of the RUS model are explained in more detail in the following paragraphs.

Nodalization

The pebble bed is modeled using 33 Control Volumes (CV), divided into 11 axial levels, and 3 radial rings. Each axial increment is 1.0 m high. The radial increments are chosen in such a way that each CV has approximately the same volume.

Pressure Drop

The flow resistance in the pebble bed is calculated from the pebble bed correlation: $K = k\lambda L\varepsilon^2/d$, where d is the pebble diameter, and L is the length. For a porosity of $\varepsilon = 0.39$, $k \approx 70.0$. For large Reynolds numbers λ is about 0.3. The length is equal to the height of a Control Volume, L = 1.0 m.

Pebble Bed

The fuel spheres are represented by 1-D Solid Conductors (SC). The pebbles are distributed equally through the core volumes. Each conductor is divided into 6 nodes of 0.005 m, for a total radius of 0.03 m. The material for the inner 5 nodes is fuel material; the outermost node consists of graphite coating. The same material properties are used for the fuel and the coating, except that no power is generated in the coating. The physical properties of the pebble material are based on the DPP.

Reactor Power

The power distribution in the reactor core is based on the DPP adjusted for the NGNP operating parameters. The coefficients in this table are used to calculate the power densities in different parts of the reactor (see [3-1]).

The power distribution shows that about 95% of the total power is generated in the pebble bed, about 1% is generated in the central reflector and about 4% in the side reflector. For simplicity's sake, the power from the central reflector is added to the pebble bed. The power that is generated in the side reflector is important, because it affects the inlet temperature of the pebble bed: the riser channels are located inside the side reflector and the helium flowing through them receives heat from the structure. The cooling flow for the control rod channels, which are also located inside the side reflector, is also receiving heat from the structure.

Reactor Kinetics

A point kinetics model has been implemented that takes into account reactivity feedback from fuel and moderator temperature. Reactivity feedback from composition changes (fuel reloading, xenon poisoning) can also be calculated. However since the NGNP calculations are done under steady state conditions with fixed power the kinetics model is not activated.

Heat Transfer in the Pebble Bed

The outer surface of each SC (representing a certain number of fuel pebbles) is thermally linked to a Control Volume (representing a part of the gas space in the pebble bed). This allows convective heat transfer between pebbles and helium. Heat transfer from one pebble to another, as well as between pebbles and other structures in the core (e.g., side reflector), is included by activating the SPECTRA thermal radiation model. It is assumed that helium acts as a non-absorbing/non-emitting gas. The following radiation paths have been modeled:

- central reflector ↔ pebbles
- pebbles ↔ pebbles
- pebbles ↔ side reflector
- side reflector ↔ core barrel
- core barrel ↔ RPV

Cooling and Leak Flows

Apart from the main flow path through the pebble bed, the following flow paths have been included in the model:

- direct bypass from core barrel outer cavity to RV outlet plenum (~6.2 kg/s)
- core bypass via the core barrel inner cavity (~4.4 kg/s)
- central reflector cooling flow (~6.2 kg/s)
- control rod channels cooling flow (~5.3 kg/s)

The numbers are based on flow data based on the DPP adjusted for the NGNP operating parameters.

Material Properties

Material properties for the fuel pebbles, central reflector graphite, side reflector graphite, SA 240 steel of the core barrel, and SA 508 steel of the reactor pressure vessel are included in the model, based on the DPP data.

3.4.2 Intermediate Heat Exchangers

The nodalization of the SPECTRA model of the intermediate heat exchanger is shown in Figure 3-4. The model is based on performance maps for the PBMR NGNP IHXs. The model consists of two heat exchangers, IHX-A and IHX-B. The basic design of IHX-B is identical to that of IHX-A, only the number of heat exchange cores (170 instead of 138) and their size is different. The text below describes the SPECTRA model of IHX-A. The numerical values in the IHX-B model that are different from IHX-A are included in Table 3-1.

Nodalization

The matrix volume is modeled using five nodes. The total volume of fluid in the matrix is V = 0.30 m^3 and V = 0.40 m^3 for the primary and secondary side respectively. Single Control Volumes are used to model the primary supply pipe, the hot flex pipes, the return flex pipes, the secondary inlet volume and the secondary outlet volume. Heat transfer through the walls of the flex pipes, as well as through the inner vessel that separates the secondary inlet and outlet

volumes, is included. However these heat losses are insignificant compared to the heat exchange that takes place in the heat exchange matrix.

Pressure Drop

The flow resistance within the matrix is determined by the friction factor. The friction factor in the heat-exchange matrix is given by the performance map provided by PBMR. The performance map defines the friction as a function of the Reynolds number. In SPECTRA it is not possible to change the default model for pressure loss due to friction. One can, however, set the *K*-factor to any desired value using control functions. This procedure, described below, is applied in the IHX models.

The friction pressure drop for flow inside the matrix is equal to:

$$\Delta P = f \frac{L}{D_h} \frac{\rho v^2}{2}$$

with f friction factor, [-], equal to: $f = 1.2039 \times \mathrm{Re}^{-0.391}$
ΔP pressure drop, [Pa]
ρ fluid density, [kg/m^3]
L friction length, [m]
D_h hydraulic diameter, [m]
v velocity, [m/s]

The singular pressure drop is equal to:

$$\Delta P = K \frac{\rho v^2}{2}$$

with K form loss coefficient, [-]

In the model the form loss coefficient is used to model the friction pressure loss, so K has to be equal to $K = fL/D_h$. For each of the junctions in the matrix a control function is defined that calculates K based on the Reynolds number for that junction. In addition, the wall roughness and friction length are set to a very small value to avoid calculating the friction pressure drop twice.

Heat Transfer Matrix

The heat exchange matrix of IHX-A is modeled as a flat plate, with a total area equal to 391 m^2 and a thickness of 3.81×10^{-4} m (which corresponds to the area and the thickness of the parting sheets). Fins are applied on both sides of the plate in order to get the correct heat exchange areas: A_{prim} = 1679 m^2, A_{sec} = 2492 m^2. The structure is modeled using 5 solid conductors (SC), or "nodes". Each node consists of two cells of 1.2×10^{-4} m and one cell of 1.41×10^{-4} m, for a total thickness of 3.81×10^{-4} m.

The primary and secondary flows are in counter-current mode. Temperature Averaging has been activated for both sides of the heat exchange matrix. Temperature Averaging is a concept in SPECTRA that allows modeling heat exchangers with relatively few nodes.

Heat Transfer Coefficient

The heat transfer coefficient (HTC) on both sides of the Solid Conductors is defined by Control Functions. These Control Functions calculate the HTC based on the fluid properties of the related Control Volume and the performance map. Below an example is given of how the HTC is calculated. This procedure is followed for all nodes, both on the primary and on the secondary side.

The performance map defines $StPr^{2/3}$ as a function of Re. Therefore:

$$HTC = Nu\frac{k}{D} = St\ Re\ Pr\frac{k}{D} = (St\ Pr^{2/3})Pr^{1/3}\frac{k}{D} = f(Re)\left(\frac{c_p\mu}{\rho k}\right)^{1/3}\frac{k}{D}$$

with

	Nu	Nusselt number, [-]
	St	Stanton number, [-]
	Re	Reynolds number, [-]
	k	thermal conductivity, [W/m^2/K]
	D	characteristic length (i.e.: hydraulic diameter), [m]
	c_p	specific heat capacity, [J/kg/K]
	μ	dynamic viscosity, [kg/m/s]
	ρ	density, [kg/m^3]

The term *f(Re)* in this equation is the performance map, defined as: $f(Re) = 0.16353\times Re^{-0.34651}$. All other terms in the equation are fluid properties that can be read from the respective Control Volume (except for *D*, which is a constant). At the end of the procedure, the calculated HTC is multiplied with the overall surface efficiency to give the effective HTC. Normally one would multiply the total heat exchange area with the efficiency, but that does not work here because the heat exchange areas in the model have to be the actual areas for the deposition calculations. A summary of the model data is given in Table 3-1.

Table 3-1 Model Data for the Primary and Secondary Side of IHX-A and IHX-B

	IHX-A		**IHX-B**	
	Primary	**Secondary**	**Primary**	**Secondary**
Total Volume [m^3]	0.30	0.40	0.82	0.78
Flow area [m^2]	1.94	2.49	2.74	2.52
Heat exchange area [m^2]	1679.12	2491.87	4575.54	5543.63
Plate length [m]	0.155		0.300	
Number of cores	138		170	
Number of plates	50540		70460	
Hydraulic diameter [m]	0.791×10^{-3}	0.676×10^{-3}	0.794×10^{-3}	0.604×10^{-3}
Overall surface efficiency	0.537	0.442	0.548	0.527

Material Properties

The high temperature heat exchanger IHX-A is made from a stainless steel type called Inconel 617. IHX-B, which operates at moderate temperatures, is made from Inconel 800H. The reactor inlet and outlet pipes, as well as the pipe that connects IHX-A to IHX-B, all consist of Inconel 800H. The properties for these materials are included in the model.

3.4.3 Circulator

The circulator in the primary loop transports the helium from IHX-B to the inlet of the reactor vessel. The circulator is modeled using the SPECTRA compressor model with the following nominal values:

- pressure ratio : 1.0434
- nominal flow : 159.6 kg/s
- nominal temperature : 337 ºC
- nominal pressure : 8626 kPa

3.4.4 Coolant Piping

The core outlet pipe is an annular pipe consisting of an inner volume for the main helium flow surrounded by an annulus through which cooling helium flows. The inner pipe is separated from the annulus by a thin metal liner, an insulation layer and a pressure pipe. Only the inner main flow of helium and the liner are modeled in SPECTRA (heat loss through the insulation is neglected). The inner pipe has a diameter of 1.034 m and a length of 11.5 m. The bend which connects the first part of the pipe to IHX-A consists of a 3.0 m long pipe with the same diameter and a loss factor of K = 0.2 for a 90˚ bend.

The pipe between the high temperature and low temperature heat exchanger has the same construction as the core outlet pipe. Again, only the inner pipe is modeled. The pipe has a length of 2.0 m. The pipe connecting the outlet of IHX-B to the inlet of the reactor vessel is a regular pipe without insulation. The inner diameter is equal to 0.710 m. The total length of the pipe is equal to 16.0 m. Two 90º bends are included, with loss factor K = 0.2. The structures representing the pipe walls are all made from Inconel 800H. The properties of this alloy are based on the DPP design.

For the secondary loop only the pipe connecting the two intermediate heat exchangers is of interest. The pipe has an inner diameter of 0.8 m and length of 10.0 m. Two 90º bends are included, with loss factor $K = 0.2$. No heat structures are modeled for this pipe, because for the purpose of the current analysis the secondary helium is assumed to be free of fission products and dust particles. Heat loss from the pipe is neglected.

3.4.5 Dust Modeling

The graphite dust is modeled using the aerosol models available in SPECTRA. The aerosol model data required to perform calculations include the aerosol particle density, size distribution, external sources, selection of suitable deposition, coagulation, and resuspension models, as well as any additional model data (filters, etc.). The following values were used for the NGNP analysis.

- Density of aerosol particles: ρ_p = 1750 kg/m^3, the value used in PBMR analyses.
- Aerosol size distribution, as specified in Section 2. Three large size sections have been added (10, 20, and 50 μm) to allow coagulation of the deposited aerosols. By default the coagulation proceeds depending on the deposited layer thickness - smaller particles are assumed to coagulate into a large particle when the layer thickness exceeds that of the larger particle. The size sections are given in Table 3-2.

Table 3-2 Aerosol Size Sections

Size section No.	D_p, [μm]
1	0.202
2	0.353
3	0.493
4	0.632
5	0.873
6	1.218
7	1.598
8	1.953
9	2.322
10	2.718
11	3.078
12	3.458
13	10.00
14	20.00
15	50.00

- All deposition models are active on all surfaces. The inertial impaction models are activated on the bends (SC-511, SC-531, and SC-532 - Figure 3-4).
- Porosity of the deposited dust is assumed to be equal to 0.5.
- All coagulation models are active for all Control Volumes. A model for coagulation of deposited particles is activated on all surfaces. This model assumes that the deposited aerosols form agglomerates of the size of the deposited layer thickness.

- The resuspension model of Vainshtein et al is active on all surfaces. This model was selected as it gave good results for the Storm experiment as well as the Reeks and Hall experiments. The alternative model (Rock'n Roll) gives higher resuspension than measured.
- The graphite dust is generated in the nuclear core and in the fuel handling system. The dust source term is given in Section 2.4 of this document. The aerosol sources ware specified using the data from Section 2. Two sources are present: core (pebble bed, side reflectors and bottom reflector) and FHSS (Fuel Handling System).

    - The total source from the core is 28 kg/fpy = 28/(365×24×3600) = 8.88×10^{-7} kg/s. The mass sources for each size section were defined by multiplying this number by the normalized volume fractions, given in Table 3-3 (in the column "Upstream the filter"). These sources were placed in CV-220 (Control Volume just below the core).

    - The total source from FHSS is 20 kg/fpy. An aerosol filter is present. The efficiency of the filter is assumed to be: 99.99% for particles larger than 0.5 μm and 0.0 for particles smaller than 0.5 μm. In the SPECTRA model, the FHSS is not modeled. The dust source from the FHSS is specified using the values downstream of the FHSS filter, calculated based on the original distribution and filter efficiencies. The values are shown in Table 3-3. The dust mass source behind the FHSS filter is 0.516 kg/fpy = 28/(365×24×3600) = 1.64×10^{-8} kg/s. The mass sources for each size section were defined by multiplying this number by the distribution fractions downstream of the filter, given in Table 3-3. These sources were placed in CV-510 (Core Outlet Pipe).

- Helium Purification System is modeled as shown in Figure 3-4. The filter efficiencies are the same as in case of the FHSS filter, 99.99% for particles larger than 0.5 μm and 0.0 for particles smaller than 0.5 μm. The flow through the HPS is forced by a fan. Typical fan characteristic maps have been used with the nominal parameters selected in such a way as to provide the desired mass flow (80 kg/hr = 0.022 kg/s) during the normal (full power) operation.

Table 3-3 Aerosol Size Distribution - FHSS Filter

Size section No.	D_p, [μm]	Filter efficiency [%]	Size distribution upstream filter [-]	Size distribution downstream filter [-]
1	0.202	0.0	3.00E-04	1.16E-02
2	0.353	0.0	4.20E-03	1.63E-01
3	0.493	0.0	2.12E-02	8.22E-01
4	0.632	99.99	4.09E-02	1.59E-04
5	0.873	99.99	4.27E-02	1.66E-04
6	1.218	99.99	9.34E-02	3.62E-04

Size section No.	D_p, [µm]	Filter efficiency [%]	Size distribution upstream filter [-]	Size distribution downstream filter [-]
7	1.598	99.99	9.99E-02	3.87E-04
8	1.953	99.99	1.16E-01	4.48E-04
9	2.322	99.99	1.28E-01	4.97E-04
10	2.718	99.99	1.37E-01	5.31E-04
11	3.078	99.99	8.51E-02	3.30E-04
12	3.458	99.99	2.32E-01	8.97E-04
13	10.00	99.99	0.00E+00	0.00E+00
14	20.00	99.99	0.00E+00	0.00E+00
15	50.00	99.99	0.00E+00	0.00E+00
Total mass source [kg/fpy]			20.0	0.516

3.4.6 Fission Product Modeling

The fission product model data required to perform calculations include the definition of the fission product decay chains, external sources, selection of suitable sorption models, as well as any additional model data (filters, etc.). The following values were used for the NGNP analysis.

- All SPECTRA built-in decay chains (10) were activated. An example of the built in chain is shown in Figure 3-6.

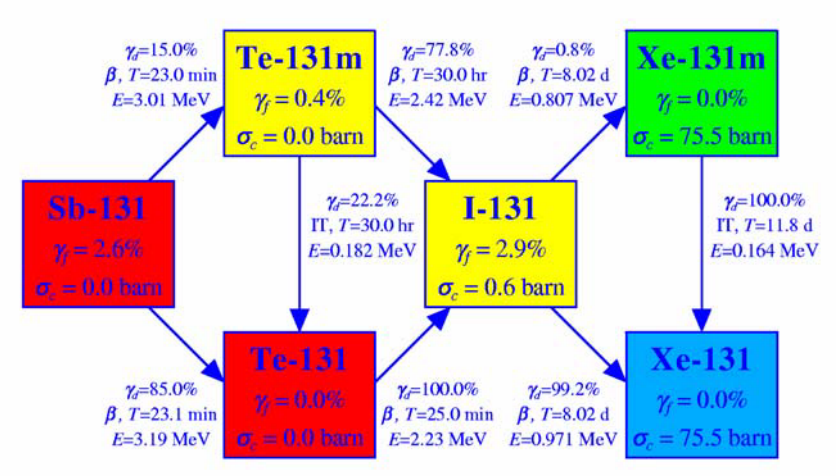

Figure 3-6 Built-in Radionuclide Chain Number 1

- Twelve additional chains were defined. The data for these chains were taken from the Table of Isotopes. The data includes decay constant, λ, energy per decay, E, and energy split between the β and the γ-radiation.

  - **User-defined Chain 11**:

    Br-83 (111)
    $\lambda = 8.056\times10^{-5}$ [1/s]
    E = 1.538×10^{-13} [J]
    β = 0.977, γ = 0.023

    Kr-83m (112)
    $\lambda = 1.052\times10^{-4}$ [1/s]
    E = 6.648×10^{-15} [J]
    β = 0.00, γ = 1.00

    Kr-83 (113)

  - **User-defined Chain 12**:

    Br-84 (121)
    $\lambda = 3.630\times10^{-4}$ [1/s]
    E = 7.449×10^{-13} [J]
    β = 0.407, γ = 0.592

    Kr-84 (122)

  - **User-defined Chain 13**:

    Ag-110m (131)
    $\lambda = 3.210\times10^{-8}$ [1/s]
    E = 4.518×10^{-13} [J]
    β = 0.0256, γ = 0.9744

    Cd-110 (132)

  - **User-defined Chain 14**:

    Kr-81 (141)
    $\lambda = 1.52\times10^{-4}$ [1/s]
    E = 6.23×10^{-13} [J]
    β = 0.90, γ = 0.10

    Rb-87 (142)

  - **User-defined Chain 15**:

    Kr-88 (151)
    $\lambda = 6.78\times10^{-5}$ [1/s]
    E = 4.66×10^{-13} [J]
    β = 0.18, γ = 0.82

    Rb-88 (152)
    $\lambda = 6.53\times10^{-4}$ [1/s]
    E = 8.51×10^{-13} [J]
    β = 1.00, γ = 0.00

    Sr-88 (153)

  - **User-defined Chain 16**:

    Kr-89 (161)
    $\lambda = 3.67\times10^{-3}$ [1/s]
    E = 7.85×10^{-13} [J]
    β = 0.71, γ = 0.29

    Rb-89 (162)
    $\lambda = 7.50\times10^{-4}$ [1/s]
    E = 7.19×10^{-13} [J]
    β = 0.28, γ = 0.72

    Sr-89 (163)
    $\lambda = 1.59\times10^{-7}$ [1/s]
    E = 2.39×10^{-13} [J]
    β = 1.00, γ = 0.00

    Y-89 (164)

  - **User-defined Chain 17**:

    Kr-91 (171)
    $\lambda = 7.88\times10^{-2}$ [1/s]
    E = 9.93×10^{-13} [J]
    β = 0.74, γ = 0.26

    Rb-91 (172)

  - **User-defined Chain 18**:

Xe-138 (181) **Cs-138** (182) **Be-138** (183)
$\lambda = 8.14\times10^{-4}$ [1/s] $\lambda = 3.59\times10^{-4}$ [1/s]
$E = 4.39\times10^{-13}$ [J] $E = 8.81\times10^{-13}$ [J]
$\beta = 0.30$, $\gamma = 0.70$ $\beta = 0.45$, $\gamma = 0.55$

- **User-defined Chain 19**:

Xe-139 (191) **Cs-139** (192) **Be-139** (193) **Le-139** (194)
$\lambda = 1.73\times10^{-2}$ [1/s] $\lambda = 1.23\times10^{-3}$ [1/s] $\lambda = 1.39\times10^{-4}$ [1/s]
$E = 7.85\times10^{-13}$ [J] $E = 6.89\times10^{-13}$ [J] $E = 3.70\times10^{-13}$ [J]
$\beta = 0.98$, $\gamma = 0.02$ $\beta = 0.95$, $\gamma = 0.05$ $\beta = 0.98$, $\gamma = 0.02$

- **User-defined Chain 20**:

Xe-140 (201) **Cs-140** (202) **Be-140** (203) **Le-140**(204) **Ce-140** (205)

$\lambda = 5.06\times10^{-2}$ [1/s] $\lambda = 1.07\times10^{-2}$ [1/s] $\lambda = 6.27\times10^{-7}$ [1/s] $\lambda = 4.79\times10^{-6}$ [1/s]
$E = 6.57\times10^{-13}$ [J] $E = 9.77\times10^{-13}$ [J] $E = 1.67\times10^{-13}$ [J] $E = 6.03\times10^{-13}$ [J]
$\beta = 0.80$, $\gamma = 0.20$ $\beta = 1.00$, $\gamma = 0.00$ $\beta = 0.99$, $\gamma = 0.01$ $\beta = 0.36$, $\gamma = 0.64$

- **User-defined Chain 21**:

Cs-134 (211) **Be-134** (212)
$\lambda = 7.88\times10^{-8}$ [1/s]
$E = 1.95\times10^{-13}$ [J]
$\beta = 0.54$, $\gamma = 0.46$

- **User-defined Chain 22**:

Ag-111 (221) **Cd-111** (222)
$\lambda = 1.07\times10^{-6}$ [1/s]
$E = 1.65\times10^{-13}$ [J]
$\beta = 1.00$, $\gamma = 0.00$

- Fission product sorption models were activated on all metallic surfaces (not on the graphite surfaces such as pebbles reflectors, etc.). The sorption model in SPECTRA is schematically illustrated in Figure 3-7. The sorption model parameters are based on [3-3].

  - Vapor class: Cs: $(1-\beta)=10^{-5}$, $\upsilon=10^{11}\exp(-28150/T)$, $\eta=0.0$
  - Vapor class: I: $(1-\beta)=0.0$, $\upsilon=10^{11}\exp(-21666/T)$, $\eta=0.0$
  - Vapor class: Ag: $(1-\beta)=10^{-5}$, $\upsilon=10^{11}\exp(-30670/T)$, $\eta=0.0$

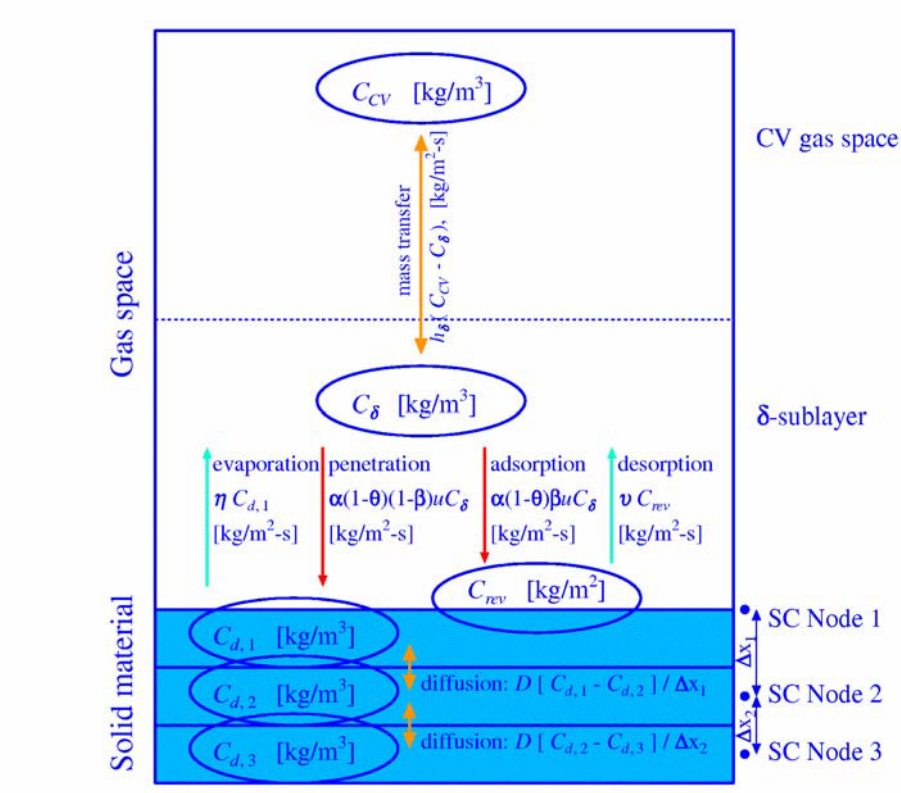

Figure 3-7 Sorption Model in SPECTRA

- The fission product sources were obtained from Section 2.3. The values are shown in Table 3-4. The original values in [atoms/s] were converted to SPECTRA input [kg/s], using the molar weights, M_W, and the Avogadro number, N_A = 6.022×10^{26} kg/kmol, as follows:

m [kg/s] = N [atoms/s] × M_W / N_A

Table 3-4 Fission Product Sources

Isotope	Molar weight	Source, [atoms/s]	Source, [kg/s]
Kr-83m	83	1.23E+10	1.70E-15
Kr-85m	85	3.92E+10	5.53E-15
Kr-85	85	4.36E+10	6.15E-15
Kr-87	87	4.85E+10	7.01E-15
Kr-88	88	8.97E+10	1.31E-14
Kr-89	89	2.23E+10	3.30E-15
Kr-90	90	1.07E+10	1.60E-15
Kr-91	91	5.34E+09	8.07E-16
Xe-131m	131	2.32E+09	5.05E-16
Xe-133m	133	6.05E+09	1.34E-15
Xe-133	133	2.75E+11	6.07E-14

Isotope	Molar weight	Source, [atoms/s]	Source, [kg/s]
Xe-135m	135	8.58E+09	1.92E-15
Xe-135	135	7.87E+10	1.76E-14
Xe-137	137	2.33E+10	5.30E-15
Xe-138	138	4.16E+10	9.53E-15
Xe-139	139	6.73E+09	1.55E-15
Xe-140	140	2.88E+09	6.70E-16
Br-83	83	1.35E+10	1.86E-15
Br-84	84	1.38E+10	1.92E-15
Br-85	85	6.14E+09	8.67E-16
I-131	131	1.44E+11	3.13E-14
I-132	132	5.97E+10	1.31E-14
I-133	133	1.54E+11	3.40E-14
I-134	134	8.04E+10	1.79E-14
I-135	135	1.08E+11	2.42E-14
I-136	136	6.29E+09	1.42E-15
Cs-137	137	1.28E+13	2.91E-12
Cs-134	134	5.71E+11	1.27E-13
Ag-110m	110	1.90E+13	3.47E-12
Ag-111	111	1.91E+11	3.52E-14
Sr-90	90	6.33E+09	9.46E-16

- The HPS filter efficiencies were estimated based on the data from Fort St. Vrain HPS [3-4]. The removal factor is defined as the fraction of the inventory of a radionuclide that is held in the delay beds of the HPS. The removal factors for the radionuclides are shown in Table 3-5.

Table 3-5 Helium Purification System Removal Factors

Isotope	Removal Factor (*RF*)
Kr-85m	0.49
Kr-85	0.999
Kr-87	0.218
Kr-88	0.314
Rb-88	0.355
Xe-131m	0.984
Xe-133m	0.92
Xe-133	0.96
Xe-135m	0.05
Xe-135	0.666

3.4.7 Boundary Conditions at Steady State

The normal operation conditions for the PHTS of the PBMR NGNP as discussed in Section 1 are:

- System pressure at the outlet of the circulator : 9 MPa
- Core inlet temperature : 350ºC
- Core outlet temperature 950ºC
- Reactor power : 500MWt
- Circulating helium mass flow : 160 kg/s
- HPS mass flow : 0.022 kg/s (80 kg/hr)

3.5 NGNP Transport Results

3.5.1 Thermal-Hydraulic Calculations

As a first step a short simulation of the SPECTRA model start-up was performed. This run does not aim at a simulation of any realistic plant transient; it is simply a step to obtain stationary conditions (temperature and pressure distributions, etc.) to be used in a long (plant lifetime) analysis of dust and fission product behavior. The start-up simulation scenario file consisted of:

- Reactor start-up. Linear power increase from zero to full power in 10 seconds.
- Circulator start-up. Linear increase of the circulator speed from zero to nominal in 3 seconds.
- The volumetric heat capacities of all materials were reduced by the factor 10,000 in order to avoid long calculation times. With the applied heat capacity stationary conditions were reached very fast. The simulation was performed for 100 s. All parameters were stable by then.

Results of the model start-up simulation are shown in Table 3-6. The main calculated operating parameters are given in Table 3-6. During the start-up calculation the time step was governed by the Courant limit and was of order of $\Delta t = 10^{-3}$ s. Since one could not perform a calculation of stationary operation of a plant-life using this short time step, the calculations described in the following sections were performed by deactivating the thermal-hydraulic solution. The thermal-hydraulic conditions calculated in this run were "frozen" and used in the subsequent long term analysis of the dust and fission products. This allows elimination of the hydraulic Courant limit and run with a large time step ($\Delta t = 10^5$ s).

Table 3-6 Numerical Model Steady State Results

Parameter	Value
Reactor power [MWt]	500
Reactor inlet pressure [kPa]	8985
Reactor outlet pressure [kPa]	8741
Primary mass flow [kg/s]	160
Secondary mass flow [kg/s]	160
Heat transfer IHX-A [MWt]	156.9
Heat transfer IHX-B [MWt]	351.6
Primary inlet temperature, IHX-A [ºC]	949
Primary outlet temperature, IHX-B [ºC]	336
Secondary inlet temperature, IHX-B [ºC]	287
Secondary outlet temperature, IHX-A [ºC]	899
Circulator pressure head [kPa]	369

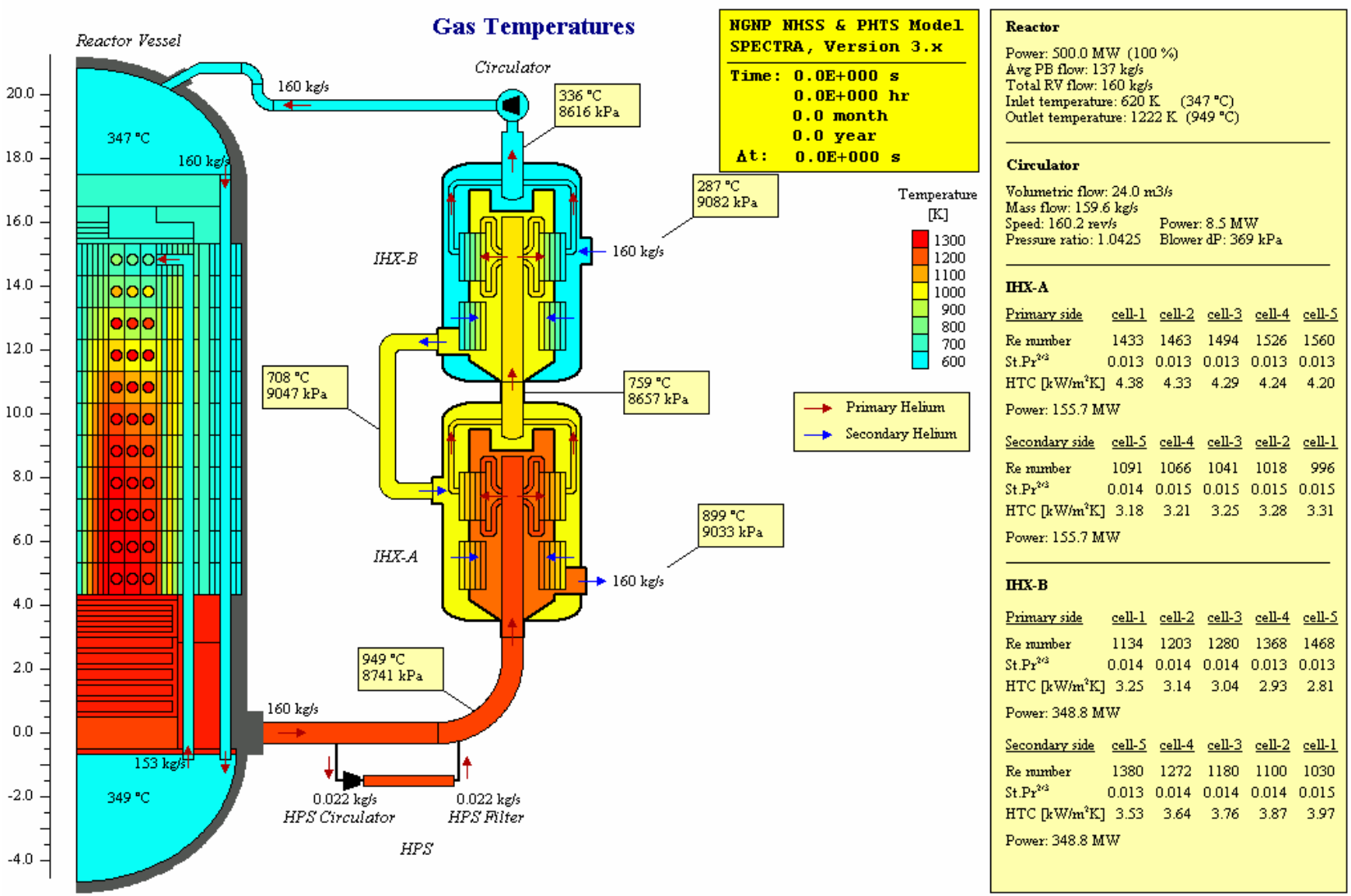

Reactor

Power: 500.0 MW (100 %)
Avg PB flow: 137 kg/s
Total RV flow: 160 kg/s
Inlet temperature: 620 K (347 °C)
Outlet temperature: 1222 K (949 °C)

Circulator

Volumetric flow: 24.0 m3/s
Mass flow: 159.6 kg/s
Speed: 160.2 rev/s Power: 8.5 MW
Pressure ratio: 1.0425 Blower dP: 369 kPa

IHX-A

Primary side	cell-1	cell-2	cell-3	cell-4	cell-5
Re number	1433	1463	1494	1526	1560
St.Pr$^{2/3}$	0.013	0.013	0.013	0.013	0.013
HTC [kW/m^{2}K]	4.38	4.33	4.29	4.24	4.20

Power: 155.7 MW

Secondary side	cell-5	cell-4	cell-3	cell-2	cell-1
Re number	1091	1066	1041	1018	996
St.Pr$^{2/3}$	0.014	0.015	0.015	0.015	0.015
HTC [kW/m^{2}K]	3.18	3.21	3.25	3.28	3.31

Power: 155.7 MW

IHX-B

Primary side	cell-1	cell-2	cell-3	cell-4	cell-5
Re number	1134	1203	1280	1368	1468
St.Pr$^{2/3}$	0.014	0.014	0.014	0.013	0.013
HTC [kW/m^{2}K]	3.25	3.14	3.04	2.93	2.81

Power: 348.8 MW

Secondary side	cell-5	cell-4	cell-3	cell-2	cell-1
Re number	1380	1272	1180	1100	1030
St.Pr$^{2/3}$	0.013	0.014	0.014	0.014	0.015
HTC [kW/m^{2}K]	3.53	3.64	3.76	3.87	3.97

Power: 348.8 MW

Figure 3-8 Thermal-Hydraulic Steady State Results

3.5.2 Dust Transport and Deposition Analysis

Calculation was performed for the expected plant life-time of 60 years with an average availability of 95%. The total run time is therefore 57 years. Continuous operation at full power during its lifetime is assumed. The time-step of $\Delta t = 10^5$ s was applied. No credit is taken for some maintenance activities that could significantly reduce the dust in the PHTS (e.g., periodic replacement of IHX-A, blow down of the IHX plates, core structure inner reflector replacement, etc.). The dust transport and deposition analysis results are shown in Table 3-7, Table 3-8, and Figure 3-9 through Figure 3-18.

Overall Deposition of Dust

Table 3-8 gives an integral overview of the transport and deposition of dust in the PHTS. The right column gives the quantities of dust deposited after 57 years of operation in different parts of the PHTS and the reactor vessel.

Table 3-7 gives a summary of the deposition of dust after 57 years full power operation and Table 3-8 presents the layer thickness of the deposited dust at different locations of the system. The labels for the different locations within the system refer to the nodalization scheme as presented in Figure 3-4. The locations with a relatively large wall thickness are marked in red.

Table 3-7 Summary of Dust Deposition During Normal Operation

Location	Deposited Dust		
	Mass [kg]	Fraction of Total [%]	Fraction within PHTS [%]
Reactor Vessel	1420.	87	
IHX-A	24.6	1.5	12
IHX-B	127.	7.8	61
Core Outlet Pipe	9.1	0.6	4
Core Inlet Pipe	28.8	1.8	14
HPS Filter	17.6	1.1	8

Airborne Dust Densities

The dust transport is also visualized in Figure 3-9, which shows also the density of dust particle density in million of particles per cubic meter (Mp/m^3) in the gas flow. In spite of deposition in IHX-A and IHX-B, the particle density increases behind the heat exchangers (the density of dust particles in the core inlet pipe is higher than in the core outlet pipe). This effect is caused by an increase of the gas density due to decreasing gas temperature.

Table 3-8 Integral Overview of Deposited Layer Thickness

NGNP NHSS & PHTS Model
SPECTRA, Version 3.x

Time: 1.8E+009 s
5.0E+005 hr
694.4 month
57.0 year
Δt: 1.0E+002 s

Deposition layers, [m] PHTS

Core Outlet Pipe		IHX-A Structures		IHX-A Plates		IHX-B Structures		IHX-B Plates		Core Inlet Pipe	
SC-510	3.74E-005	SC-300	2.63E-005	SC-320	1.37E-005	SC-400	3.49E-005	SC-420	1.71E-005	SC-530	5.40E-005
SC-511	8.99E-004	SC-310	2.86E-005	SC-321	1.48E-005	SC-410	3.71E-005	SC-421	2.99E-005	SC-531	5.14E-003
SC-520	2.89E-005	SC-330	8.33E-005	SC-322	1.64E-005	SC-430	5.09E-005	SC-422	3.28E-005	SC-532	4.23E-003
		SC-360	0.00E+000	SC-323	1.74E-005	SC-460	0.00E+000	SC-423	3.64E-005	SC-533	5.40E-005
		SC-380	0.00E+000	SC-324	1.77E-005	SC-480	0.00E+000	SC-424	4.13E-005		

Deposition layers, [m] RPV

Inner Reflector		Ring 1		Ring 2		Ring 3		Outer Reflector 1		Outer Reflector 2		CRD tubes	
SC-110	2.17E-005	SC-111	2.90E-005	SC-112	3.50E-005	SC-113	4.63E-005	SC-114	3.59E-005	SC-115	3.15E-005	SC-118	1.18E-002
SC-120	2.34E-005	SC-121	2.92E-005	SC-122	2.88E-005	SC-123	3.14E-005	SC-124	2.47E-005	SC-125	3.12E-005	SC-128	2.04E-002
SC-130	2.94E-005	SC-131	3.39E-005	SC-132	2.39E-005	SC-133	2.58E-005	SC-134	2.01E-005	SC-135	3.10E-005	SC-138	1.66E-002
SC-140	1.39E-005	SC-141	1.79E-005	SC-142	2.49E-005	SC-143	3.12E-005	SC-144	2.69E-005	SC-145	3.10E-005	SC-148	1.59E-002
SC-150	3.00E-005	SC-151	3.33E-005	SC-152	1.77E-005	SC-153	1.92E-005	SC-154	1.55E-005	SC-155	3.11E-005	SC-158	1.53E-002
SC-160	2.34E-005	SC-161	2.63E-005	SC-162	3.13E-005	SC-163	3.39E-005	SC-164	3.39E-005	SC-165	3.12E-005	SC-168	1.24E-002
SC-170	2.22E-005	SC-171	2.49E-005	SC-172	2.94E-005	SC-173	3.21E-005	SC-174	4.42E-005	SC-175	3.13E-005	SC-178	1.20E-002
SC-180	2.15E-005	SC-181	2.40E-005	SC-182	2.83E-005	SC-183	3.10E-005	SC-184	2.14E-005	SC-185	3.14E-005	SC-188	1.16E-002
SC-190	2.09E-005	SC-191	2.34E-005	SC-192	2.74E-005	SC-193	3.02E-005	SC-194	2.35E-005	SC-195	3.15E-005	SC-198	9.36E-003
SC-200	2.00E-005	SC-201	2.10E-005	SC-202	2.75E-005	SC-203	3.05E-005	SC-204	2.86E-005	SC-205	3.16E-005	SC-208	9.12E-003
SC-210	2.29E-005	SC-211	2.27E-005	SC-212	2.60E-005	SC-213	3.17E-005	SC-214	3.06E-005	SC-215	3.18E-005	SC-218	1.20E-002

Lower Reflector	SC-220	2.71E-005
Outlet slots (1)	SC-221	4.48E-005
Outlet slots (2)	SC-222	3.50E-005

Locations with large deposition: pipe bends, CRD tubes, are marked in red

Dust Deposition within the Heat Exchangers

Dust deposition within the heat exchangers is shown in Figure 3-10 through Figure 3-14. Figure 3-10 gives the total dust deposited on the plates of the heat exchangers IHX-A and IHX-B. Figure 3-11 and Figure 3-12 present the layer thickness of the deposited dust on the plates of IHX-A and IHX-B. The layer thickness of the deposited dust on the structures of the heat exchangers is shown in Figure 3-13 and Figure 3-14.

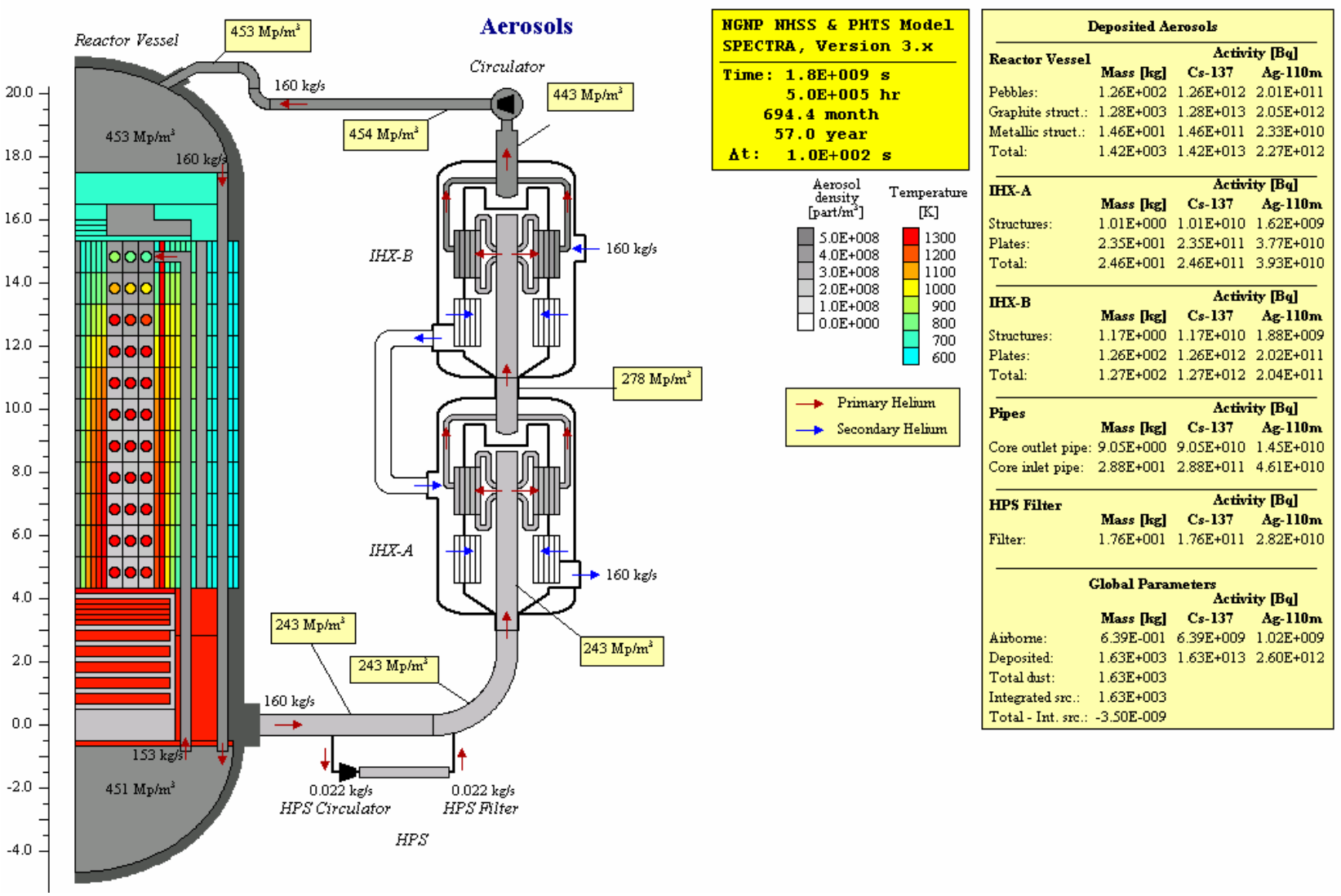

Deposited Aerosols

	Mass [kg]	Activity [Bq] Cs-137	Activity [Bq] Ag-110m
Reactor Vessel			
Pebbles:	1.26E+002	1.26E+012	2.01E+011
Graphite struct.:	1.28E+003	1.28E+013	2.05E+012
Metallic struct.:	1.46E+001	1.46E+011	2.33E+010
Total:	1.42E+003	1.42E+013	2.27E+012
IHX-A			
Structures:	1.01E+000	1.01E+010	1.62E+009
Plates:	2.35E+001	2.35E+011	3.77E+010
Total:	2.46E+001	2.46E+011	3.93E+010
IHX-B			
Structures:	1.17E+000	1.17E+010	1.88E+009
Plates:	1.26E+002	1.26E+012	2.02E+011
Total:	1.27E+002	1.27E+012	2.04E+011
Pipes			
Core outlet pipe:	9.05E+000	9.05E+010	1.45E+010
Core inlet pipe:	2.88E+001	2.88E+011	4.61E+010
HPS Filter			
Filter:	1.76E+001	1.76E+011	2.82E+010
Global Parameters			
Airborne:	6.39E-001	6.39E+009	1.02E+009
Deposited:	1.63E+003	1.63E+013	2.60E+012
Total dust:	1.63E+003		
Integrated src.:	1.63E+003		
Total - Int. src.:	-3.50E-009		

Figure 3-9 Aerosol Transport and Deposition Results for the RUS and PHTS

Because the coagulation model is active on all surfaces, the deposited aerosols are assumed to form agglomerates of the size of the deposited layer thickness. The large agglomerates are easily resuspended. Resuspensions of agglomerated particles are clearly visible on the heat exchanger plates (Figure 3-11 and Figure 3-12).

- For IHX-A these resuspensions occur when particles coagulate into 20 μm particles.
- For IHX-B resuspension occurs when particles coagulate into 50 μm particles. The 20 micron particles are not resuspended in IHX-B because the velocities are lower than in IHX-A (lower temperature, thus higher density).
- Because the deposited layer is <20 μm in IHX-A and <50 μm in IHX-B, the deposited mass is much larger in IHX-B than in IHX-A.
- The results depend strongly on the assumed size sections (20, 50 μm). Therefore it would be better to use more size sections, minimizing the section-to section size difference, for example by using sections 20, 30, 40, and 50 μm.

Deposition layers on the IHX structures are shown in Figure 3-13 and Figure 3-14. The deposition is smaller than 50 μm except for the return flex pipes where the layer of up to 150 μm is observed. The thick layer is caused by relatively small gas velocities in the return flex pipes.

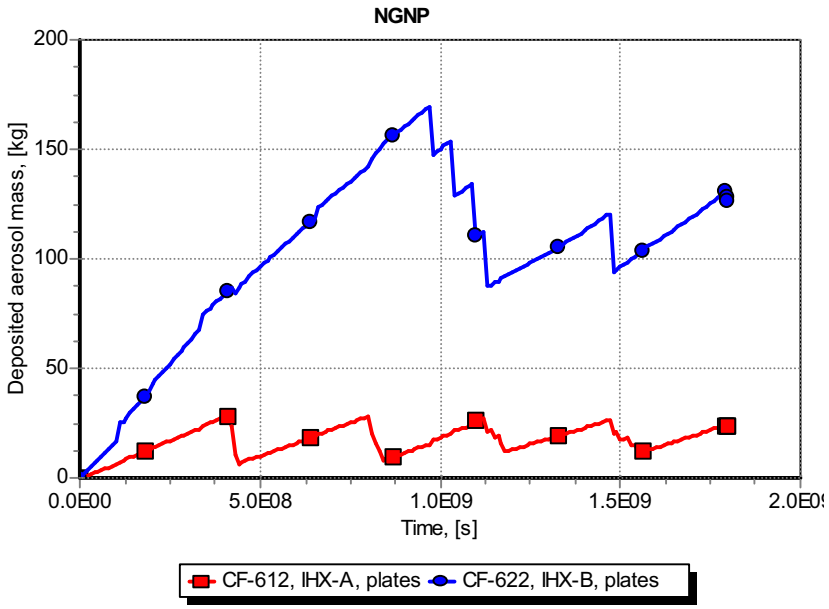

Figure 3-10 Deposited Mass in Heat Exchangers

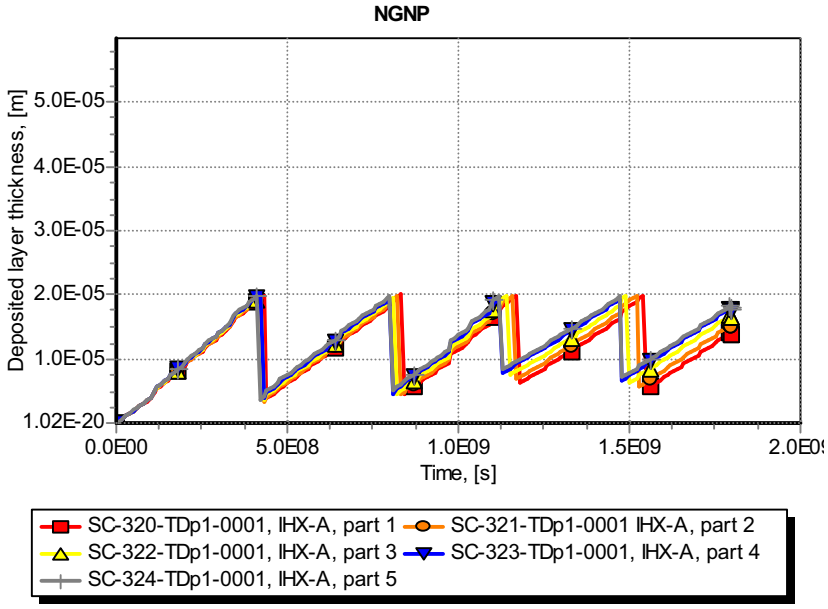

Figure 3-11 Deposited Layer Thickness, IHX-A Plates

.

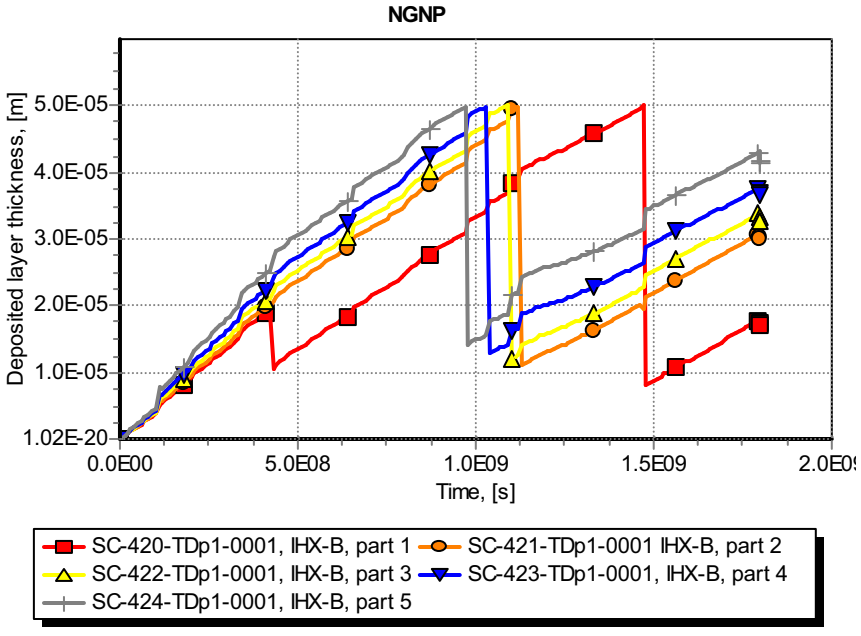

Figure 3-12 Deposited Layer Thickness, IHX-B Plates

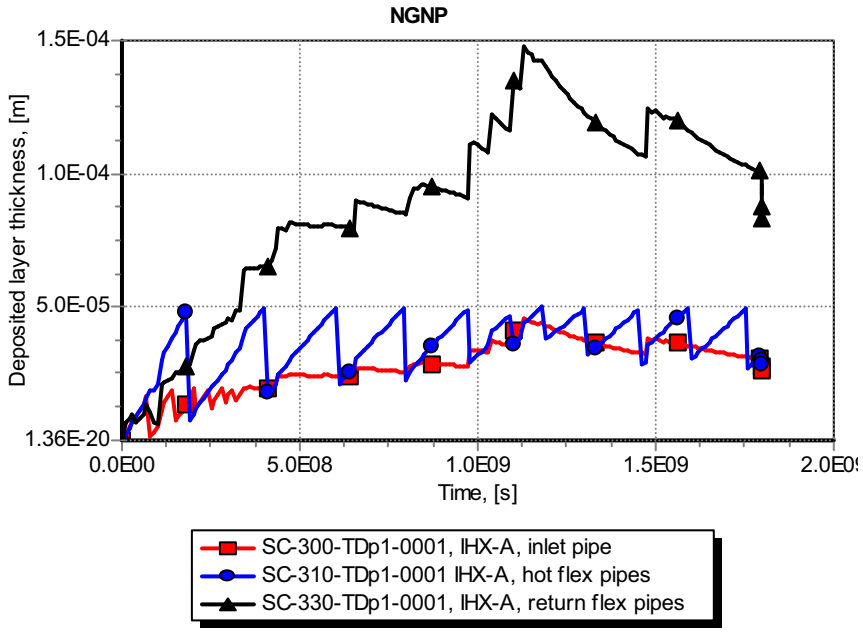

Figure 3-13 Deposited Layer Thickness, IHX-A Structures

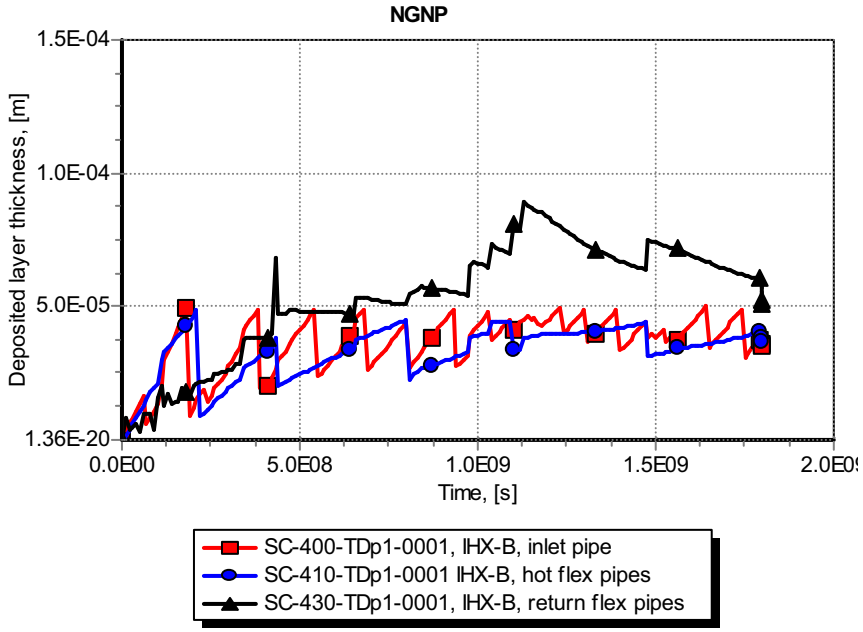

Figure 3-14 Deposited Layer Thickness, IHX-B Structures

Dust Deposition within the Pipes

Deposition of dust in the core inlet and outlet pipes is shown in Figure 3-15 through Figure 3-17. Figure 3-15 gives the total deposited mass in the core inlet and outlet pipe. Deposition on the core inlet pipe is larger than the deposition on the core outlet pipe because gas velocity is smaller there (larger gas density). Therefore fewer particles are resuspended in the core inlet pipe and more mass remains on the walls.

The layer thickness of the deposited dust is shown in Figure 3-16 and Figure 3-17. In the figures the layer thickness is presented for different parts of the inlet and outlet pipes (the labels in the figures refer to the numbers in the nodalisation scheme as presented in Figure 3-4). During the periods of resuspension from the IHX plates a large amount of large particles enters the gas. These particles deposit mainly on the pipe bends because the inertial impaction is important for large particles. The deposited layer thickness is more than two orders of magnitude larger on the bends than on the straight pipes.

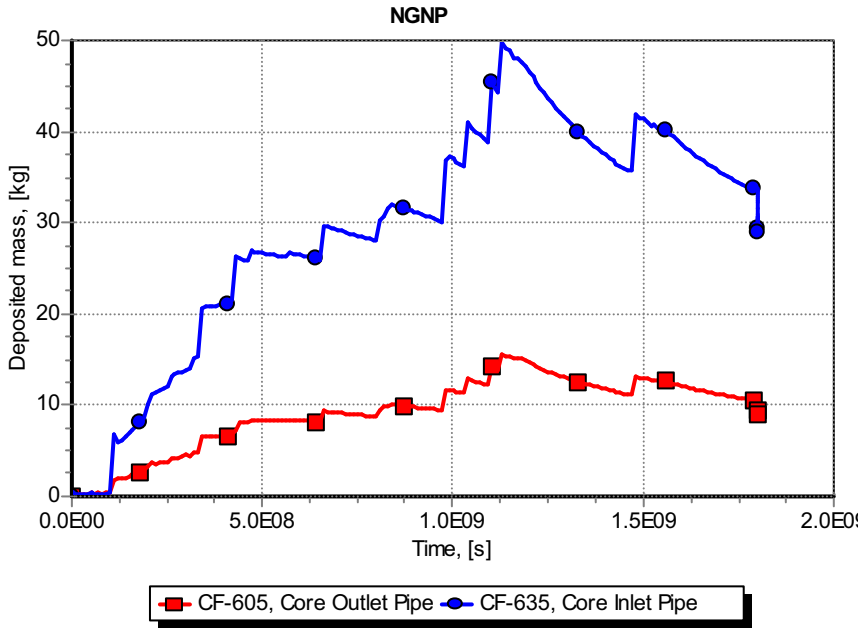

Figure 3-15 Deposited Mass, Coolant Pipes

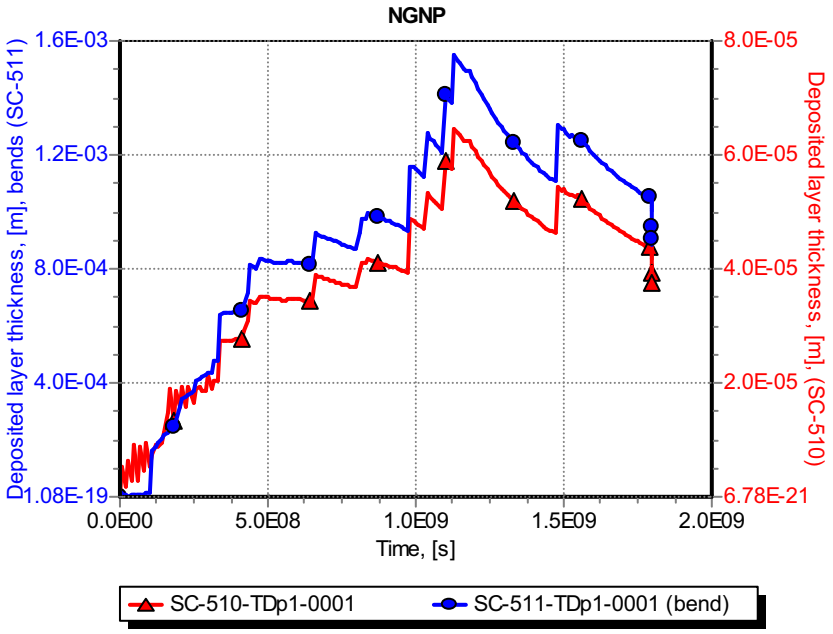

Figure 3-16 Deposited Layer Thickness, Core Outlet Pipe

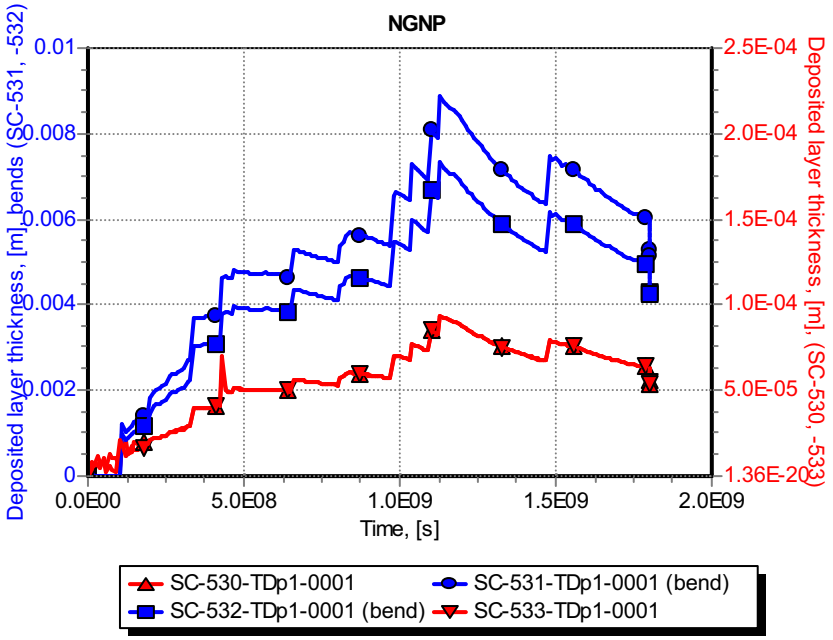

Figure 3-17 Deposited Layer Thickness, Core Inlet Pipe

Dust Deposition within the Reactor Vessel

By far the largest amount of generated dust is deposited within the reactor vessel, mainly on the graphite structures. The deposited dust distribution is shown in the right part of Figure 3-9. There is almost 1300 kg of dust deposited on the different graphite structures in the reactor vessel. Deposition on the metallic structures (core barrel, RPV walls) is rather small (about 15 kg). A large deposited layer is observed on the Control Rod Drive (CRD) channels. Figure 3-18 gives the layer thickness of the deposited dust at different locations in the CRD channels. While on other surfaces in the system the deposited layer thickness is at most hundreds of microns (10^{-4} m), the layer on CRD channels is of order of centimeters (10^{-2} m). The reason for this large deposition is very small gas velocities (~1 m/s) in the CRD channels that result in an almost stagnant gas region. As a consequence of the stagnant gas, the dust layer accumulates undisturbed (i.e. there are no occasional resuspensions), which is clearly visible in Figure 3-18.

The maximum layer thickness is 2 cm (Figure 3-18). Since the total diameter of the CRD channels is 13 cm, the open fraction is reduced to 9 cm in the narrowest place. This may cause problems with the CRD operation.

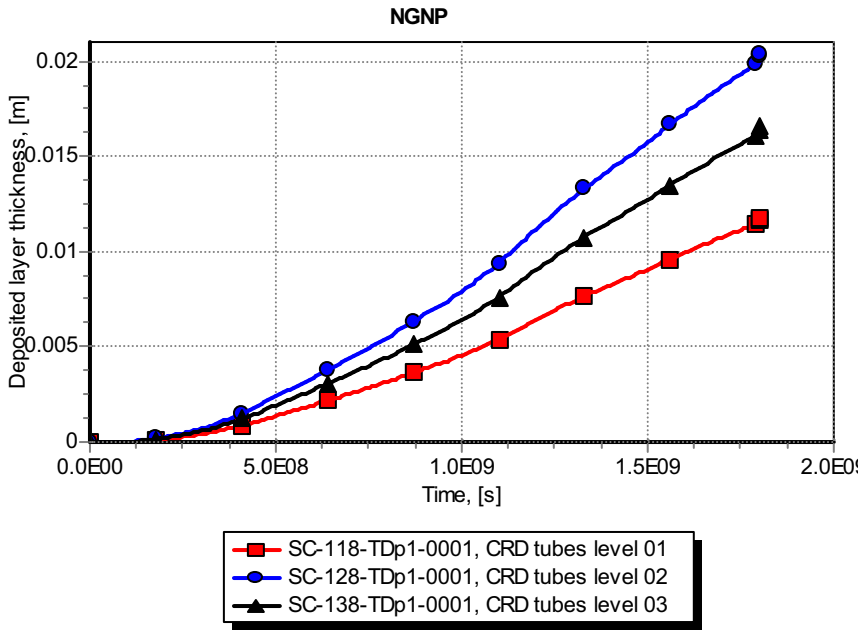

Figure 3-18 Deposited Layer Thickness, CRD Channels

3.5.3 Fission Products Transport and Plate-out Analysis

For this part of the analysis also 60 years of continuous operation at full power with an average availability of 95% is assumed. No credit is taken for some maintenance activities that could reduce the presence of fission products in the PHTS. The fission product plate-out results are shown in Table 3-9 and the amount of fission products circulating in the helium flow is presented

in Table 3-10. The activity of the Cesium and Silver on metallic surfaces is shown in Figure 3-19 and Figure 3-20.

Dust-bound Activities

Activities of the fission products attached to the dust particles were estimated in a simplified way, since no suitable model coefficients are available for sorption on graphite dust particles. The AVR measured dust-bound activities were 10^6 to 10^8 Bq/g for Cs-137 and 5×10^4 to 5×10^7 Bq/g for Ag-110m ([3-3], Table 6-1). The geometrical average values were taken for the present analysis:

$$\sqrt{10^6\times10^8} = 10^7\ Bq/g \qquad = 1.0\times10^{10}\ Bq/kg$$
$$\sqrt{5\times10^6\times5\times10^8} \approx 1.6\times10^6\ Bq/g \qquad = 1.6\times10^9\ Bq/kg$$

The activity of the dust bound Cesium and Silver, calculated using the coefficients shown above, are presented in the far right table of Figure 3-9. The dust-bound activities are 1-2 orders of magnitude smaller than the plate-out activities (see Table 3-9).

As seen from the above values, the present method has an inaccuracy of approximately 1 order of magnitude. A literature search should be performed in the future to find the sorption coefficients for dust particles and calculate dust activities more accurately. Since the dust-bound activities are 1-2 orders of magnitude smaller than the activities of fission products adsorbed on metallic surfaces, this inaccuracy is an immediate concern for the present analysis.

Transport of Fission Products

Table 3-9 gives the activities of the radionuclides that are plated out on the metallic surfaces. The table presents all isotopes that are adsorbed on the metallic surfaces of the structures outside the reactor vessel after 57 years of operation. The table shows that most of the fission products are adsorbed on the heat exchangers. There is somewhat larger deposition of fission products on IHX-B than IHX-A, because the airborne concentrations in the helium flow are higher (higher density of gas due to lower temperatures). Figure 3-19 and Figure 3-20 present the activity for Ag-110m and Cs-137 for different locations outside the core as a function of time. Both figures show that most of the silver and cesium is deposited on the heat exchangers with an order of magnitude higher deposition on IHX-B than on IHX-A. The Ag-110m reaches equilibrium between deposition on the surface and decay in a few years. The Cs-137 activity is slowly increasing during the whole period.

It should be noted that from Table 3-9 the noble gasses, such as Xe-131m, are removed although the detailed SPECTRA analysis shows that noble gasses are adsorbed. The presence of noble gases in the structures is caused by the assumption that both penetrated and adsorbed molecules remain on the structure upon decay. What is adsorbed on the surface is the I-131, which upon decay is transformed to Xe-131 (Figure 3-6). The main reason for this assumption is that there are no data and/or models available that describe the phenomena.

Table 3-10 gives the activities of the radionuclides that are circulating in the gas after 57 years of operation. In the table the activity of the noble gases is presented for the different locations outside the core and the total activity in the helium flow outside the core. It should be noted that tritium is not included in this table because tritium was not included in the transport analysis, but is treated separately in Section 2.1 of this report.

Table 3-9 Activities of Radionuclides Adsorbed onto Metallic Structures

NGNP NHSS & PHTS Model
SPECTRA, Version 3.x

Time: 1.8E+009 s
5.0E+005 hr
694.4 month
57.0 year
Δt: 1.0E+002 s

Activities [Bq]
Isotopes present in the metallic surfaces
(daughter-products not included)

Adsorbed isotopes:
- Vapor class 2 : Cs, Rb
- Vapor class 4 : I, Br
- Vapor class 12 : Ag

Isotope	Core Outlet Pipe	IHX-A	IHX-B	Core Inlet Pipe
Cs-134	1.98E+010	2.18E+012	5.14E+013	7.43E+011
Cs-135	1.35E+004	1.58E+005	8.65E+006	3.35E+005
Cs-137	1.53E+010	2.90E+011	1.15E+013	3.81E+011
Cs-138	5.54E+007	1.54E+010	4.83E+010	2.28E+009
Cs-139	2.03E+007	6.73E+009	1.59E+010	7.18E+008
Cs-140	4.25E+007	1.45E+010	3.30E+010	1.47E+009
Rb-90m	5.64E+007	1.90E+010	4.40E+010	1.98E+009
Rb-90	1.35E+006	4.48E+008	1.05E+009	4.76E+007
Rb-88	1.99E+008	5.98E+010	1.60E+011	8.10E+009
Rb-89	2.91E+007	8.91E+009	2.35E+010	1.19E+009
I-131	1.82E+008	5.65E+009	1.23E+011	4.78E+009
I-132	8.75E+007	2.05E+010	1.22E+011	2.66E+009
I-133	2.03E+008	1.49E+010	1.67E+011	5.47E+009
I-134	1.17E+008	3.49E+010	1.87E+011	3.74E+009
I-135	1.52E+008	2.17E+010	1.62E+011	4.27E+009
I-136	1.16E+007	3.93E+009	1.94E+010	3.58E+008
Br-83	1.98E+007	4.56E+009	2.72E+010	5.98E+008
Br-84	2.01E+007	6.32E+009	3.28E+010	6.44E+008
Br-85	1.02E+007	3.47E+009	1.72E+010	3.21E+008
Ag-110m	1.90E+010	9.52E+011	1.80E+013	1.24E+011
Ag-111	1.91E+008	9.74E+009	1.81E+011	1.24E+009

Table 3-10 Activities of Radionuclides Present in the Gas

NGNP NHSS & PHTS Model
SPECTRA, Version 3.x

Time: 1.8E+009 s
5.0E+005 hr
694.4 month
57.0 year
Δt: 1.0E+002 s

Activities [Bq]
Noble gases present in the gas

Isotope	Total
Xe-131m	1.02E+007
Xe-133m	1.25E+008
Xe-133	2.63E+009
Xe-135m	8.00E+008
Xe-135	6.44E+010
Xe-137	2.23E+009
Xe-138	3.89E+009
Xe-139	0.00E+000
Xe-140	0.00E+000
Kr-83m	2.04E+009
Kr-85m	5.03E+009
Kr-85	1.33E+006
Kr-87	4.30E+009
Kr-88	1.35E+010
Kr-89	2.15E+009
Kr-90	0.00E+000
Kr-91	0.00E+000

Isotope	Core Outlet Pipe	IHX-A	IHX-B	Core Inlet Pipe
Xe-131m	2.90E+006	1.72E+006	2.53E+006	3.02E+006
Xe-133m	3.56E+007	2.12E+007	3.11E+007	3.71E+007
Xe-133	7.50E+008	4.46E+008	6.55E+008	7.81E+008
Xe-135m	2.28E+008	1.35E+008	1.99E+008	2.37E+008
Xe-135	1.83E+010	1.09E+010	1.60E+010	1.91E+010
Xe-137	6.35E+008	3.78E+008	5.55E+008	6.61E+008
Xe-138	1.11E+009	6.58E+008	9.68E+008	1.15E+009
Xe-139	0.00E+000	0.00E+000	0.00E+000	0.00E+000
Xe-140	0.00E+000	0.00E+000	0.00E+000	0.00E+000
Kr-83m	5.81E+008	3.46E+008	5.08E+008	6.06E+008
Kr-85m	1.43E+009	8.52E+008	1.25E+009	1.49E+009
Kr-85	3.77E+005	2.25E+005	3.30E+005	3.93E+005
Kr-87	1.22E+009	7.28E+008	1.07E+009	1.28E+009
Kr-88	3.83E+009	2.28E+009	3.35E+009	4.00E+009
Kr-89	6.13E+008	3.65E+008	5.35E+008	6.38E+008
Kr-90	0.00E+000	0.00E+000	0.00E+000	0.00E+000
Kr-91	0.00E+000	0.00E+000	0.00E+000	0.00E+000

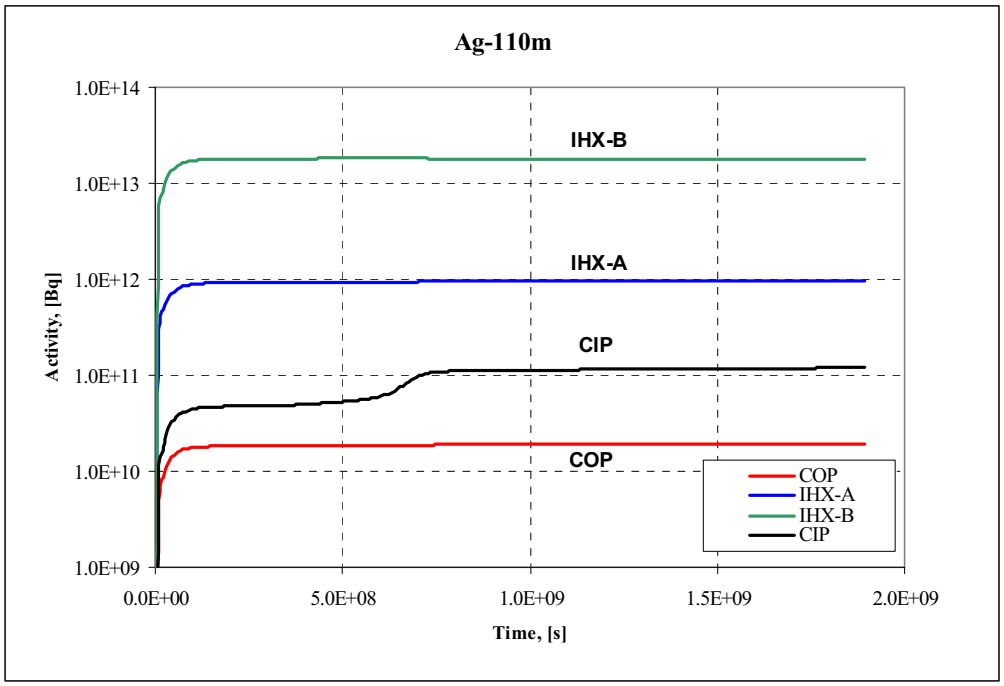

Figure 3-19 Activities of Ag-110m Adsorbed on Metallic Structures

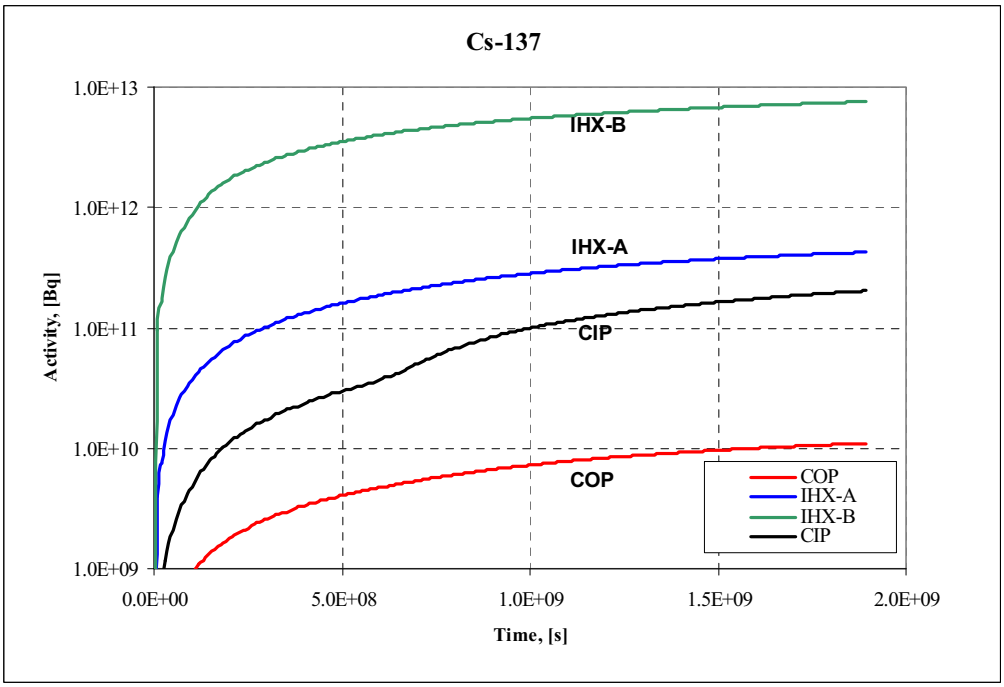

Figure 3-20 Activities of Cs-137 Adsorbed on Metallic Structures

3.6 Summary

The transport of dust and fission products within the PBMR NGNP was analyzed based on the assumption of 60 years of continuous full power operation with an availability of 95%. No credit was taken for changes in system conditions related to power operation and maintenance activities.

The total amount of graphite dust generated in the nuclear core region and the FHSS that enters the helium flow is approximately 1627 kg. About 87% of the dust settles in the graphite heat structures in the reactor vessel. Of the remaining graphite dust, 2/3 collects in Intermediate Heat Exchanger B.

Agglomeration of dust from smaller into larger particles is observed at all locations. The resuspension of agglomerated dust particles is an important phenomena that limits the build-up of a dust layer on the heat exchange surface of the IHX and causes a large deposition of dust within the reactor vessel.

The present method of estimating the dust-bound activities has an inaccuracy of ±1 order of magnitude. Since the dust-bound activities are 1 - 2 orders of magnitude smaller than the activities of fission products adsorbed on metallic surfaces, this inaccuracy is an immediate concern for the present analysis.

The effect of the filters in the HPS is negligible because of the relatively small mass flow of the system (only 1% of the generated dust is trapped in the HPS filter). The filter in the FHSS removes 97% of the dust generated in the FHSS.

3.7 Conclusions

The present analysis led to the following main conclusions:

- 87% of the dust generated in the core region and FHSS is deposited in the reactor vessel. The remaining graphite dust is deposited in the IHX A and B and on the pipe bends. Excluding the reactor vessel, the largest amount of dust is deposited in IHX-B (approximately 60% of the deposited dust outside the reactor vessel).

- Because of the very small flow through the HPS, the effect of the HPS filters on the dust in the PHTS is rather small (only about 1% of the total amount of generated dust is trapped by the filter).

- Activities of the fission products attached to the dust particles were estimated in a simplified way, since no suitable model coefficients are available for sorption on graphite

dust particles. The present method has an inaccuracy of approximately one order of magnitude.

- A large deposited layer is observed on the Control Rod Drive (CRD) channels. This large layer may have some effect on the control rod movement.

3.8 Recommendations

Based on the previous conclusions and the discussions in the previous sections the following recommendations are made:

- Because the deposition layer in the IHX is strongly affected by resuspension of agglomerated particles, the influence of using different size sections for the agglomerated (large) particles) should be investigated.

- In the present calculation the additional resistance for the heat transfer and for the gas flow caused by the deposited dust was neglected. It is recommended to address this issue for future work.

- A literature search should be performed to find the sorption coefficients for dust particles and calculate the dust activity more accurately.

- It is possible that the graphite layer has influence on the plate-out of fission products on metals. This may be taken into account in the analysis if the sorption coefficients for dust particles are found.

- The present analysis has been performed by assuming a continuous operation at full power during its lifetime. The expected plant life-time is 60 years with an average availability of 95%. The calculations were performed for 57 years full power operation. A more realistic approach would be to perform a 60-year simulation taking into account periodic outages with zero power, start up of the plant and maintenance activities.

- Because of the large deposition of dust within the reactor vessel, in particular the observed large deposition in the CRD tubes, a detailed study of the transport of dust within the reactor vessel under realistic conditions is recommended.

3.9 References

[3-1] *E.A.R. de Geus, H.G.W. Idink, "NGNP Contamination Control Study – SPECTRA Model Description and Calculation Results", NRG Report 22194/08.88401.*

[3-2] *I.E. Idelchik, "Handbook of Hydraulic Resistance", Hemisphere Publishing Corp., 1986.*

[3-3] *"Fuel Performance and Fission Product Behaviour in Gas-Cooled Reactors", IAEA-TECDOC-978, November 1997.*

[3-4] *Fort St. Vrain Final Safety Analysis Report, Chapter Number and Title, Public Service Company of Colorado, Revised March 1983.*

4 EXPECTED RADIATION EXPOSURES

4.1 Estimation of Worker Exposure

Due to deposition of carbon dust contaminated with fission products and metallic fission products that are plated out on the inner walls of the channels and the heat exchangers of the primary heat transfer system (PHTS), personnel occupying the surrounding rooms of the heat exchanger hall can be exposed to ionizing radiation. Also gaseous fission products, like noble gasses (Kr, Xe) and halogens (Cl, Br) as well as tritium are released from the core and transported with the carrier gas through the PHTS. Except from tritium, which emits only weak beta radiation that cannot penetrate through the walls, these circulating gasses also contribute to the external dose rates outside the PHTS.

The results of the SPECTRA calculations (see Section 3) show where radioactive dust particles and fission products are deposited in the different parts of the primary circuit of the reactor. Also the activity concentrations of the circulating gaseous fission products in the different parts of the PHTS are calculated.

With these results the main sources of radioactive contamination outside the reactor vessel are qualitatively and quantitatively determined. With the point kernel calculation tool MicroShield the dose rates at relevant parts of the installation, where workers can be exposed during maintenance or inspection work, are estimated. The calculations take account of the reactor building and shielding design.

For estimating the dose rates, five locations are evaluated, which are denoted A to E in Figure 4-1 and Figure 4-2.

Except for locations B and D, radiation originating from radioactivity inside the PHTS is shielded by the concrete building structures. The shielding consists of 100 cm concrete for dose points A and E and 150 cm concrete for dose point C. Furthermore the radiation is shielded by the metallic boundaries, in total 27 cm of steel/Inconel of the Core Outlet Pipe (COP) and 2.8 cm of steel of the Core Inlet Pipe (CIP). The relevant parts of the heat exchangers IHX-A and IHX-B (heat exchange plates and inner structures) are shielded by the IHX vessels of about 9 cm of steel.

Table 4-1 presents an overview of the assumed source geometries and dimensions and the shielding parameters. The total nuclide specific activities in or on the different items of the PHTS after 60 years of operation with 95% availability, as calculated with the SPECTRA code, are given in Section 3.

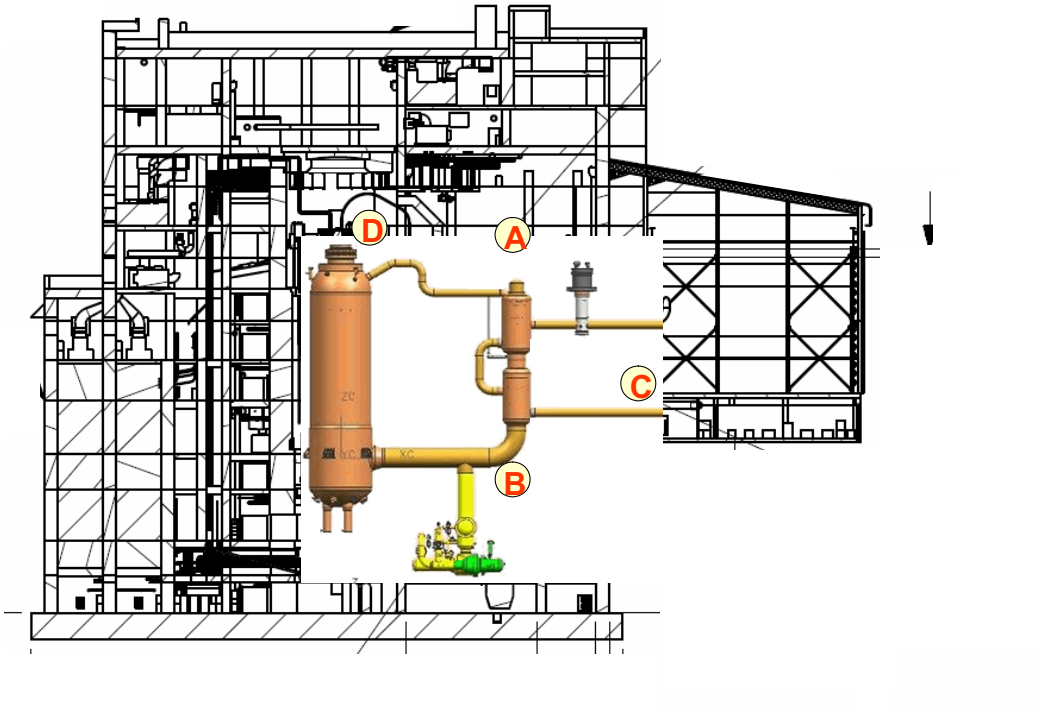

Figure 4-1 Locations of Dose Points A to D

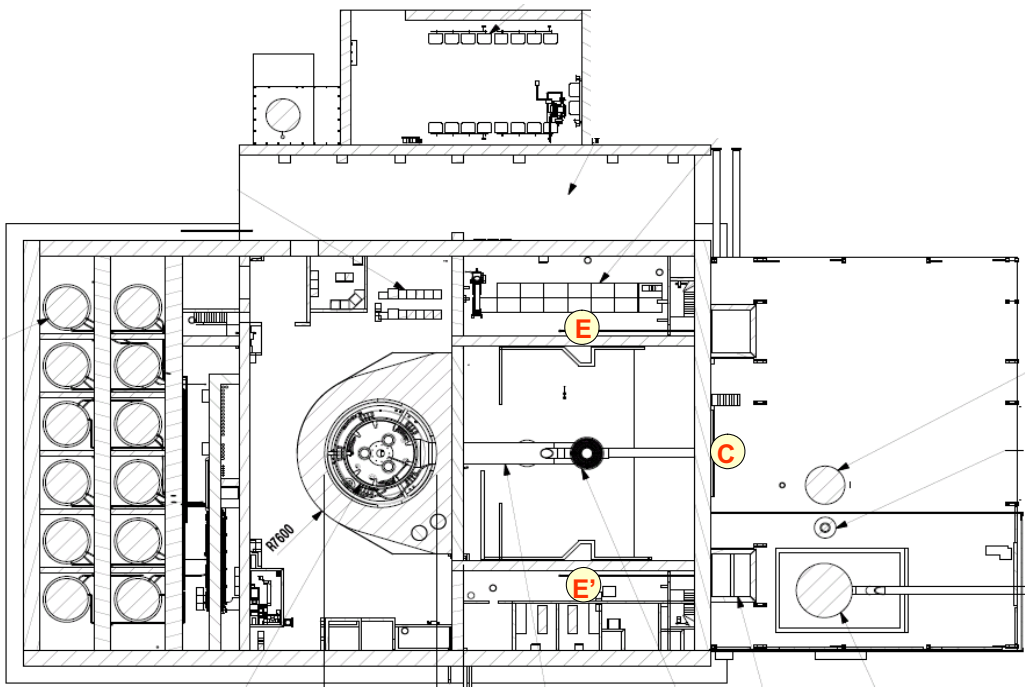

Figure 4-2 Location of Dose Points C and E

Table 4-1 Source Volumes and Geometrical Data

Source		A	B	C	D	E
COP **V = 9.0 m^3**	Distance (cm) Iron (cm) Concrete (cm)		350 11.1 -			
IHX-A **V = 37.1 m^3**	Distance (cm) Iron (cm) Concrete (cm)		840 8.8 -	1250 8.8 150		1200 8.8 100
IHX-B **V = 37.1 m^3**	Distance (cm) Iron (cm) Concrete (cm)	500 8.8 100		1310 8.8 150		1260 8.8 150
CIP **$V_{A,B}$ = 2.8 m^3** **V_D = 1.2 m^3**	Distance (cm) Iron (cm) Concrete (cm)	500 2.8 100	2100 2.8 -		140 2.8 -	

4.2 MicroShield Code

Microshield v. 5.05 [4-1] is a comprehensive photon/gamma ray shielding and dose assessment program, using the point kernel method for integrating dose contributions from each point in a source. Up to sixteen different source geometries can be calculated for as many as twenty-five energy groups. Source-to-dose-point geometries include up to ten standard shields, source self attenuation and cylindrical cladding.

Microshield is widely used for designing shields, estimating source strength from radiation measurements, minimizing exposure to people, such as operators, maintenance and inspection technicians as well as members of the public, and for teaching shielding principles.

4.3 Results of Exposure Calculations

The results of the exposure calculations are presented in Table 4-2 with respect to the five identified dose points (locations) and for each location the most relevant sources of radiation. The dose points are situated at a height of 1 m above the floors or at a distance of 1 m from the walls. For point D the dose point is at 1 m from the Core Inlet Pipe. The dose rate as a function of the distance to the core inlet pipe for this location is given in Figure 4-3. The calculated dose rates are given as effective dose in μSv per hour.

Annual doses to operators should be calculated with respect to their maximum exposure time during inspection and maintenance work.

Table 4-2 Calculated External Dose Rates at Identified Locations

Source		Dose Rates (µSv per hour)				
		A	**B**	**C**	**D**	**E**
Core Outlet Pipe	Dust		0.15			
	MFP		0.45			
	GFP		14.5			
IHX-A	Dust		0.3	9.4×10^{-9}		3.2×10^{-6}
	MFP		53	4.7×10^{-5}		3.2×10^{-3}
	GFP		0.5	1.2×10^{-6}		8.3×10^{-5}
IHX-B	Dust	8.3×10^{-5}		5.2×10^{-8}		1.8×10^{-5}
	MFP	1.7×10^{-1}		6.5×10^{-4}		4.9×10^{-2}
	GFP	1.5×10^{-4}		2.0×10^{-7}		1.8×10^{-5}
Core Inlet Pipe	Dust	4.0×10^{-4}	11.5		880	
	MFP	3.3×10^{-2}	96		7290	
	GFP	3.0×10^{-3}	6.1		470	
Total		**2.1×10^{-1}**	**183**	**7.0×10^{-4}**	**8640**	**5.2×10^{-2}**

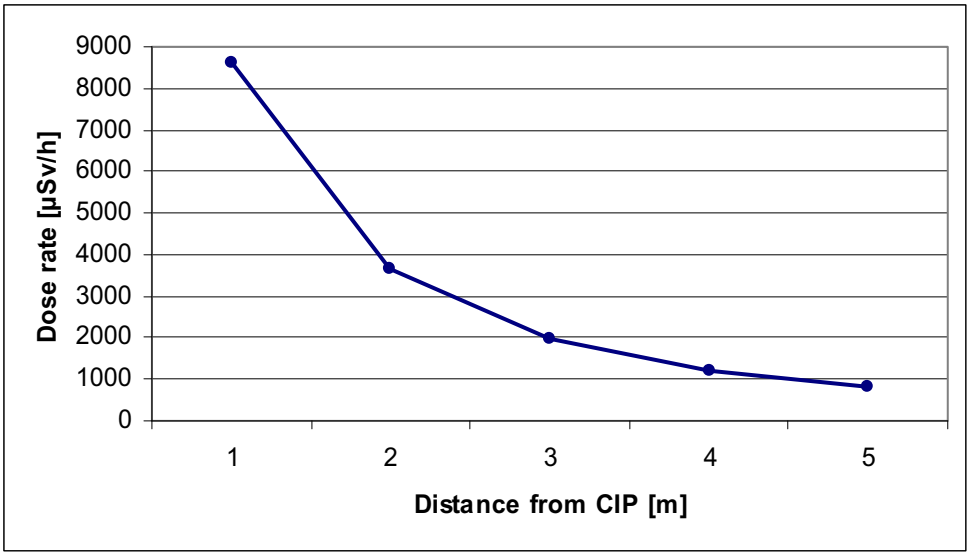

Figure 4-3 Dose Rate as a Function of Distance for Location D

With respect to the maximum allowable occupational whole body dose in a calendar year, as given in Section 3.2.2, the calculated dose rates can be converted to a maximum allowable exposure time. Assuming a whole body dose limit of 50 mSv per year the maximum allowable exposure times are 275 hours and 6 hours for respectively locations B and D. For the other locations additional dose rates are so low that there are no restrictions on the occupancy in these rooms. One should realize that during maintenance and inspection activities, due to changing conditions within the PHTS, the activity of dust may be much more important than plated out activity.

During maintenance the reactor will be shut down so the contribution of circulating activity to the dose will be zero. However the main contribution is from deposited metallic fission products, so that the dose rate near the Core Inlet Pipe will still be very high. Additional shielding around the pipe may help to reduce the dose rate.

Dose rates are calculated for the maximum deposition of dust and metallic fission products after 60 years of operation with 95% effective operation time. Since the contributions to the calculated dose rates of the circulating gaseous fission products are relatively small, the total dose rates in the first years of operation will be much smaller and therefore maximum allowable exposure times will be higher.

4.4 Summary

Based on SPECTRA calculations of deposited dust and metallic fission product and the circulating activity in the helium flow of the PHTS of NGNP, dose rates are estimated at five different locations around the PHTS. Three locations are shielded by concrete structures from radioactivity inside the PHTS. The other two locations are located within the building where the PHTS is located. The dose rates at locations outside the building with the PHTS are less than 1 μSv per hour. The dose rate inside the PHTS building near the IHX is approximately 0.2 mSv per hour and near the core inlet pipe approximately 9 mSv per hour. Assuming a whole body dose limit of 50 mSv per year the maximum allowable exposure time near the core inlet pipe is approximately 6 hours.

4.5 Conclusions and Recommendations

The analysis of the dose rates at different locations within NGNP led to the following main conclusions:

- The dose rates outside the PHTS building, due to dust and fission products in the PHTS, are low and no extra measures are necessary to prevent exposure to personnel.

- The dose rates within the PHTS building are significantly higher (up to several mSv per hour) which might limit the presence of maintenance workers.

Based on the conclusions and analysis it is recommended to perform the following studies for future work:

- The approach of 60 years of full power operation with 95% availability dose rates results in a gradual build up of dust and fission products. It is recommended to investigate the effect of power operation (power steps, start up, etc.) and maintenance work on the location and build up of dust and fission products.

- It is recommended to take radiation protective measures to avoid exposure to free coming dust, besides the direct radiation of it, during maintenance activities of the IHX and other components.

- It is recommended to analyze in detail the effect of condition changes within the PHTS on the resuspension of dust and the effect on the dose rates.

4.6 References

[4-1] *MicroShield v. 5.05, Grove Engineering, Rockville, Maryland.*

5 TRITIUM PERMEATION THROUGH HEAT EXCHANGERS

5.1 Introduction

The production rate for tritium is approximately 2.1×10^{-9} mol/s, as calculated from Figure 2-1 in Section 2.1. This tritium production occurs mainly in the fuel spheres from which the tritium is rapidly released into the PHTS due to its high permeability. There are several mechanisms causing the tritium release from the PHTS:

- The helium gas in the PHTS leaks out of the PHTS at a rate of about 0.12%/day. This causes the tritium to leak out at the same rate. Replacement helium is entered into the PHTS to compensate for this helium loss.
- Tritium permeates through the IHX from the PHTS into the SHTS.
- Tritium permeates through the other parts of the primary system (other than the IHX) into the space surrounding the PHTS.
- A small fraction of the tritium is removed by the HPS.

Besides the above release mechanisms there is also the radioactive decay, which decreases the tritium concentration. However, due to the relatively long half life (12 year) of tritium, this effect has a relatively small impact on the tritium concentration and will not be discussed in this section.

Due to the large area and thin walls of the compact IHXs and the high temperature of operation significant tritium contamination of the SHTS is likely. If the tritium partial pressure in the SHTS becomes too large, significant amounts of tritium can also be released from the SHTS into the Hydrogen Production System process coupling heat exchanger, into the Power Conversion System steam generator, and into the buildings surrounding these systems.

In order to limit the tritium concentration in the SHTS, the permeation through the IHX should be smaller than the other PHTS removal mechanisms.

Without changing the geometry of the IHX, the permeability of the alloys used in the IHX may be reduced in two ways:

1. Enhancement of surface oxidation of the construction metals.
2. Application of a dedicated coating layer (in practice a foreign oxide or carbide).

NRG is performing tritium breeding tests for fusion applications in the High Flux Reactor (HFR) in Petten. These experiments confirm that the tritium permeation through bare metal walls is very high, requiring engineered features to prevent tritium release to the environment. In the case of the HFR this is solved by giving the experiment a triple gas containment.

The following paragraphs give options for permeation reduction, and their suitability for the IHX. This is followed by a conservatively high estimation of the permeation rate from the

PHTS into the SHTS of NGNP, and quantified values for the influence of coatings on this permeation rate. Moreover recommendations are given to reduce tritium in the SHTS, based on literature studies and experience gained at the HFR Petten.

5.2 Oxidation of IHX Alloys

Under nominal (mildly oxidizing) PHTS conditions, an oxide scale with a thickness of a few to tens of micrometers will form on the IHX structural alloys during operation, due to impurities (H_2O, CO, CH_4) in the helium flow [5-8]. Both Incoloy 800H and Inconel 617 contain by design a significant amount of chromium [5-7], and since chromium is the most readily oxidized component in these alloys, this layer consists mostly of Cr_2O_3 [5-10]. In addition to corrosion protection, the oxide layer brings a permeation reduction factor (PRF) of up to 10^3 depending on the material and oxidation conditions ([5-6], [5-14] and [5-15]).

In the case of Incoloy 800H, obtained PRFs are in the range 10^2-10^3. Fütterer et al reviewed permeation reducing layers in the context of tritium breeding blankets, with a focus on Incoloy 800 [5-13]. The following conclusions were drawn regarding this material:

- Surface oxidation produces higher PRF values when performed at higher temperatures: PRF@(750 ^oC)>PRF@(660 ^oC)>PRF@ (520 ^oC).
- After oxide formation at higher temperatures, the higher PRF is retained when the temperature is slowly dropped.
- Fast temperature cycling results in the formation of cracks, which strongly reduces the PRF. However, self-healing occurs under oxidizing conditions within 1-5 days if mildly oxidizing conditions are maintained.

For Inconel 617, permeation reduction factors of only 45-150 have been obtained by Schaefer et al [5-6]. However, since its chromium content is close to that of Incoloy 800H, it is likely that similar PRFs can be reached if oxidation is performed at higher temperatures (~750 ^oC).

The stability region of these oxides is limited. Since the composition of the oxide scale depends dynamically on the coolant composition, the amounts of trace gases in the PHTS need to be controlled in order to maintain it. From reviews of helium chemistry on the oxide scales of HTGR alloys it can be concluded that concentrations of CO and CH_4 in the gas flows should be kept to a minimum to avoid carburization, while minimum H_2O and/or O_2 levels need to be maintained to stabilize the oxide layer at higher temperatures ([5-8] and [5-17]). If carbides are allowed to form, cracks occur on the alloy surface, with a large drop in PRF as a result [5-9]. Note that the estimated gas composition of the NGNP promotes a stable oxide layer at moderate temperatures [5-8].

Under HTGR conditions, carburization rapidly increases above a critical temperature due to reduction of the oxide layer. In particular, a critical temperature of 980 ^oC has been found for Inconel 617 in an advanced gas-cooled reactor helium atmosphere [5-10]. The Cr_2O_3 scale may

react to form the volatile CrO_2 above a temperature of ca. 950 ^oC ([5-11] and [5-17]). The uncertainties with respect to volatilization are increased due to the high gas velocities in the NGNP. This means that for Inconel 617 and Incoloy 800H, PRFs of ~10^3 may not be maintainable above 950 ^oC even under relatively beneficial helium chemistry. Nevertheless, a stable chromia scale has been observed on Inconel 617 in a test loop under conditions approaching that of the NGNP (T=950 ^oC, 7000 hours) [5-12].

Sakaba et al have recently compared laboratory permeation experiments with direct measurements from the Japanese HTTR operating at 950 ^oC [5-31]. The authors find that the laboratory experiments were representative; permeation reduction in the IHX by a factor ~10^2 compared to laboratory experiments were explained in terms of in-situ oxidation of the IHX alloy Hastelloy XR.

Based on the data as described above, the following observations can be made:

- The growth of a natural oxide layer to reduce permeation is a realistic option for the IHX B (Incoloy 800H at 760 ^oC). The operating temperature and helium composition in the IHX B are suitable for the formation of a stable oxide layer. Initial oxidation could be performed before start of reactor operation in order to grow a higher-quality oxide under more controlled conditions (i.e., a carbon-free flow and controlled temperature [5-10]). PRFs in the order of 10^3 may be reached.
- In the case of IHX A (Inconel 617 at 950 ^oC), the NGNP operates near the limit of the Cr_2O_3 stability range. There are uncertainties with respect to volatilization and reduction of the oxide scale; both processes have an onset at about 950 ^oC. More experimental test results under NGNP conditions are necessary before an oxidation layer can be considered as a realistic option for permeation reduction.

5.3 Application of External Permeation Barriers

The most extensively researched coating material is alumina (Al_2O_3), due in large part to its thermodynamic stability and high mechanical strength and wear resistance. Thermodynamic stability in particular makes the issues of helium chemistry and temperature limits much less important.

There is no evidence available on PRFs of alumina specific to Inconel 617 and Incoloy 800H, but alumina coatings produced under laboratory conditions are found to produce PRFs of 10^2-10^4 for different substrate metals ([5-16], [5-17] and [5-18]), with large scatter in data. In a strict sense, these numbers are only meaningful when specifying both the substrate and the coating materials and the thicknesses of both the substrate and the coating. However, considering the PRF of the coating material independent of the substrate seems acceptable because the substrate and coating dimensions of tested materials are similar to those in the IHX.

Hollenberg et al. [5-20] reviewed the research in the early 80s and 90s on permeation-reducing coatings in fusion technology, with the following conclusions on alumina coatings:

1. A higher surface content of aluminum before oxidation yields higher PRFs.
2. Coatings are robust; in addition, extensive temperature cycling does not influence the PRF.
3. The PRF is mainly determined by the presence of a relatively thin (< 1 μm) oxide layer. The thickness of the aluminum-rich metallic layer is unimportant with respect to the PRF, but a minimum layer is recommended to provide the possibility of self-healing of the permeation barrier.

Different methods have been tried to fix the alumina coating on a substrate, which fall into the broad categories of aluminizing and vapor deposition techniques. Aluminizing, the application of an aluminum-rich metallic coating, has been performed by hot-dipping, pack-aluminizing, chemical vapor deposition and sputtering [5-16]. The coating material is advised to be an alloy tailored to match (as far as possible) the thermal expansion of the substrate. The application of the aluminum-rich coating is followed by a heat treatment by which diffusion of aluminum produces a composition gradient that increases bonding with the substrate. During the heat treatment performed under an inert atmosphere, the aluminum-rich layer will be slowly oxidized due to the presence of traces of CO_2, CO or H_2O.

Commercial packed-bed aluminizing methods have been tested by Forcey et al [5-18]. The main conclusions of these authors were:

- Pack-aluminizing can readily be performed on an industrial scale; the aluminum-rich layer has been shown to be resistant to thermal and mechanical shock.
- The protective oxide layer may be formed in-situ, during operation. This has been tested at temperatures up to 600 ^{o}C, and oxidation was found to be more effective at higher temperatures (as was the case for oxidation of Inconel 617 and Incoloy 800).
- Depending on the aluminizing method, PRFs of 10^{2}-10^{4} were found.
- Permeation reduction is obtained by very thin oxide layers (30-200 nm is enough [22,33]), while there is no dependence on the thickness of the metallic layer (1-50 μm).
- Removal of the oxide layer by reduction does not occur at NGNP temperatures.
- The aluminum content of the coating should be smaller than 30% because of brittleness at higher concentrations (close to 30% is recommended).

A 7 micrometer Fe–Al/Al_2O_3 layer made by the pack-cementation process at CEA has been tested in the Exotic 8.10 experiment, carried out at the HFR Petten [5-32]. In this experiment, a PRF of up to 10^{+3} was found, depending on temperature (280 ^{o}C -480 ^{o}C). During irradiation the permeation barrier did not deteriorate with respect to tritium permeation. Also no dependence on hydrogen concentration was observed except for a slight increase at hydrogen concentrations below 0.1% (a factor 10^{+3} higher than values estimated for the NGNP). This shows that the oxide layer is not reduced even at high hydrogen contents, but that the presence of hydrogen inhibits tritium permeation. However, it is unknown if the latter effect is significant at the low concentrations present in the NGNP.

Alternatively, at the Forschungszentrum Karlsruhe (Germany) the hot-dip method has been developed ([5-20] and [5-21]). After a 30-hour heat treatment under argon atmosphere at 950 ^{o}C, a PRF of ~10^3 was found; this may serve as an indication of the PRF obtained by in-situ oxidation in the NGNP. However, a drawback of the hot-dip method as performed by Forschungszentrum Karlsruhe is that it produces an aluminum-rich layer with a thickness of tens of micrometers. On the approximately 400-μm thick separation plates in the IHX, this could significantly change mechanical and heat transfer properties. A reduction in the heat transfer characteristics of the IHX may lead to an unacceptable reduction of the performance of the power production of the reactor.

Vapor deposition techniques offer better control over the layer thickness and application temperature compared to aluminizing/oxidation methods, with similar PRFs. Very thin coatings of crystalline alumina have been applied directly to substrate metals on a laboratory scale ([5-23], [5-24], [5-25] and [5-26]). In particular, a 1-μm layer on Eurofer, deposited by running an arc discharge on an aluminum cathode and introducing oxygen into the sample chamber at 700 ^{o}C and a -100 V substrate bias, produced a PRF of 10^3, with perfect stability under temperature cycling. Serra et al observed a PRF of 10^4 of a 1.5-μm layer sputtered on Manet steel [5-26]. The question remains if these methods can be scaled up to the level of the IHX separation plates.

Levchuk et al have recently shown erbia (Er_2O_3) to be an alternative to alumina that can be applied at room temperature ([5-24] and [5-22]). Erbia was found to have similar performance as a permeation barrier. However, data on the stability and characteristics of this oxide is still limited. Currently research is being done into industrial scale deposition of erbia in the framework of the European ExtreMat project.

Other alternatives to alumina that have been tested to a certain extent are silicon carbide, titanium carbide and mixed titanium carbide/nitride, applied by vapor deposition techniques (chemical vapor deposition and plasma spraying). All of these coatings have excellent resistance to heat cycling. In the case of titanium carbide, processing can alternatively be performed by sputtering of the metal followed by carburization.

Shan et al ([5-29] and [5-30]) and Checchetto et al [5-27] obtained PRFs of 10^4-10^5 for TiC and mixed TiC/TiN, TiC/TiN/TiC and TiC/TiN/SiO_2 coatings of 1-2 μm on 316L stainless steel, a possible order of magnitude increase in PRF compared to alumina. In contrast, Forcey et al have compared the permeation reduction of TiC, TiC/TiN and Al_2O_3/TiC/TiN layers of similar thickness and applied by the same method [5-19], and found PRFs of about 10. This shows that the PRF, as in the case of oxides, depends heavily on the quality of the coating layers; cracks in the coating severely increase permeation. Finally, Wang et al have reported a PRF of ~10^5 for a <2 μm amorphous or superfine-grained SiC coating applied to the same substrate [5-28]. The layer was produced by ion-beam assisted deposition/ion implantation. Silicon carbide also has excellent thermal shock resistance and offers a factor of 10 in thermal conductivity.

In conclusion three coating options are available to reduce the high permeability of tritium from the PHTS through the heat exchange surface of the IHX to the SHTS side.

- The solution with the highest reduction of tritium transport from PHTS to SHTS is the application of a 1-2 μm layer of SiC or TiC/TiN by vapor deposition. This option offers the largest PRF for coatings (10^4-10^5). The applicability of this option on an industrial scale should however be checked.
- Alumina offers a similar degree of stability and can be applied by available industrial aluminizing techniques. An alumina layer of a few micrometers should be applied and this layer can be oxidized in-situ at IHX temperatures, before and/or during operation. PRFs approaching 10^3 can be expected.
- The most economic solution is surface oxidation of the alloys used in the IHX. This is a realistic option for the IHX B, since it operates at a moderate temperature and experimental results of oxidation of Incoloy 800 are available. Oxidation may be achieved before reactor operation in a controlled atmosphere for increased quality of the oxide layer. A PRF of approximately 10^3 can be reached. Because the IHX A operates at the limit of stability of the oxide layer, the surface oxidation process is not recommended without an extensive testing of the oxide layer at IHX A conditions.

All the experimental results show that the actual permeation reduction depends strongly on the quality of the oxide layers.

5.4 Calculation of Tritium Permeation in IHX A/B

In the literature, permeation through bare (uncoated) alloys is generally considered to be diffusion-limited unless barriers of very high quality are present. Within this diffusion-limited regime, the permeation rate can be obtained using Sievert's Law:

$$k(t) = \frac{\Phi}{PRF} \cdot \frac{A}{L} \cdot \left(\sqrt{p_{T,PHTS}(t)} - \sqrt{p_{T,SHTS}(t)} \right)$$

with $k(t)$ = permeation rate (mol/s)
Φ = permeability of the material (mol /m /s $Pa^{-0.5}$).
$p_{T,i}(t)$ = tritium partial pressures in PHTS and SHTS.
A = total area of the heat exchanger materials.
L = total thickness of the heat exchanger materials.
PRF = permeation reduction factor, useful (but simplified) way of accounting for permeation reduction by coatings.

Permeation of tritium out of the PHTS takes place through the walls of the pipes and vessel of the PHTS and to the SHTS through the heat exchange surface of the IHX. Assuming comparable permeability for the wall and vessel material and for the heat exchange surface of the IHX, the ratio of wall area/wall thickness determines the ratio of the permeation rate out of the PHTS and permeation rate into the SHTS. The ratio of wall area/wall thickness is for the pipe and vessel walls of the PHTS and is < 2% of the ratio for the heat exchange surface of the IHX.

Therefore permeation through walls of tritium from the PHTS will only be considered for the heat exchange surface of the IHX. Due to the very thin walls and the large heat exchange surface of the IHX, permeation into the SHTS is very efficient. Below we give separate upper limits for tritium permeation rates in the IHX A and IHX B when no permeation barriers (coatings) are present.

For a conservatively realistic estimation of the tritium permeation from PHTS to SHTS, we make the following assumptions:

- Diffusion-limited permeation (Sievert's Law).
- Isotope effects are negligible (they tend to become smaller at high temperatures).
- Literature values for permeabilities (we assume that permeation is not reduced by surface or bulk saturation by He or other trace gases).
- Diffusion of tritium within the gas flow does not limit permeation.
- The permeation rate is not limited by thermal equilibrium between molecular hydrogen and water; i.e., all tritium exists in the form of molecular tritium (HT).
- The interface area between the PHTS and SHTS is the total separation plate area as presented for the secondary loop (Table 2).
- Partial tritium pressure in the SHTS is assumed to remain zero.
- No feedback from permeation rate on the partial pressure in the SHTS
- Dependency of permeation on the rate of helium flow is not considered.

According to earlier PBMR studies, it is assumed that the tritium partial pressure $p_{T,PHTS}$ in the PHTS drops from an initial value of about 5.3 Pa (~0.3 mol in the PHTS) to a steady-state value which is lower by a factor of 2 after roughly four years of normal operation. Geometrical characteristics and the temperatures in the IHX are given in Table 5-1. Numbers in bold italic are used as input for the analysis.

Table 5-1 Relevant Physical and Geometrical Data of the NGNP IHX System

Parameter	IHX A		IHX B	
	Primary	Secondary	Primary	Secondary
PHTS volume (m^3)	***492***			
He mass in PHTS (kg)	3463			
Inlet temperature (^0C)	***950***	710	***760***	287
Inlet pressure (kPa)	8751	9011	8683	9082
Required exit pressure (kPa)	8697	8970	8643	9026
Obtained pressure difference (kPa)	52.62	39.95	39.39	58.26
Differential pressure (PHTS/SHTS) (kPa)	219.0		343.0	
Fin thickness (10^{-3} m)	0.102	0.102	0.102	0.102
Height between separation plates (10^{-3} m)	1.905	2.590	1.93	1.930
Height of fin (10^{-3} m)	1.905	1.295	1.93	0.965
Plate thickness (10^{-3}m)	***0.381***		***0.381***	
Total finned surface area (m^2)	1355.0	2100.2	3701.0	4486.7
Total separation plate area (m^2)	324.1	***391.7***	874.5	***1056.9***
Total heat exchanger area (m^2)	1679.1	2491.9	4575.5	5543.6

Table 5-2 gives permeabilities for the bare alloys used in the NGNP (Inconel 617 for IHX A and Incoloy 800H for IHX B). These numbers are estimates based on Arrhenius parameters extracted from measurements at lower temperatures. Numbers in bold **italic** are used as input for the analysis.

Table 5-2 Hydrogen Permeabilities of Uncoated IHX Materials

Material	Permeability (mol s^{-1} m^{-1} $Pa^{-0.5}$)	
	Temp. 760 ^{0}C (IHX B)	Temp. 950 ^{0}C (IHX B)
Incoloy 800H		
Reference [5-1] hydrogen	***2.76E-10***	9.64E-10
Reference [5-2] hydrogen	***1.27E-09***	4.04E-09
Reference [5-3] hydrogen	***1.67E-10***	6.38E-10
Reference [5-4] deuterium	7.06E-11	2.70E-10
Reference [5-5] deuterium	6.08E-11	1.66E-10
Inconel 617		
Reference [5-6] hydrogen	1.67E-10	***5.39E-10***
Reference [5-7] hydrogen	3.01E-10	***1.01E-09***

Table 5-2 indicates that the permeabilities of the different alloys have the same order of magnitude, and increase by a factor of 3 - 4 when going from IHX B to IHX A temperatures. The permeabilities of these high nickel alloys are on average about 2 to 4 times larger than that of austenitic stainless steels. As input into Sievert's law, the average of the values obtained for hydrogen was used for calculations.

With the input described above (this includes the assumption of a non-oxidized heat exchange material), the permeation rate into the SHTS is calculated with Sievert's law. The partial pressure of tritium in IHX A/B was calculated from PBMR results for the expected tritium concentration in the PHTS of NGNP. The estimated concentration of tritium in the PHTS drops in about 4 years from 5.7 x 10^{-4} to 2.9 x 10^{-4} mol/m^3 and remains constant after 4 years of operation. This concentration was estimated based on the following assumptions:

- The tritium production rate in the fuel is known.
- The tritium will diffuse rapidly from the fuel and enter into the PHTS.
- About 0.12%/day of the gas in the PHTS leaks out of the PHTS and pure helium is entered into the PHTS in order to compensate for this loss.
- No permeation of tritium through walls is assumed.

The results of the permeation calculation are presented in Table 5-3. The computation yields that approximately 5x10^{-3} mol/s permeates from the PHTS into the SHTS through the IHX.

Table 5-3 Permeation Rate from PHTS to SHTS

Time (years)	Partial tritium pressure (Pa)		Permeation rate (mol/s)			Leakage from PHTS (mol/s)
	IHX A	IHX B	IHX A	IHX B	Total	
0	5.73	4.84	1.91×10^{-3}	3.79×10^{-3}	5.70×10^{-3}	3.85×10^{-9}
4	3.02	2.55	1.38×10^{-3}	2.75×10^{-3}	4.14×10^{-3}	2.03×10^{-9}

A conclusion is that the tritium concentration assumed in the PHTS is too high, and that under the above assumptions, the main path of the tritium out of the PHTS is permeation through the IHX, and not the 0.12% leakage per day as assumed by PBMR. With these results, a steady state condition will be reached in which tritium permeation is essentially equal to the production rate of tritium in the PHTS. The steady state concentration of tritium in the PHTS will then depend on the permeability of the IHX.

The above calculated permeation of tritium from SHTS to PHTS is based on the upper limit of the permeability of the IHX alloys. There are several effects that will decrease the permeation significantly:

- Permeation will decrease by a factor of approximately 10 due to a combination of overestimated temperature of the IHX materials, the isotope effect and partial (<10%) oxidation of the tritium gas. In addition, a lower partial tritium pressure in the SHTS will decrease the permeation and the presence of helium and hydrogen blocking some of the diffusion sites will have an impact which is difficult to estimate.
- A permeation reduction factor (PRF) of 10^2 might be considered due to surface oxidation of the IHX alloys during operation.
- By applying high-quality carbide coatings, the PRF may be increased to 10^5 (maximum value obtained from literature).

A strong reduction of the permeation through the IHX heat exchange surface is needed in order to reduce the permeation so much that the leakage (0.12%/day) becomes the dominant release path of the tritium. Only in that case a significant reduction of the tritium permeation into the IHX can be achieved. For this reason the permeation rate from PHTS to SHTS is also calculated, taking into account the feedback of the permeation rate on the amount of tritium inside the PHTS. For this calculation the following approach is applied:

- A steady state configuration is assumed in which the sum of tritium leakage and permeation equals the tritium production (mass balance).
- The tritium production rate is for steady state normal operation conditions, 2.08×10^{-9} mol/s and the helium gas leaks out of the PHTS at a rate of about 0.12%/day
- For different PRFs, the mass balance is solved for the tritium amount in the PHTS.
- From the total amount of tritium in the PHTS, both the tritium leakage and the permeation rate are calculated. This in turn yields the fraction of tritium permeating into the SHTS for different values of the PRF.

Results are given in Table 5-4. The table shows that PRFs larger than 10^6 are needed in order to reduce the amount of permeated tritium into the SHTS by a factor of 10. These values are not realistic to achieve. The highest reported PRFs for coatings are in the order of 10^4 to 10^5, while the highest estimated values using industrial-scale coating techniques are about 10^3.

Table 5-4 Cases for Tritium Transfer from PHTS

PRF coating (-)	Tritium amount in PHTS (mol)	Permeation rate to SHTS (mol/s)	Leak rate (mol/s)	Permeation to SHTS as fraction of production
$1.0 \times 10^{+2}$	4.14×10^{-8}	2.08×10^{-9}	5.75×10^{-16}	1.00
$1.0 \times 10^{+3}$	4.14×10^{-6}	2.08×10^{-9}	5.75×10^{-14}	1.00
$1.0 \times 10^{+5}$	2.76×10^{-2}	1.70×10^{-9}	3.83×10^{-10}	0.82
$1.0 \times 10^{+6}$	1.24×10^{-1}	3.61×10^{-10}	1.72×10^{-9}	0.17
$1.0 \times 10^{+7}$	1.47×10^{-1}	3.93×10^{-11}	2.04×10^{-9}	0.02

For more precise values of relative tritium levels in the different loops of the NGNP, a detailed description of the tritium kinetics is needed that also takes into account:

- Permeation through the walls of the piping.
- The mass balance of tritium in the SHTS and the hydrogen production system.
- Possible effects of the pressure of He and trace gases on tritium permeability.
- A possible transfer to a linear dependence of the permeation rate on tritium partial pressure for high-quality coatings.

However, the above calculations indicate that permeation barriers on the heat exchange surfaces of the IHX will likely be of limited value when trying to reduce tritium levels in the SHTS. This means that alternative or perhaps complementary routes to lower SHTS tritium levels have to be pursued. Two routes suggest themselves:

- Reduction of the tritium concentration in the PHTS through:
  - Consider adsorption of tritium by graphite fuel spheres and reflector elements, which offers the potential for holding much of the tritium that is produced [5-33].
  - Increasing the mass flow through the HPS (currently the ratio of HPS mass flow and helium mass flow in the PHTS is approximately 1.4×10^{-4}).
  - Add oxidants to the helium inventory of the PHTS to oxidize tritium into tritium oxide (HTO). The product, HTO, permeates much more slowly through the IHX. If this approach results in a significant reduction of the tritium concentration in the PHTS, additional application of a permeation barrier on the heat exchange surface of the IHX might help to reduce the permeation of tritium to the SHTS even more.
- Direct removal of tritium from the coolant in the SHTS through:
  - Consider retention of a SHTS helium purification system with a high tritium removal rate.

- Add oxidants to the SHTS coolant to oxidize tritium to tritium oxide. At NRG Petten, a copper oxide bed is used to form HTO, after which the water is removed from the tritium stream by a molecular sieve bed.

As stated in Section 1.2, a conservative tritium target for offsite drinking water is 100Bq/l. In order to determine how close the above results are to this limit a detailed analysis is required as the design progresses that is both application- and site-dependent.

However, an upper bound order of magnitude estimate of the tritium retention required within the plant can be made now by assuming that the water flow rate from the site is on the order of 200 l/s (representative for a steam process application with injection into the ground). Then the acceptable release to meet the 100Bq/l limit is $2x10^4$ Bq/s. This compares with the amount produced as shown in Figure 2-1 of $7x10^6$ Bq/s, so that a factor of 350 is needed from one or more of the mechanisms and design selections mentioned above. Prior work [5-33] has indicated that through a combination of retention in the reactor graphite and with a high-volume flow HPS on the SHTS that this is achievable.

5.5 Conclusions and Recommendations

The permeation of radioactive tritium out of the PHTS into the SHTS of NGNP is a known safety concern. Due to the large area and thin walls of the IHX heat exchange surface, and the high operating temperature, a considerable amount of tritium might permeate through the heat exchanger surface of the IHX. If the tritium partial pressure in the SHTS becomes too large, significant amounts of tritium can contaminate the hydrogen product stream of the NGNP.

The possibilities for permeation-reducing coatings, and estimates of their effectivity, have been assessed. Main results are that the maximum permeation reduction factor observed in the literature is about 10^4 to10^5 (for SiC or TiC/TiN coatings on the heat exchange surface material). However, these coatings are not tested for industrial applications. A maximum permeation reduction factor of 10^3 can be reached by commercially available aluminizing techniques. If no coatings are applied to reduce the permeation, oxidation during operation of the IHX materials will provide limited permeation reduction of 10^2 or less.

Due to a combination of the large area, small thickness of the boundary between PHTS and SHTS and the high temperature of operation, the permeation of tritium from the PHTS into the SHTS is very efficient. Preliminary calculations that do not take into account permeation through the walls of the PHTS and build-up of tritium in the SHTS, indicate that under normal NGNP operation conditions nearly 100% of the tritium that is produced in the PHTS permeates through the heat exchange surface of the IHX into the SHTS, and that this fraction cannot significantly be reduced by the application of coating materials. Even SiC or TiC/TiN coatings, currently considered to be the most effective permeation reduction coatings, cannot reduce the permeation rate sufficiently.

Therefore it is recommended:

- Focus primarily on tritium removal in the PHTS (graphite, HPS and oxidants) and reduction of the tritium source term in order to reduce the tritium concentration in the SHTS.
- After sufficient reduction of the tritium concentration in the PHTS is realized by one of the above mentioned countermeasures, application of coatings on the heat exchange surface of the IHX will result in a further reduction
- Reduction of tritium concentration in the SHTS (helium purification system and oxidants).
- Perform a detailed study of tritium kinetics taking into account tritium build-up in the SHTS and hydrogen production system as well as permeation through the walls of the transport systems. This will be both an application- and site-dependent analysis.

5.6 References

[5-1] *K. Masui, H. Yoshida and R. Watanabe, Trans. ISIJ 19 (1979), 547.*

[5-2] *Y. Mori and T. Nakada, BNES Conf. on the HTR and Process Appl., Inst. Of Civil Eng., Westminster, London, 26-28 Nov. 1974, Paper 49.*

[5-3] *H.D. Rohrig, R. Hecker, J. Blumensaat and J. Schaefer, Nucl. Eng. Des. 34 (1975), 157.*

[5-4] *R.A. Strehlow and H.C. Savage, Nucl. Tech. 22 (1974), 127.*

[5-5] *G.A. Esteban, A. Perujo, L.A. Sedano, F. Legarda, B. Mancinelli and K. Douglas, JNM 300 (2002), 1.*

[5-6] *J. Schaefer, D. Stoever and R. Hecker, Nucl. Technol. 66 (1983), 537.*

[5-7] *R.N. Wright, Kinetics of gas reactions and environmental degradation in NGNP Helium, INL report for the NGNP program, June 2006*

[5-8] *K. Natesan, A. Purohit and S.W. Tam, Materials behavior in HTGR environments, ANL report, July 2003.*

[5-9] *A. Pisarev, I. Tsvetkov and S. Yarko, Fus. Eng. Des. 82 (2007), 2120.*

[5-10] *H.J. Christ, U. Kunecke, K. Meyer and H.G. Sockel, Oxidation of Metals 30 (1988), 27.*

[5-11] *H.J. Grabke and G. Horz, Ann. Rev. Of Mat. Science 7 (1977), 155.*

[5-12] *R. Harth, W. Jansing and H. Teubner, Nucl. Eng. Des. 121 (1990), 173.*

[5-13] *M.A. Futterer, X. Raepsaet and E. Proust, Fus. Eng. Des. 29 (1995), 225.*

[5-14] *A. Perujo, J. Reimann, H. Feuerstein and B. Mancinelli, JNM 283-287(2000), 1292.*

[5-15] *J.T. Bell, J.D. Redman and H.P. Bittner, Metall. and Mater. Trans. A 11 (1980), 775.*

[5-16] *G.W. Hollenberg, E.P. Simonen, A. Terlain and G. Kalinin, Tritium/Hydrogen barrier development, PNL report for the DOE, 1994.*

[5-17] *P.S. Korinko, High Temperature Environmental Interactions of Inconel 617: A Paper Study for the TEF, Westinghouse Report for DOE, htttp://sti.srs.gov/fulltext/tr2000136/tr2000136.html.*

[5-18] *K.S. Forcey, D.K. Ross and C.H. Wu, JNM 182 (1991), 36.*
[5-19] *K.S. Forcey, A. Perujo, F. Reiter and P.L. Lolli-Ceroni, JNM 299 (1993), 417.*
[5-20] *H. Glasbrenner, K. Stein-Fechner, J. Konys, Z. Voss, O. Wedemeyer, Development of a tritium permeation barrier on F82H-mod. Sheets and on MANET tubes by hot dip aluminizing and subsequent heat treatment, FZK Scientific report, 1998.*
[5-21] *H. Glasbrenner, A. Perujo and E. Serra, Fusion Technol. 28 (1995), 1159.*
[5-22] *D. Levchuk, S. Levchuk, H. Maier, H. Bolt and A. Suzuki, JNM 367-370 (2007), 1033.*
[5-23] *D. Levchuk, F. Koch, H. Maier and H. Bolt, JNM 328 (2004), 103.*
[5-24] *F. Koch, R. Brill, H. Maier, D. Levchuk, A. Suzuki, T. Muroga and H. Bolt, JNM 329-333 (2004), 1403.*
[5-25] *R. Brill, F. Koch, J. Mazurelle, D. Levchuk, M. Balden, Y. Yamada-Takamura, H. Maier and H. Bolt, JNM 174 (2003), 606.*
[5-26] *E. Serra, P.J. Kelly, D.K. Ross, R.D. Arnell, JNM 257 (1998), 194.*
[5-27] *R. Checchetto, M. Bonelli, L.M. Gratton, A. Miotello, A. Sabbioni, L. Guzman, Y. Horino and G. Benamati, Surf. Coat. Techn. 83 (1996), 40.*
[5-28] *P. Wang, J. Liu, Y. Wang and B. Shi, Surf. Coat. Tech. 128-129 (2000), 99.*
[5-29] *Z. Yao, J. Hao, C. Zhou, C. Shan and J. Yu, JNM 283-287 (2000), 1287.*
[5-30] *C. Shan, A. Wu, Y. Li, Z. Zhao, Q. Chen, Q. Huang and S. Shi, JNM 191-194 (1992), 221.*
[5-31] *N. Sakaba, H. Ohashi and T. Takeda, JNM 353 (2006), 42.*
[5-32] *A.J. Magielsen, K. Bakker, C. Chabrol, R. Conrad, J.G. van der Laan, E. Rigal and M.P. Stijkel, JNM 307-311 (2002), 832.*
[5-33] *W. Steinwarz, Tritium in HTR Plants, Juel-2138, Nuclear Research Center Juelich, July 1987.*

6 CONTAMINATION CONTROL RECOMMENDATIONS

The recommendations to be pursued from this study are presented in the context of identifying what was learned in each task, and suggesting what actions may be needed in the future to improve the operation of the NGNP.

6.1 Plant Tritium Source Term Recommendations

The key finding was that the activation of He^3 and Li^6 resulted in a steady state production rate of tritium in the PHTS of 7 x 10^6 Bq/s. The transport analysis performed in subsequent tasks indicates that this quantity, when allowed to permeate to the SHTS, is high. Recommendations for further actions related to the source are:

- Evaluate the specifications for make-up helium, to decrease the allowable He^3.
- Evaluate the specifications for the carbon materials in fuel spheres and in reactor reflectors, to decrease the allowable Li^6.
- Evaluate the design of all plant systems containing helium, with the goal of decreasing the amount of make-up helium required.
- Evaluate lowering the coolant gas temperature entering the IHX.

6.2 Plant Gaseous Carbon-14 Source Term Recommendations

The steady state C^{14} activity in coolant was calculated to be 1.6E+10 Bq, which originates from the activation of nitrogen. The subsequent transport and radiation exposure tasks indicated that this is an acceptable level. If there should be a future need to decrease this quantity, the operating procedures for the plant should be examined to reduce the startup and maintenance operations that allow nitrogen (air) to enter the PHTS.

6.3 Fission Product Source Term Recommendations

The expected fission product sources were calculated for all relevant gaseous and metallic fission products entering the PHTS. The database and models used in the analysis have been extended from the HTR programs carried out in the Federal Republic of Germany. The retention of fission products within the NGNP fuel spheres will depend strongly on fabricating fuel that meets the same quality specifications as the German fuel. The recommendations for meeting the fission product source term goals are:

- Demonstrate the fuel fabrication process so that the product is of equal quality to the earlier German fuel.
- Complete the planned irradiation test program for PBMR fuel.

6.4 Dust Source Term Recommendations

An expected dust generation rate of 48 kg/fpy is based on scaling from the measured dust production in the AVR and THTR plants. Measurements of dust generation should be carried out, as planned, in the PBMR DPP plant.

6.5 Dust and Fission Product Transport Recommendations

The SPECTRA code demonstrated the capability to calculate the quantities and location of dust in the PHTS. The key findings were that small dust particles tend to agglomerate into larger particles while in transit, that 87% of the dust settles in the reactor vessel, that metallic fission products are absorbed quickly by circulating dust, and that a dust layer of up to 50 μm thickness builds up in the IHX. The recommendations related to dust and fission product transport are the following:

- Consider more detailed analysis of the re-suspension model, particularly to increase the number of groups for dust particle size, and to determine the effects of changes in coolant flow rate on re-suspension.
- Evaluate the effects of dust layers in the IHX on the heat transfer.
- Evaluate dust accumulation in the CRD channels to assure there is no impact on control rod insertion.
- Analyze more fully the deposition of Ag-110, to determine the cause of high deposition in some local areas of the PHTS.
- Analyze the content of iodine and metallic fission products in the HPS, as transported by dust.

6.6 Radiation Exposure Recommendations

The locations in the plant for potential radiation exposure have been defined, and the dose rates have been quantified. The results are presented in terms of dose rates as a function of distance from the dose source. The recommendations for further actions are:

- Analyze specific worker actions, which would include the number of workers and the time that they would be exposed.

6.7 Permeation of Tritium Recommendations

The study found that nearly 100% of the tritium source reached the SHTS, and a large fraction would potentially reach a product gas. While the treatment of metallic surfaces to reduce the permeability shows promise, current surface treatments provide insufficient holdup of tritium. The recommendations for improving the retention of tritium are the following:

- Decrease the source from the reactor by the methods identified in Section 6.1.

- Increase the flow rate through the helium purification system, in particular that of the SHTS.
- Develop ceramic IHX materials which greatly increase retention of tritium.

7 LIST OF ASSUMPTIONS

No. **Description**

1. The reactor vessel size, the reactor core, the reflector design, the nuclear control system design and the fuel handling system design are the same for the NGNP as the PBMR DPP.

2. The NGNP power level of 500MWt is scaled from the 400MWt PBMR DPP, and is achieved by lowering the core inlet gas temperature, decreasing the fuel sphere exposure time and accepting a higher off-normal fuel temperature.

3. Core neutron flux distributions for NGNP are derived from detailed analyses performed for the PBMR DPP.

4. Leak rate from the HPB boundary is assumed to be 0.12% per day.

5. ^{3}He content in charged primary coolant is assumed to be 1E-07, as for He extracted from terrestrial sources.

6. Mass of nitrogen in primary circuit from first evacuation and at 6-year maintenance operations is assumed to be 5 Kg.

7. For the source term calculations, the CO and CH_4 concentrations in He coolant are assumed to be 2.2 and 12 ppmv.

10. The GETTER thermo-hydraulic model of the core assumes a cylindrical and not annular geometry. This influences the fuel spheres and mass transfer from the fuel spheres, and both have conservative effects on fission product source calculations.

11. Fuel performance for retention of radionuclides is equal to that of fuel demonstrated in the German HTR programs, as documented in IAEA TECDOC-978.

12. The 60 years of plant operation at 95% capacity factor was assumed in transport calculations to be 57 years continuously, with no variations in coolant flow rate.

13. The specific activities of fission products adsorbed to dust were not calculated explicitly; but rather, the activities measured in AVR were used as a basis.

APPENDIX A: 90% Review Presentation Slides

Contamination Control Study

90% Design Review

April 24, 2008

Westinghouse NGNP Team

Objectives of Study

- Determine sources of radionuclides and dust in primary and secondary circuits during normal operation
- Determine transport rates and deposition of dust and fission products in the primary circuit
- Evaluate potential radiation exposure and maintenance impact due to contaminants in the primary circuit
- Provide information on tritium permeation through metals

Presentation Outline

Background: Scope of Contamination Control Study

Task 1: Radionuclides and Dust Source Terms

- Subtask 1.1: Plant Tritium Source Term
- Subtask 1.2: Plant Gaseous C14 Source Term
- Subtask 1.3: Fission Product Source Terms
- Subtask 1.4: Dust Source Term

Task 2: Dust and Fission Product Transport

- Subtask 2.1: Development of Analytical Model
- Subtask 2.2: SPECTRA Transport Analyses

Task 3: Expected Radiation Exposures

Task 4: Permeation of Tritium

Final Report Outline

Section	
	Summary and Conclusions
	Introduction
1.0	NGNP Description and Operational Requirements
2.0	Radionuclide and Dust Source Terms (Task 1)
3.0	Dust and Fission Product Transport (Task 2)
4.0	Expected Radiation Exposures (Task 3)
5.0	Permeation of Tritium (Task 4)
6.0	Contamination Control Recommendations
7.0	List of Assumptions

Reference PBMR Nuclear Heat Supply for Contamination Control Study

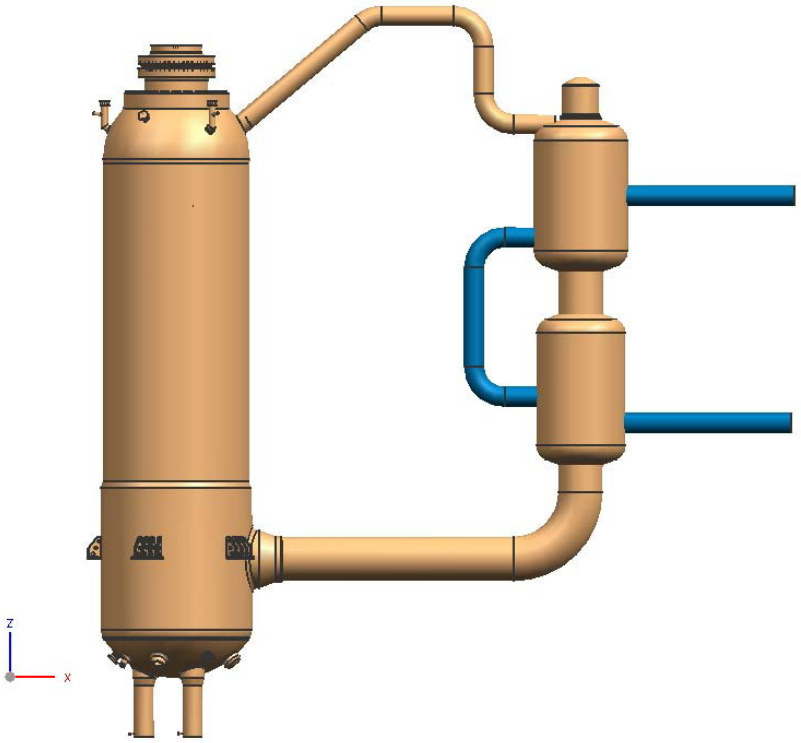

- Reactor Unit from PBMR Demonstration Power Plant
- Primary Heat Transport System (PHTS) coupled to Secondary Heat Transport System (SHTS) via two Intermediate Heat Exchangers (IHX A & IHX B) in series
- Pressure biasing from SHTS to PHTS
- PHTS circulator mounted at top of IHX B vessel
- Fuel Handling System and Helium Purification System also form portions of primary Helium Pressure Boundary

IHX Coolant Flow Paths

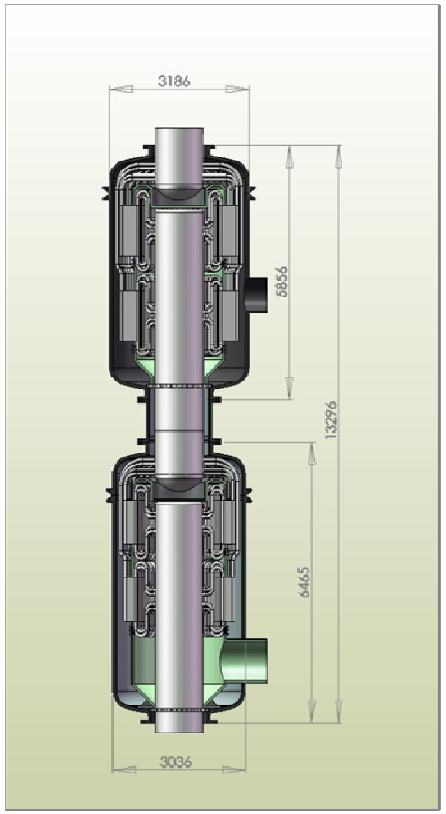

IHX B

IHX A

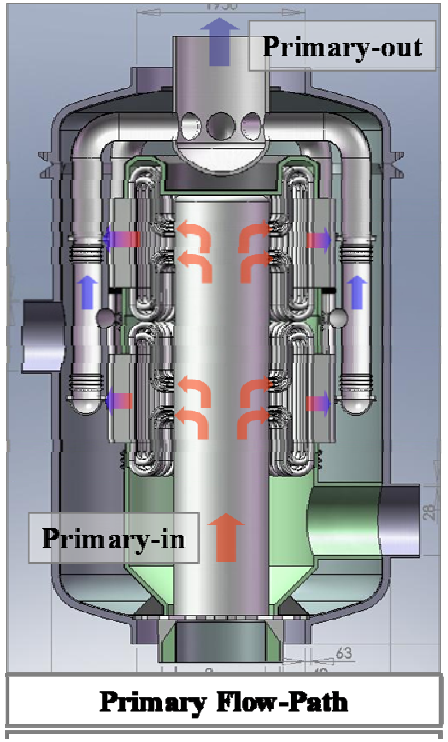

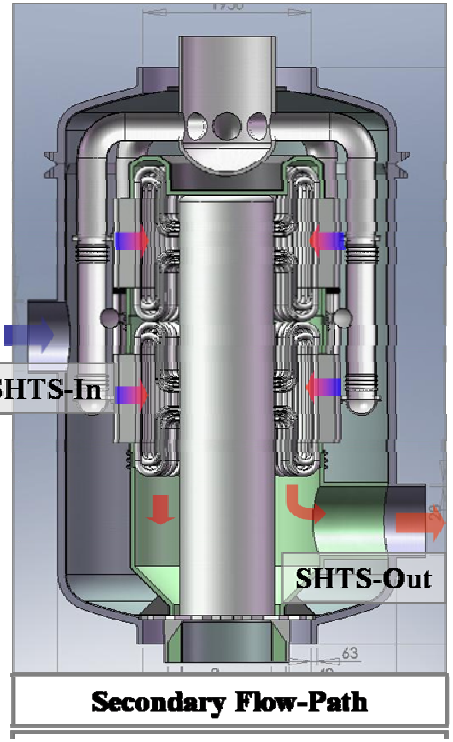

- Internal flow paths are the same for IHX A/B
- Vessel liner (not shown) required for active cooling of IHX A vessel

Westinghouse NGNP Team

Key NHSS Parameters

Parameter	NHSS Value
Module power, MWt	500
Reactor coolant T_{in} , °C	350
Reactor coolant T_{out} , °C	950
Coolant pressure, MPa	9.0
Coolant flow rate, Kg/sec	160
Fuel sphere cycles over life	6
Fuel spheres in core	452,000
Average fuel sphere life, Yr	2

Subtask 1.1: Tritium Source Term Historical Basis

- Tritium mass balances were measured in past HTGRs
  - AVR
  - Peach Bottom Unit 1
  - Fort St Vrain
  - THTR
- Tritium source was primarily from activation of He-3 and Li-6
- Tritium in circulation correlated with make-up helium histories

Subtask 1.1: Tritium Source Term Background

- PBMR DPP parameters and fluxes adapted for NGNP
- $^{3}He(n,p)^{3}H$ and $^{6}Li(n,\alpha)^{3}H$ two dominant production mechanisms
- Differential equations provide time-dependent tritium production rates

Details of Tritium Source Term Model

- Average Helium mass-weighted RU + PHTS neutron flux obtained for $^{3}He(n,p)^{3}H$ production calculation
- Average core neutron flux obtained for $^{6}Li(n,\alpha)^{3}H$ production calculation
- ^{3}He content taken as 1E-07, as for He extracted from terrestrial sources
- ^{6}Li content of Fuel Spheres (FS) taken from PBMR DPP specifications

Time-dependent Tritium Production Rate

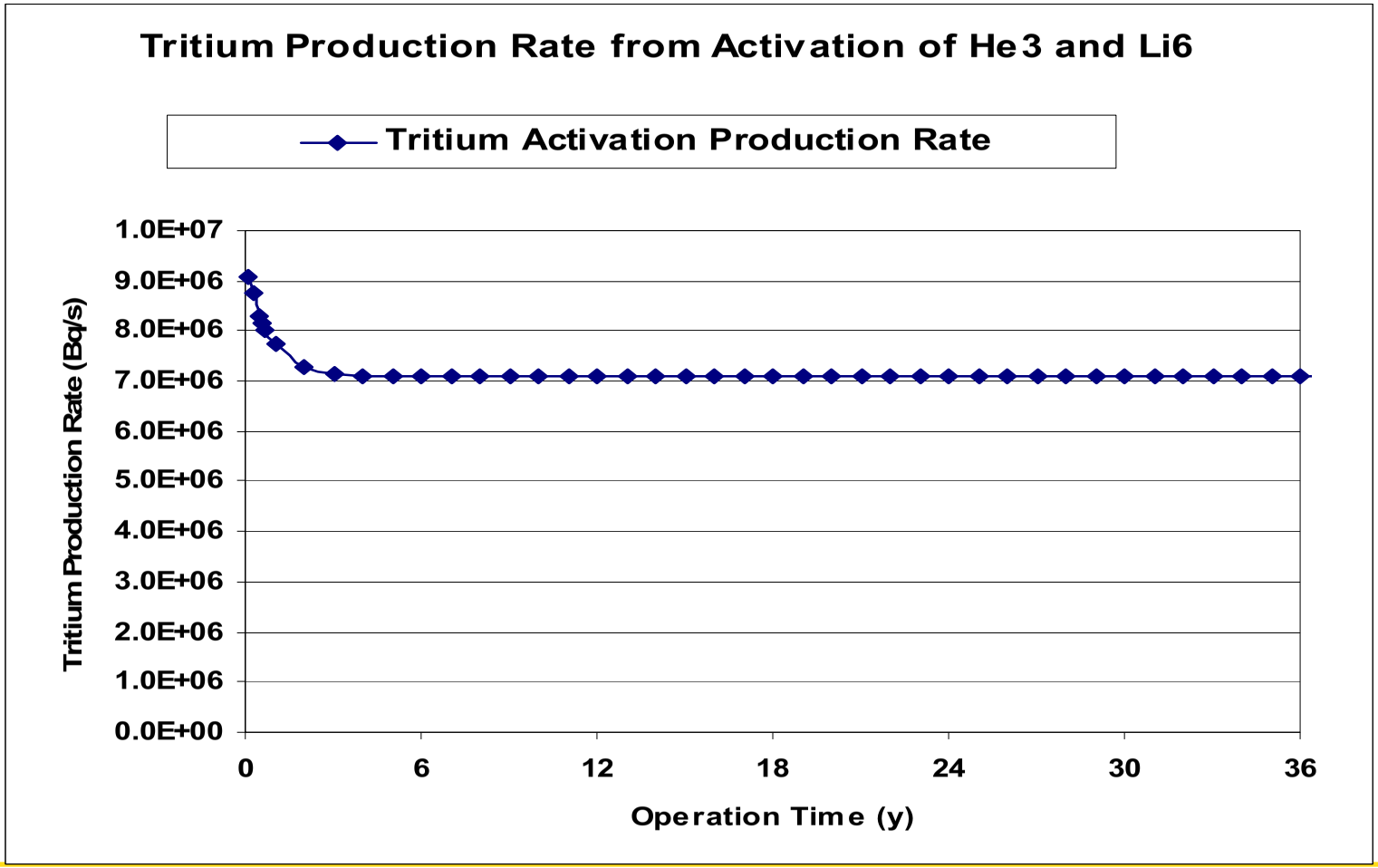

Westinghouse NGNP Team

Subtask 1.2: Gaseous C-14 Source Term Historical Basis

- C-14 inventories were measured in past gas cooled reactors
  - AVR
  - Peach Bottom Unit 1
  - Fort St Vrain
  - THTR
  - Advanced Gas Cooled Reactors in UK

- Source of C-14 is predominantly from activation of nitrogen

Gaseous C-14 Source Term Background

- PBMR DPP parameters and fluxes adapted for NGNP ^{14}C source terms
- Differential equations provide time-dependent ^{14}C production rate

Details of Gaseous C-14 Source Term

- $^{14}N(n,p)^{14}C$ reaction considered for production
- Mass of N_2 from first evacuation and 6 year maintenance is 5 kg
- N_2 from FS migrating into primary coolant is 40 ppm (N_2 per C)
- Mass of carbon per fuel sphere is 189 g
- Ratio of C atoms in FS to number of C atoms at surface is 630
- CO and CH_4 concentrations in He coolant are 2.2 and 12 ppmv

Time-dependent C-14 Coolant Activity

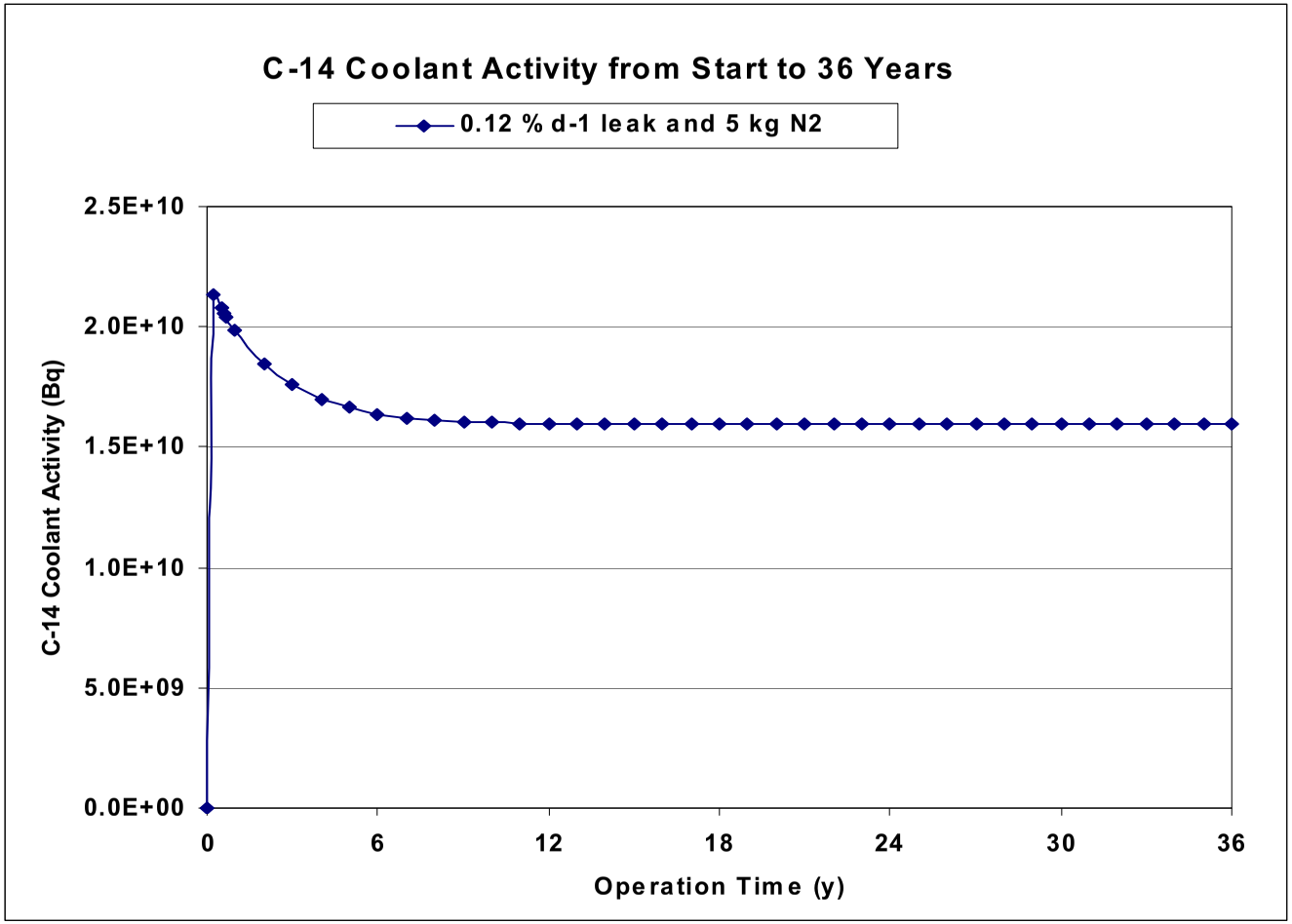

Westinghouse NGNP Team

Subtask 1.3: Fission Product Source Term Background

- Based on German (HRB)calculation models
- Fuel performance parameters from German tests (IAEA TECDOC 978)
- Models from PBMR DPP applied to NGNP
  - Gaseous fission product release model (Kr, Xe, I and Br):
    - Based on the Booth model, applied in the NOBLEG code
    - Steady state approximations
  - Metallic fission product release model (Cs, Ag, Sr):
    - Based on Fick's 2nd law of diffusion, applied in the GETTER code
    - Dynamic release from fuel spheres

Approach for Fission Product Source Term

- Neutronic design and thermal conditions calculated from PBMR DPP (400 MWt, 500 °C RIT, 900 °C ROT design)
- Power raised for NGNP 500 MWt
- Mass flow rates adjusted for NGNP (350 °C RIT, 950 °C ROT)
- Parameters and correlations used are based on German reference data
- Only steady state conditions considered
- Constant failed particle fraction of 1.44×10^{-5}
- Effective uranium contamination in the matrix material of 2.0×10^{-6}

Fission Product Model Validation

- All software has been reverse engineered, and numerical and analytical solutions mathematically verified
- Specific subroutines have been compared with other software products and benchmarked against some irradiation test results
- Complete lifecycle V&V plans are available that include integral effects testing against existing and planned irradiation tests and eventual evaluation of plant performance

Expected Key Gaseous Fission Product Releases

Nuclide	Half-life (hours)	Activity Released from Core (Bq)
Kr-85	9.40E+04	4.36E+10
Kr-88	2.80E+00	8.97E+10
Kr-90	8.97E-03	1.07E+10
Xe-133	1.27E+02	2.75E+11
I-131	1.93E+02	1.44E+11

Expected Key Metallic Fission Product Releases

	^{137}Cs	^{134}Cs	^{110m}Ag	^{111}Ag	^{90}Sr
Core release rate (atoms/s)	1.28×10^{13}	5.71×10^{11}	1.90×10^{13}	1.91×10^{11}	6.33×10^{9}
Core activity release rate (Bq/s)	9 330	6 110	604 000	206 000	4.83

Subtask 1.4: Dust Source Term
Background

- AVR data from dust experiments provide dust quantities, characterization, and radionuclide content
  - Dust measured in helium purification gas filters
  - Dust sampled from in-reactor Vampyr-I and Vampyr-II probes
- THTR examined dust in primary system components
  - Values reported for quantity of dust and specific activities
- PBMR DPP analysis predicted sources using AVR/THTR data
  - Quantity, particle size, specific activity, and deposition locations determined by analyses

Approach to Dust Source Term

- Identify dust production mechanisms
  - Locate sources in Core and FHSS
  - Identify metallic dust
- Assess dust production rate
  - Show expected rate based on AVR and THTR
  - Calculate NGNP values from 400 MWt PBMR DPP
- Assess size of dust generated
  - Provide tables of dust size distribution
- Identify mechanisms for dust-bound activity
  - Provide logic for radionuclides attaching to dust

Key Data from German Program

- AVR determined quantitative values
  - Dust was predominantly graphite
  - Rate was correlated to operating conditions
  - Mean particle size was 0.8 micron
  - Principal activity was Co-60, Cs-137 and Ag-110m
- THTR determined qualitative values
  - Dust posed no problems for operation or safety
  - Principal activity was Co-60, Sr-95, Hf-181 and Pa-235
- Siemens estimated rate for 200 MWt Modul design
  - Dust rate of 10 mg per FS per pass

Calculation of NGNP Dust Rate

- German test data scaled to PBMR DPP
  - Scaled for thermal power, core height, fuel cycle rate, core temperature and coolant chemistry
- PBMR DPP values adjusted for NGNP parameters
  - Dust generation rate and particle size are quantified

NPNG Dust Generation Rate

Graphite dust source	Dust generation rate (kg/fpy)
Core (pebble bed, side reflectors and bottom reflector)	28
FHSS (dust before filtering)	20
Total other sources	<1

Dust Size Distribution for NGNP
Based on AVR Tests

Average Dust Particle Size (µm)	Normalised Number Distribution (%)	Normalised Volume Distribution (%)
0.202	6.09	0.03
0.353	14.43	0.42
0.493	27.01	2.12
0.632	24.77	4.09
0.873	9.79	4.27
1.218	7.90	9.34
1.598	3.74	9.99
1.953	2.37	11.57
2.322	1.56	12.82
2.718	1.04	13.69
3.078	0.45	8.51
3.458	0.85	23.15

Task 2: Dust & FP Transport
Background

- Analytical Model for NGNP follows PBMR DPP application
- Graphite dust and fission products circulate with helium coolant through PHTS and reactor unit, and deposit in different PHTS locations
- Deposited dust may have negative effect on behavior of PHTS components (circulator and IHX)
- Fission products deposited in PHTS and attached to dust particles cause potential radiation exposure to maintenance workers

Approach for Dust & FP Transport

- The PHTS and reactor unit of NGNP are included in the SPECTRA model
- Analyses represent normal operation conditions during NGNP lifetime
- Graphite dust and fission products are included in the model through source terms
- Effects of helium purification system and system leakage are represented as negative sources (sinks) for fission products and dust

Subtask 2.1: Development Analytical Model
SPECTRA Code

- NRG developed in-house SPECTRA code as system analysis code for nuclear and non-nuclear systems
- Thermal hydraulic models are based on RELAP5, TRAC, ATHLET, CATHARE experience and literature studies
- Fission product and dust transport models are based on AVR, THTR experience, and best available models from literature survey
- SPECTRA extensively used for V&V of thermal hydraulic analysis for PBMR DPP design S201 and older DPP designs
- SPECTRA recently used for fission product and dust transport analysis for PBMR DPP design S201

SPECTRA Application

SPECTRA (Sophisticated Plant Evaluation Code for Thermal-hydraulic Response Assessment) is a fully integrated system analysis code, that models thermal-hydraulic behavior of Nuclear Power Plants, including reactor cooling system, emergency and control systems, containment and reactor building of various plant types:

- BWR,
- PWR,
- HTR.
- It can also be used to assess thermal-hydraulic response of non-nuclear plants, for example cooling systems of chemical reactors.

SPECTRA
Code organization

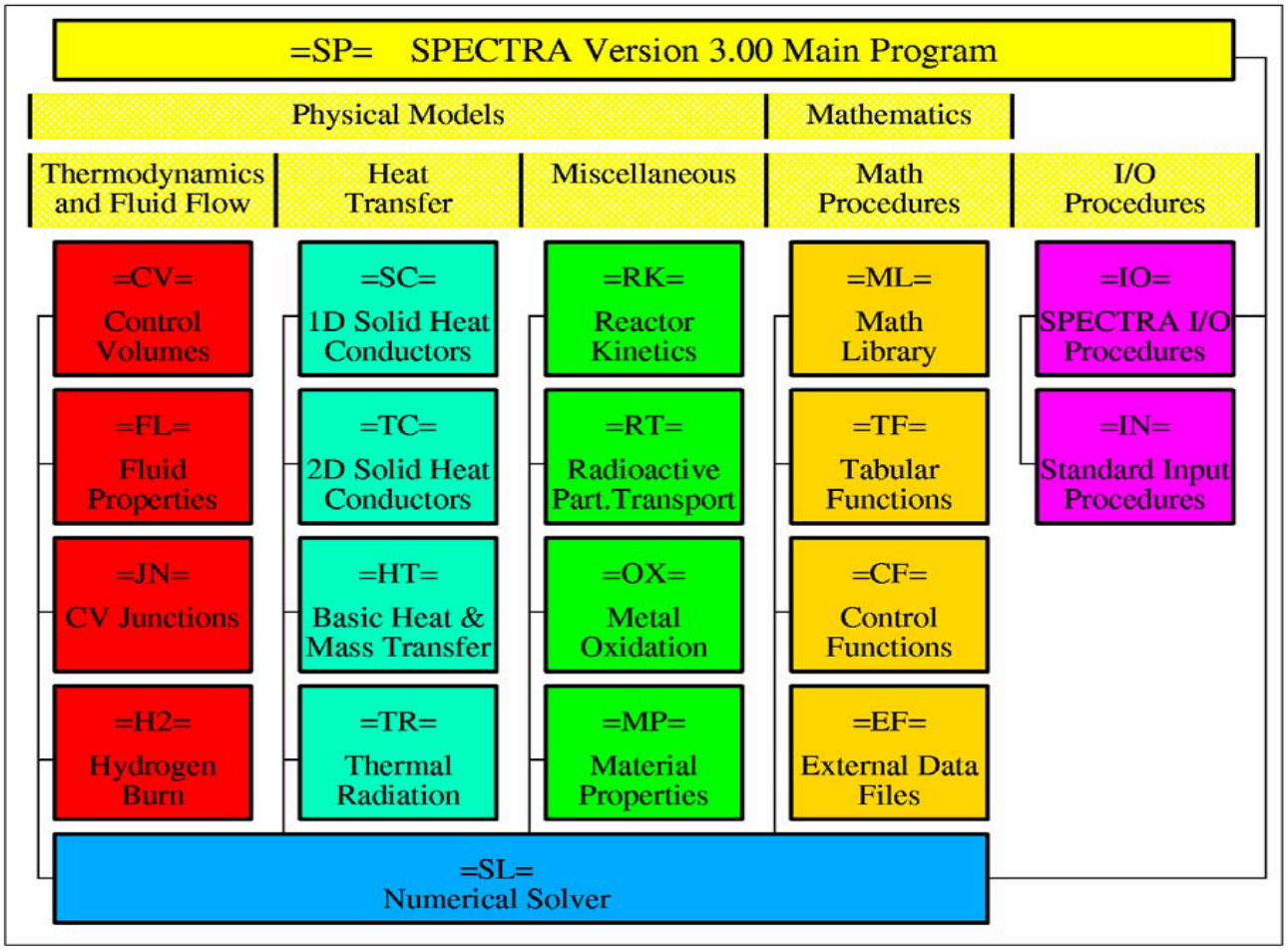

SPECTRA
RT Package

- A detailed description of the code is provided in the Code Manuals
- The most important part of the code for the NGNP analysis is the Radioactive Particle Transport Package – the RT Package
- The RT Package deals with:
  - Aerosol (dust) particles transport, deposition and re-suspension.
  - Fission product release and transport and interactions..

SPECTRA
Aerosol Dynamics

- The aerosol particles, which vary in size, are represented in the code using discrete size sections

- Each size section is characterised by its characteristic (average) particle size, diameter and shape factors. The maximum number of aerosol size sections is 20

- Shape factors may be used to account for non-spherical shape of particles. Values may be found in literature

SPECTRA
Aerosol Deposition

- The following deposition mechanisms are considered:
  - Gravitational deposition
  - Brownian
  - Thermophoresis
  - Diffusiophoresis
  - Turbulent impaction
  - Inertial impaction
  - Pool scrubbing
  - Filters
- Aerosols can deposit on the surfaces of 1-D and 2-D Solid Heat Conductors, as well as on a pool surface.

SPECTRA
Aerosol Coagulation

- The coagulation kernel is calculated in SPECTRA taking into account three mechanisms:
  - Gravitational coagulation, K_{grav}
  - Brownian coagulation, K_{Brown}
  - Turbulent coagulation, K_{turb}

- The total coagulation kernel, K, is calculated assuming that the three kernels may be added, similarly as in most aerosol codes:

$$K = K_{grav} + K_{Brown} + K_{turb}$$

SPECTRA
Coagulation Deposited Particles

- In SPECTRA the deposited aerosol particles of a given size section are assumed to coagulate into a larger size section (characterized by its diameter, d_j) if the deposited layer thickness, t, exceeds the particle diameter, d_j, multiplied by a user-defined factor (XDC1RT).

- Default value of the factor is 1.0.

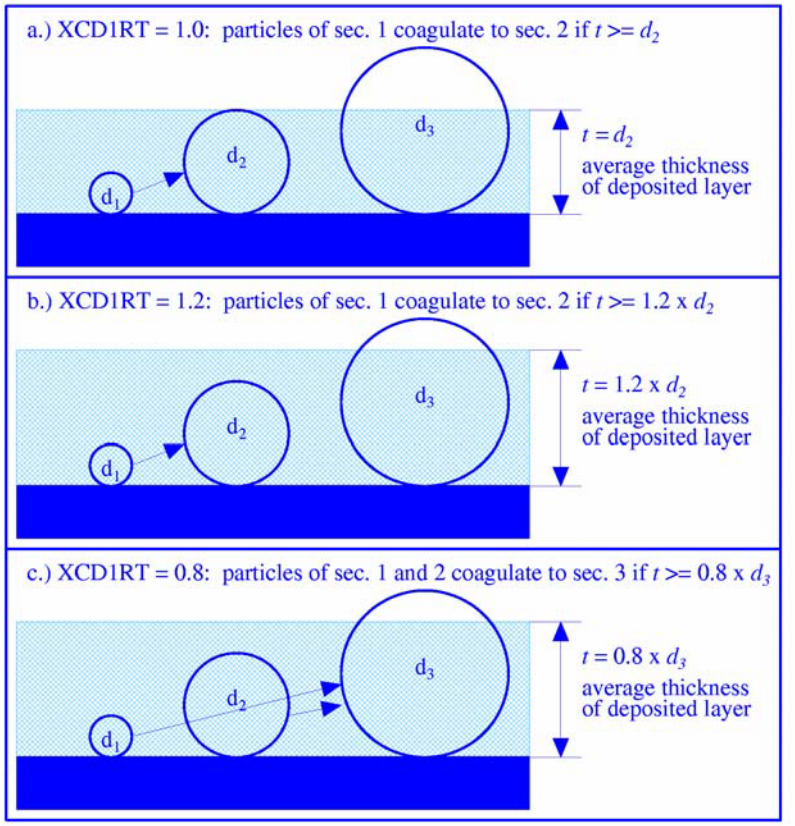

SPECTRA
Re-Suspension

- Two existing models, the Rock'n Roll model and the Vainshtein et al. model are available. Additional two problem-specific models, developed at NRG, are implemented.
- Adhesion force distribution is approximated by a discrete sections, called: "F_a-sections". Typically a log-normal distribution is used. Upon resuspension the distribution changes as the weakly-bound particles are resuspended.

Initial distribution

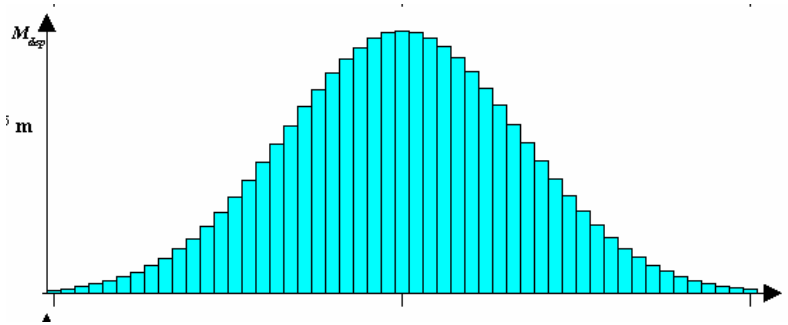

Resuspension

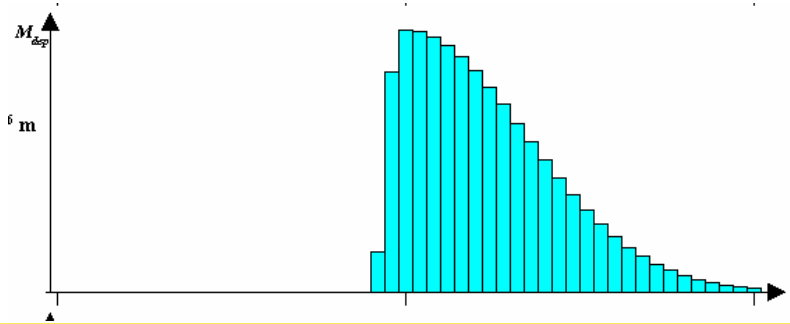

SPECTRA
Re-Suspension Models, continued

- The Rock'n Roll model gives somewhat more conservative results (higher re-suspension). Therefore the Vainshtein model can be considered as a best-estimate model, while the Rock'n Roll as a conservative model.
- A key factor in successful re-suspension predictions is a good knowledge of the adhesion force and its distribution for dust particles deposited on rough surfaces.
- Although a re-suspension model is typically used to calculate liftoff of particles during accident conditions, it is also important to use the re-suspension model for stationary state calculations. During stationary state particles, are continuously deposited. The weakly bound particles are immediately blown off, therefore the remaining particles are those with higher adhesion force. Therefore the adhesion force distribution is a result of gas flow during stationary state.

SPECTRA
Fission Products

- Decay chains
  - About 300 isotopes may be tracked
  - Built-in data include 10 decay chains (about 50 isotopes) of the most important fission products
  - Initial masses of isotopes
    - Calculated outside SPECTRA (for example ORIGEN code).
    - Calculated internally, using an average fuel burn-up, defined by the user.

SPECTRA
Fission Products

- Fission products are divided into classes. A fission product class groups isotopes which have similar properties. There are 12 default classes.

Release class	Member elements	Default member elements
1	Xe, He, Ne, Ar, Kr, Rn, H, N	Xe, Kr
2	Cs, Li, Na, K, Rb, Fr, Cu	Cs, Rb
3	Ba, Be, Mg, Ca, Sr, Ra, Es, Fm	Ba, Sr
4	I, F, Cl, Br, At	I, Br
5	Te, O, S, Se, Po	Te, Se
6	Ru, Rh, Pd, Re, Os, Ir, Pt, Au, Ni	Ru, Rh, Pd
7	Mo, V, Cr, Fe, Co, Mn, Nb, Tc, Ta, W	-
8	Ce, Ti, Zr, Hf, Th, Pa, Np, Pu, C	Zr
9	La, Al, Sc, Y, Ac, Pr, Nd, Pm, Sm, Eu, Gd, Tb,Dy, Ho, Er, Tm, Yb, Lu, Am, Cm, Bk, Cf	Y -
10	U	-
11	Cd, Hg, Zn, As, Sb, Pb, Tl, Bi	Sb
12	Sn, Ga, Ge, In, Ag	-

SPECTRA
Fission Product Release

- Each isotope is assigned to a release class. For each release class one of three models is available for release calculation:
  - CORSOR-M (for LWR-s)
  - ARSAP (for LWR-s)
  - User-defined Control Function (general, possible for HTR)

SPECTRA
Fission Product Vapors

- Each isotope is assigned to a fission product vapor class. The vapor classes do not need to be the same as the release classes
- The vapor saturation pressures are provided for all vapor classes
- The fission product vapors may condense on cold surfaces or in the atmosphere (gas space) of a Control Volume. If a vapor condenses in the atmosphere, it is assumed to condense on the surface of existing aerosols, or form new aerosols
- The fission product vapors may react with surfaces (sorption)

SPECTRA
Fission Product Sorption on Surfaces

- Three models are implemented in SPECTRA:
  - User-defined function.
  - Simple model similar to the MELCOR model.
  - Full model – discussed below.

- Transport of the vapor from the bulk gas to the δ-sublayer (mean free path).
- Adsorption of the vapor from the δ-sublayer to the wall material, where the part β remains on the surface as reversibly bound molecules, while the part (1–β) penetrates into the material (absorption).
- Desorption of the molecules that are reversibly bound at the surface back to the δ-sublayer.
- Eventual evaporation of the molecules that have penetrated into the material from the surface node into the δ-sublayer.

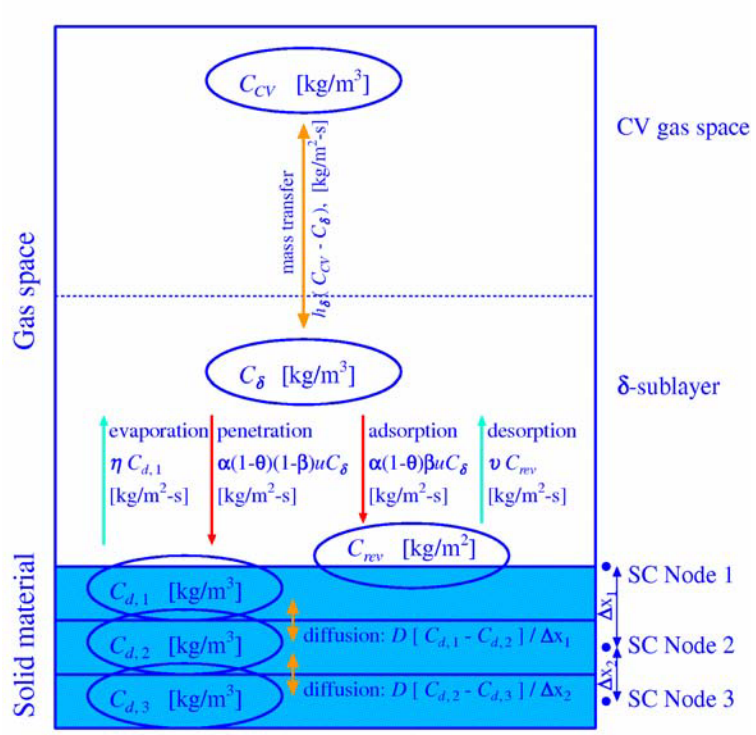

Westinghouse NGNP Team

SPECTRA
NGNP Nodals

- Pebble bed: 33 Control Volumes (CV), divided into 11 axial levels, and 3 radial rings
- Fuel spheres: 1-D Solid Conductors (SC).
  - Each SC is divided into 6 nodes of 0.005 m
  - Inner 5 nodes: fuel material; outermost node: graphite coating.
- Heat transfer in pebble bed:
  - Convective heat transfer between pebbles and helium.
  - Pebble-to-pebble radiation and between pebbles and other structures.
- Heat exchangers A and B: five nodes with the Temperature Averaging (TA) concept, allowing to model a heat exchanger using relatively few nodes.
- Heat transfer – the default correlation set in SPECTRA replaced by the correlation specific to the heat exchangers.

SPECTRA
NGNP Nodal Scheme

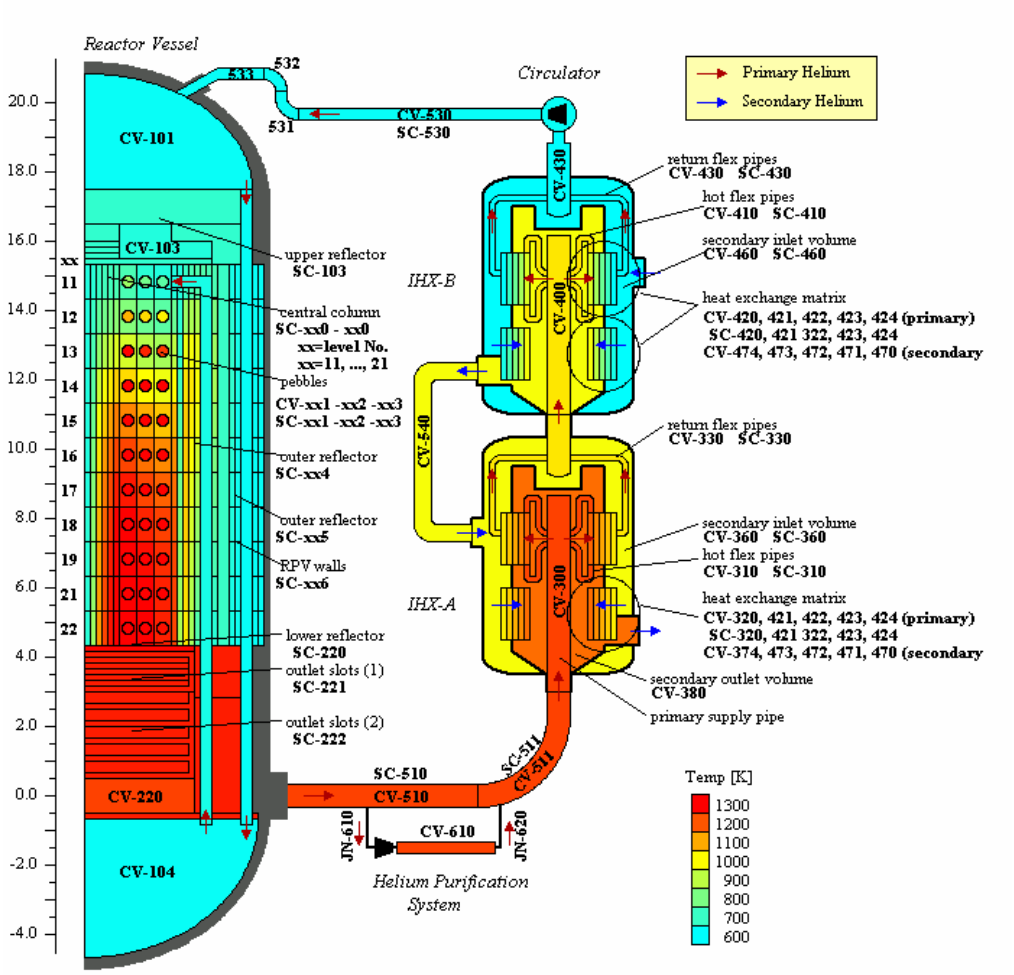

Westinghouse NGNP Team

NGNP Model
NGNP Aerosol Modeling

- Aerosols are divided into 15 size sections
  - 12 sections based on reference data from PBMR.
  - 3 additional sections are used to allow coagulation of deposited particles.

Size section No.	D_p, μm
1	0.202
2	0.353
3	0.493
4	0.632
5	0.873
6	1.218
7	1.598
8	1.953
9	2.322
10	2.718
11	3.078
12	3.458
13	10.00
14	20.00
15	50.00

SPECTRA
Aerosol Modeling of Source

- Aerosol sources - Core
  - Total core source: 28 kg/fpy = 8.88×10^{-7} kg/s.
  - The mass sources for each size section were defined by multiplying this number by the normalized volume fractions for the sections. These sources were placed in CV-220 (Control Volume just below the core).
- Aerosol sources – Fuel Handling System (FHSS)
  - Total source from FHSS: 20 kg/fpy. An aerosol filter is present. The efficiency of the filter is assumed to be: 99.99% for particles larger than 0.5 μm and 0.0 for particles smaller than 0.5 μm. The dust mass source behind FHSS filter is 0.516 kg/fpy = 1.64×10^{-8} kg/s.
  - The mass sources for each size section were defined by multiplying this number by the distribution fractions downstream the filter. These sources were placed in CV-510 (Core Outlet Pipe).

SPECTRA
Aerosol Modeling

- **Deposition**
  - All deposition models are active on all surfaces. The pipe bend inertial impaction models are activated on the bends (SC-511, SC-531, SC-532)
- **Coagulation**
  - All coagulation models are active for all Control Volumes.
  - Coagulation of deposited particles is activated on all surfaces (XCD1RT=1.0).
- **Re-Suspension**
  - The re-suspension model of Vainshtein is active on all surfaces. This model was selected as it gave good results for the Storm experiment as well as the Reeks and Hall experiments. The alternative model (Rock'n Roll) gives higher re-suspension than measured.

SPECTRA
Sorption Modeling

- Full sorption model is used.
- Sorption of three FP vapor classes is modeled. The sorption coefficients are obtained from IAEA-TECDOC-978:

	Penetration	Desorption	Evaporation
– Class 2:	$(1-\beta)=10^{-5}$	$u=10^{11}\exp(-28150/T)$	$\eta=0.0$
– Class 4:	$(1-\beta)=0.0$	$u=10^{11}\exp(-21666/T)$	$\eta=0.0$
– Class 12:	$(1-\beta)=10^{-5}$	$u=10^{11}\exp(-30670/T)$	$\eta=0.0$

- Note that these classes include several isotopes that are being adsorbed in the same way:
  - Vapor class: 2: Cs, Rb
  - Vapor class: 4: I, Br
  - Vapor class: 12: Ag
- Neither sorption nor desorption model is active for other vapor classes. This means that the decay daughter products of the adsorbed isotopes are remaining inside the material.

SPECTRA
HPS Filters

- HPS filter efficiency for dust is 90% for particles >0.5 μm
- The HPS fission product filter data was obtained from Fort St Vrain SAR. The values shown there are stationary activities for the cases with and without the filter.
- The filter removal factor is defined as the ratio of the activity with the filter to one without the filter.
- The filter efficiency (SPECTRA input) is for the analysis defined as:

  $\eta = RF$

Subtask 2.2: Transport Analysis
Steady State 100% Power (1)

A quick plant start-up was simulated, with reactor power reaching 100% in 10 seconds, and the circulator reaching the nominal speed in 3 seconds.

Calculations were performed until all parameters (temperatures, pressures) were stable.

The results are summarised in the table and the visualization of the results presented in the next slide.

Parameter	Value
Reactor power [MWt]	500
Reactor inlet pressure [kPa]	8985
Reactor outlet pressure [kPa]	8741
Primary mass flow [kg/s]	160
Secondary mass flow [kg/s]	160
Heat transfer IHX-A [MW]	156.9
Heat transfer IHX-B [MW]	351.6
Primary Temp in, IHX-A [°C]	949
Primary Temp out, IHX-B [°C]	336
Secondary Temp in, IHX-B [°C]	287
Secondary Temp out, IHX-A [°C]	899
Circulator power [MW]	8.5

Transport Analysis Results
Steady State 100% Power (2)

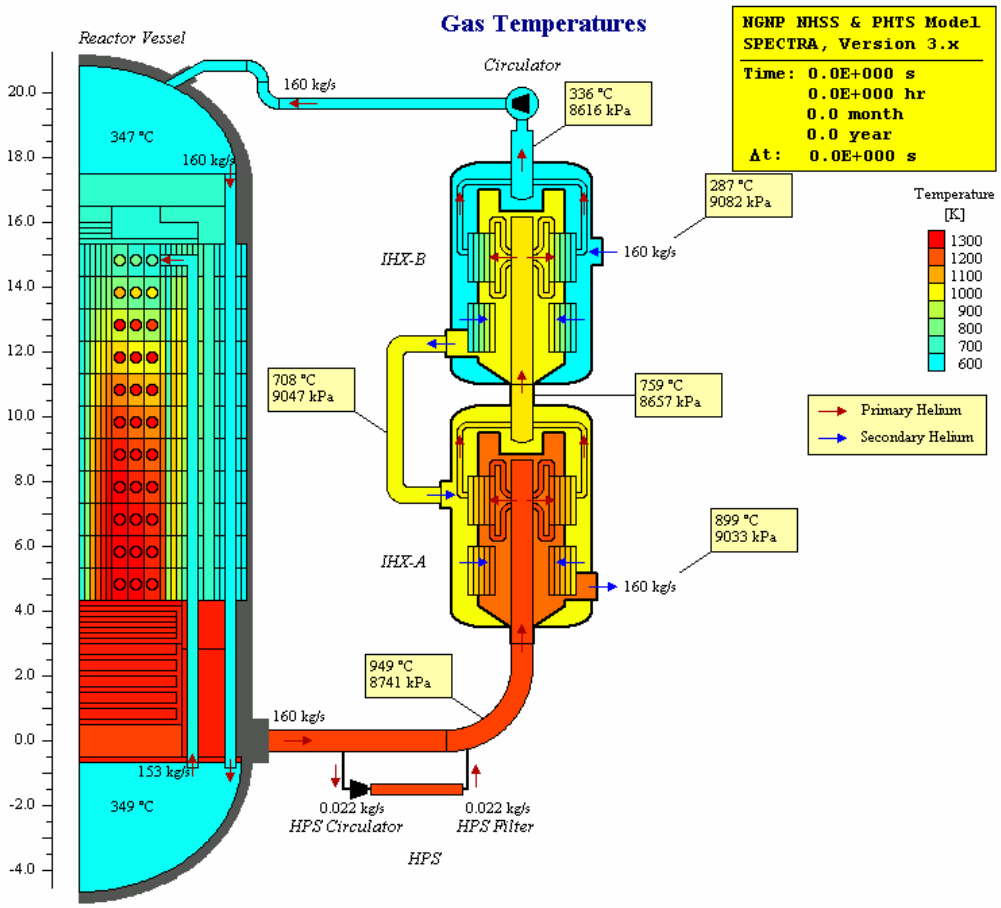

Reactor

Power: 500.0 MW (100 %)
Avg PB flow: 137 kg/s
Total RV flow: 160 kg/s
Inlet temperature: 620 K (347 °C)
Outlet temperature: 1222 K (949 °C)

Circulator

Volumetric flow: 24.0 m3/s
Mass flow: 159.6 kg/s
Speed: 160.2 rev/s Power: 8.5 MW
Pressure ratio: 1.0425 Blower dP: 369 kPa

IHX-A

Primary side	cell-1	cell-2	cell-3	cell-4	cell-5
Re number	1433	1463	1494	1526	1560
St.Pr$^{2/3}$	0.013	0.013	0.013	0.013	0.013
HTC [kW/m^{2}K]	4.38	4.33	4.29	4.24	4.20

Power: 155.7 MW

Secondary side	cell-5	cell-4	cell-3	cell-2	cell-1
Re number	1091	1066	1041	1018	996
St.Pr$^{2/3}$	0.014	0.015	0.015	0.015	0.015
HTC [kW/m^{2}K]	3.18	3.21	3.25	3.28	3.31

Power: 155.7 MW

IHX-B

Primary side	cell-1	cell-2	cell-3	cell-4	cell-5
Re number	1134	1203	1280	1368	1468
St.Pr$^{2/3}$	0.014	0.014	0.014	0.013	0.013
HTC [kW/m^{2}K]	3.25	3.14	3.04	2.93	2.81

Power: 348.8 MW

Secondary side	cell-5	cell-4	cell-3	cell-2	cell-1
Re number	1380	1272	1180	1100	1030
St.Pr$^{2/3}$	0.013	0.014	0.014	0.014	0.015
HTC [kW/m^{2}K]	3.53	3.64	3.76	3.87	3.97

Power: 348.8 MW

Westinghouse NGNP Team

Transport Analysis Results
Dust Deposition (1)

- Calculation was performed for the expected plant life-time of 60 years with an average availability of 95%. The total run time is therefore 57 years

- The next slide shows transport of dust in the PHTS. This transport is characterized by the dust particles per unit volume (in millions of particles per cubic meter, Mp/m^3)

- In spite of deposition in IHX-A & IHX-B, the particle density increases behind the heat exchangers. This effect is caused by an increase of the gas density due to decreasing gas temperature

Transport Analysis Results
Dust Deposition (2)

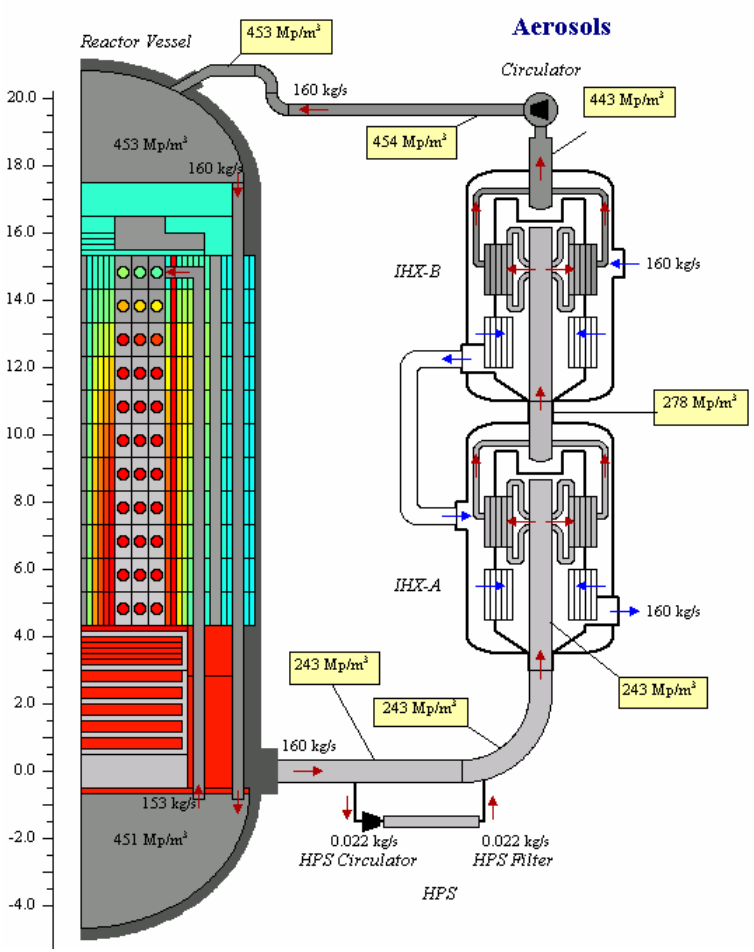

NGNP NHSS & PHTS Model
SPECTRA, Version 3.x

Time: 1.8E+009 s
5.0E+005 hr
694.4 month
57.0 year
Δt: 1.0E+002 s

Aerosol density [part/m³]	Temperature [K]
5.0E+008	1300
4.0E+008	1200
3.0E+008	1100
2.0E+008	1000
1.0E+008	900
0.0E+000	800
	700
	600

Primary Helium
Secondary Helium

Deposited Aerosols

Reactor Vessel	Mass [kg]	Activity [Bq] Cs-137	Ag-110m
Pebbles:	1.26E+002	1.26E+012	2.01E+011
Graphite struct.:	1.28E+003	1.28E+013	2.05E+012
Metallic struct.:	1.46E+001	1.46E+011	2.33E+010
Total:	1.42E+003	1.42E+013	2.27E+012

IHX-A	Mass [kg]	Activity [Bq] Cs-137	Ag-110m
Structures:	1.01E+000	1.01E+010	1.62E+009
Plates:	2.35E+001	2.35E+011	3.77E+010
Total:	2.46E+001	2.46E+011	3.93E+010

IHX-B	Mass [kg]	Activity [Bq] Cs-137	Ag-110m
Structures:	1.17E+000	1.17E+010	1.88E+009
Plates:	1.26E+002	1.26E+012	2.02E+011
Total:	1.27E+002	1.27E+012	2.04E+011

Pipes	Mass [kg]	Activity [Bq] Cs-137	Ag-110m
Core outlet pipe:	9.05E+000	9.05E+010	1.45E+010
Core inlet pipe:	2.88E+001	2.88E+011	4.61E+010

HPS Filter	Mass [kg]	Activity [Bq] Cs-137	Ag-110m
Filter:	1.76E+001	1.76E+011	2.82E+010

Global Parameters	Mass [kg]	Activity [Bq] Cs-137	Ag-110m
Airborne:	6.39E-001	6.39E+009	1.02E+009
Deposited:	1.63E+003	1.63E+013	2.60E+012
Total dust:	1.63E+003		
Integrated src.:	1.63E+003		
Total - Int. src.:	-3.50E-009		

Westinghouse NGNP Team

Transport Analysis Results
Dust Deposition (3)

Dust deposition - steady state

Location	Deposited dust		
	Mass [kg]	Fraction Total [%]	Fraction PHTS [%]
Reactor vessel	1420.	87	
IHX-A	24.6	1.5	12
IHX-B	127	7.8	61
Core Outlet Pipe	9.1	0.6	4
Core Inlet Pipe	28.8	1.8	14
HPS filter	17.6	1.1	8

Dust deposition on IHX plates

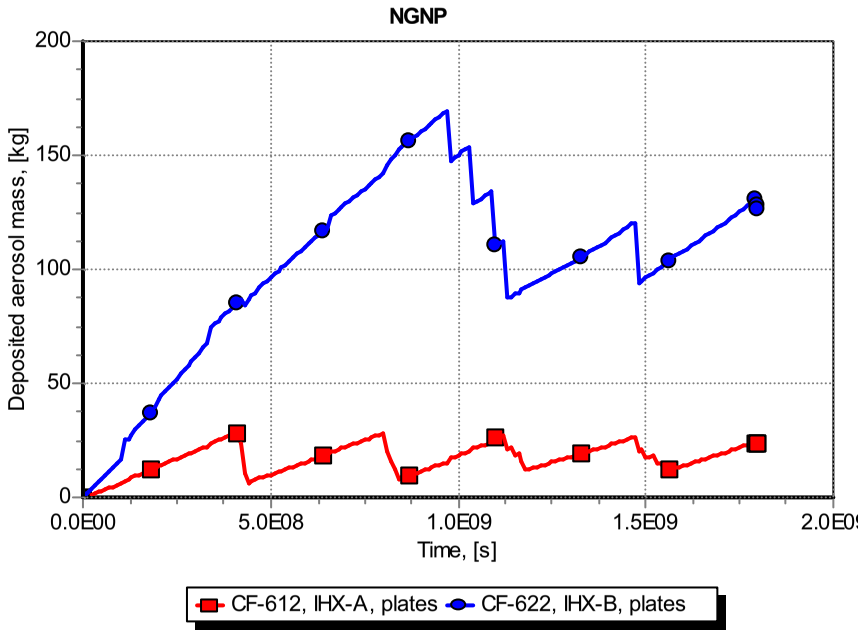

Westinghouse NGNP Team

Transport Analysis Results
Dust Deposition (4)

Deposited layer on IHX-A plates

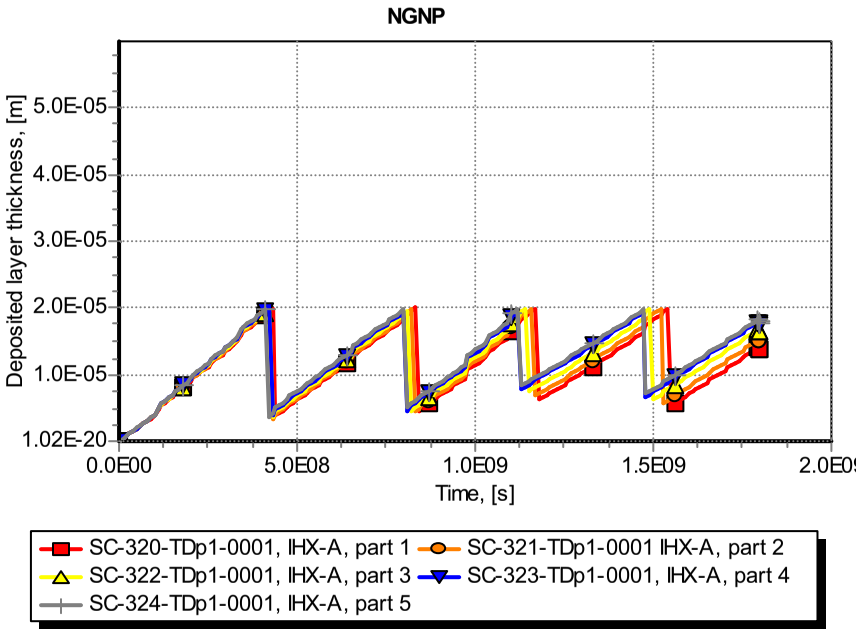

Deposited layer on IHX-B plates

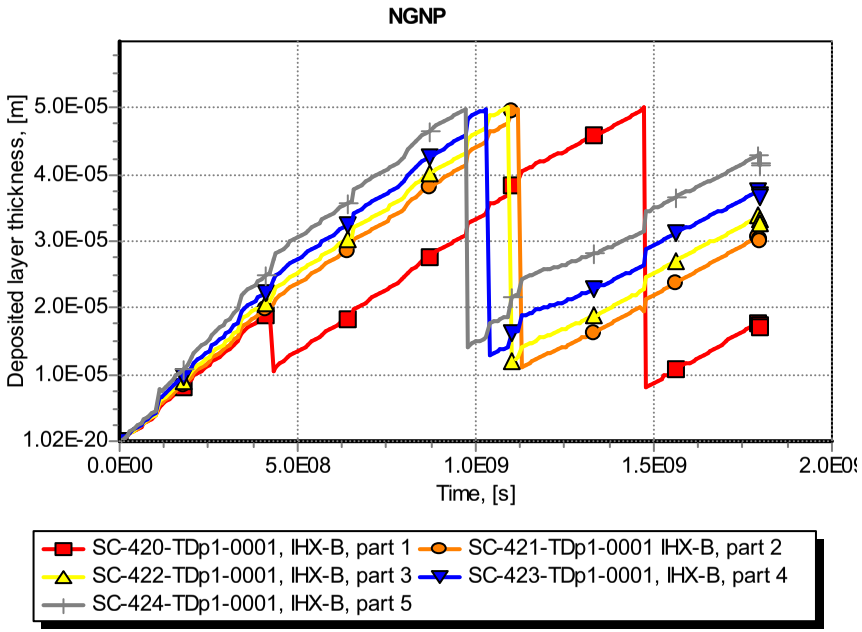

Transport Analysis Results
Dust Deposition (5)

- Dust deposited on the IHX plates agglomerates into larger particles, that are easily resuspended. Resuspensions of agglomerated particles are clearly visible on the heat exchanger plates:
  - For IHX-A these resuspensions occur when particles coagulate into 20 μm particles.
  - For IHX-B these resuspension occurs when particles coagulate into 50 μm particles (size section 15). The 20 micron particles are not resuspended in IHX-B because the velocities are lower than in IHX-A (lower temperature, thus higher density)
- Because the deposited layer is <20 μm in IHX-A and <50 μm in IHX-B, the deposited mass is much larger in IHX-B than in IHX-A.
- The results depend strongly on the assumed size sections (20, 50 μm). Therefore it would be better to use more size sections.

Transport Analysis Results
Dust Deposition (6)

Deposited mass in pipes

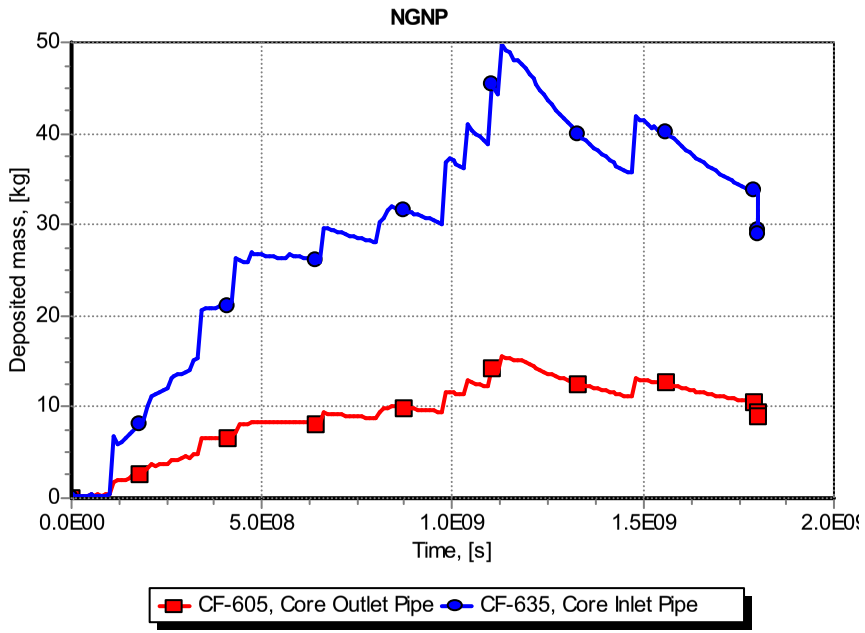

Westinghouse NGNP Team

Transport Analysis Results
Dust Deposition (7)

Deposited layer on Core Outlet Pipe

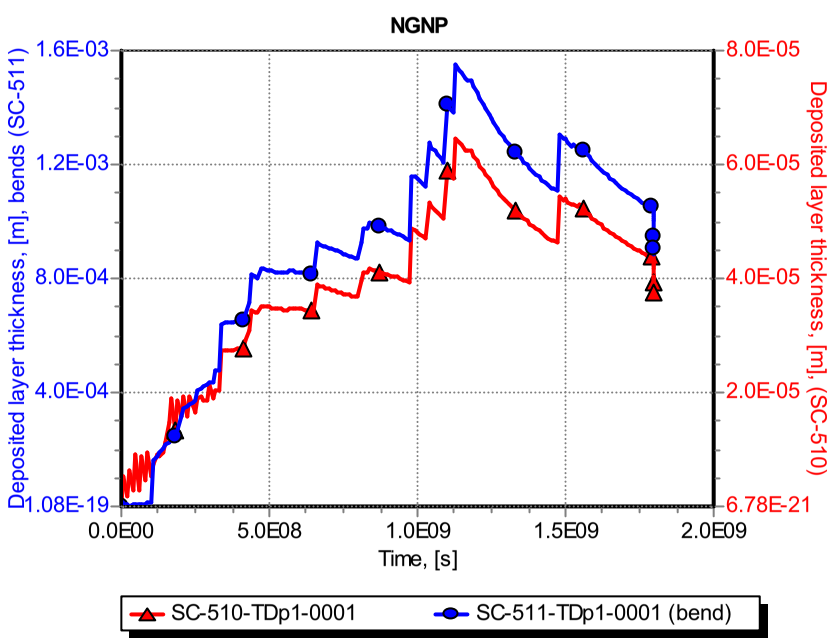

Deposited layer on Core Inlet Pipe

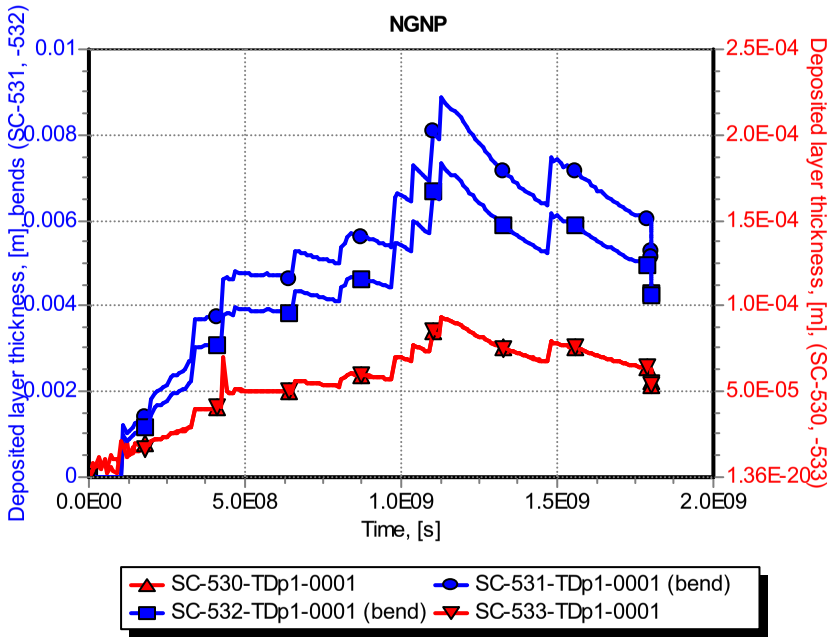

Westinghouse NGNP Team

Transport Analysis Results
Dust Deposition (8)

- Deposition on the core inlet pipe (CIP) is larger than the deposition on the core outlet pipe (COP) because gas velocity is smaller there (larger gas density). Therefore fewer particles are resuspended in core inlet pipe.
- During the sudden resuspensions from the IHX plates a large amount of large particles enter the gas.
- These particles deposit mainly on the pipe bends because the inertial impaction is important for large particles.
- Deposited layer is more than an order of magnitude larger on the bends than on the straight pipes.

NGNP Transport Analysis
Activity Dust

- Activities of the fission products attached to the dust particles were estimated in a simplified way, since no suitable model coefficients are available for sorption on graphite dust particles. The AVR measured dust-bound activities were 10^6 to 10^8 Bq/g for Cs-137 and 5×10^4 to 5×10^7 Bq/g for Ag-110m (IAEA-TECDOC-978, Table 6-1).

- The geometrical average values were taken for the present analysis to estimate the dust-bound activities:

$$\sqrt{10^6\times10^8} = 10^7\ Bq/g \qquad = 1.0\times10^{10}\ Bq/kg$$
$$\sqrt{5\times10^6\times5\times10^8} \approx 1.6\times10^6\ Bq/g \qquad = 1.6\times10^9\ Bq/kg$$

Transport Analysis Results
Dust Deposition Summary

The dust related results are summarized as follows:

- 87% of the dust generated in the core region and from the FHSS settles down inside the reactor vessel
- The remaining dust is deposited within the PHTS, mainly in the Intermediate Heat Exchangers and on the pipe bends
- Because of the very small flow through the HPS, the effect of the HPS filters on the dust in the PHTS is rather small (only about 8% as much dust is trapped by the filter as is deposited within the PHTS).

Transport Analysis Results
Fission Products on Structures (1)

Table on next slide gives the activities of the radionuclides Iodine, Cesium and Silver that are adsorbed after 57 years of operation on the metallic structures of the PHTS:

- Core Outlet Pipe
- IHX A
- IHX-B
- Core Inlet Pipe
- HPS Filter

Neither sorption nor desorption model is used for noble gases. Therefore the decay daughter products of the adsorbed isotopes are remaining inside the material.

Transport Analysis Results
Fission Products on Structures (2)

NGNP NHSS & PHTS Model
SPECTRA, Version 3.x

Time: 1.8E+009 s
5.0E+005 hr
694.4 month
57.0 year
At: 1.0E+002 s

Activities [Bq]
Isotopes present in the metallic surfaces (daughter-products not included)

Adsorbed isotopes:
- Vapor class 2 : Cs, Rb
- Vapor class 4 : I, Br
- Vapor class 12 : Ag

Isotope	Core Outlet Pipe	IHX-A	IHX-B	Core Inlet Pipe
Cs-134	1.98E+010	2.18E+012	5.14E+013	7.43E+011
Cs-135	1.35E+004	1.58E+005	8.65E+006	3.35E+005
Cs-137	1.53E+010	2.90E+011	1.15E+013	3.81E+011
Cs-138	5.54E+007	1.54E+010	4.83E+010	2.28E+009
Cs-139	2.03E+007	6.73E+009	1.59E+010	7.18E+008
Cs-140	4.25E+007	1.45E+010	3.30E+010	1.47E+009
Rb-90m	5.64E+007	1.90E+010	4.40E+010	1.98E+009
Rb-90	1.35E+006	4.48E+008	1.05E+009	4.76E+007
Rb-88	1.99E+008	5.98E+010	1.60E+011	8.10E+009
Rb-89	2.91E+007	8.91E+009	2.35E+010	1.19E+009
I-131	1.82E+008	5.65E+009	1.23E+011	4.78E+009
I-132	8.75E+007	2.05E+010	1.22E+011	2.66E+009
I-133	2.03E+008	1.49E+010	1.67E+011	5.47E+009
I-134	1.17E+008	3.49E+010	1.87E+011	3.74E+009
I-135	1.52E+008	2.17E+010	1.62E+011	4.27E+009
I-136	1.16E+007	3.93E+009	1.94E+010	3.58E+008
Br-83	1.98E+007	4.56E+009	2.72E+010	5.98E+008
Br-84	2.01E+007	6.32E+009	3.28E+010	6.44E+008
Br-85	1.02E+007	3.47E+009	1.72E+010	3.21E+008
Ag-110m	1.90E+010	9.52E+011	1.80E+013	1.24E+011
Ag-111	1.91E+008	9.74E+009	1.81E+011	1.24E+009

Transport Analysis
Fission Products in Gas Flow (1)

Table in next slide gives the activities (Bq) of the noble gasses that are circulating in the gas at 57 years for the following fluid volumes of the PHTS:

- Core Outlet Pipe
- IHX A
- IHX-B
- Core Inlet Pipe

Transport Analysis Results
Fission Products in Gas Flow (2)

Table gives the activities (Bq) of the noble gasses that are circulating in the gas at 57 years.

Isotope	Activity (Bq)
Xe-131m	1.02×10^{7}
Xe-133m	1.25×10^{8}
Xe-133	2.63×10^{9}
Xe-135m	8.00×10^{8}
Xe-135	6.44×10^{10}
Xe-137	2.23×10^{9}
Xe-138	3.89×10^{9}
Xe-139	-
Xe-140	-

Isotope	Activity (Bq)
Kr-83m	2.04×10^{9}
Kr-85m	5.03×10^{9}
Kr-85	1.33×10^{6}
Kr-87	4.30×10^{9}
Kr-88	1.35×10^{10}
Kr-89	2.15×10^{9}
Kr-90	-
Kr-91	-

Transport Analysis Results
Fission Products Ag-110m and Cs-137

- Figure in next slide shows summed activities of Cs-137 and Ag-110m for:
  - Core Outlet Pipe
  - IHX A
  - IHX-B
  - Core Inlet Pipe
- The Ag-110m reaches equilibrium between source and decay in a few years
- The Cs-137 activity is slowly increasing during the whole period

Transport Analysis Results
Adsorbed Ag-110m Activity

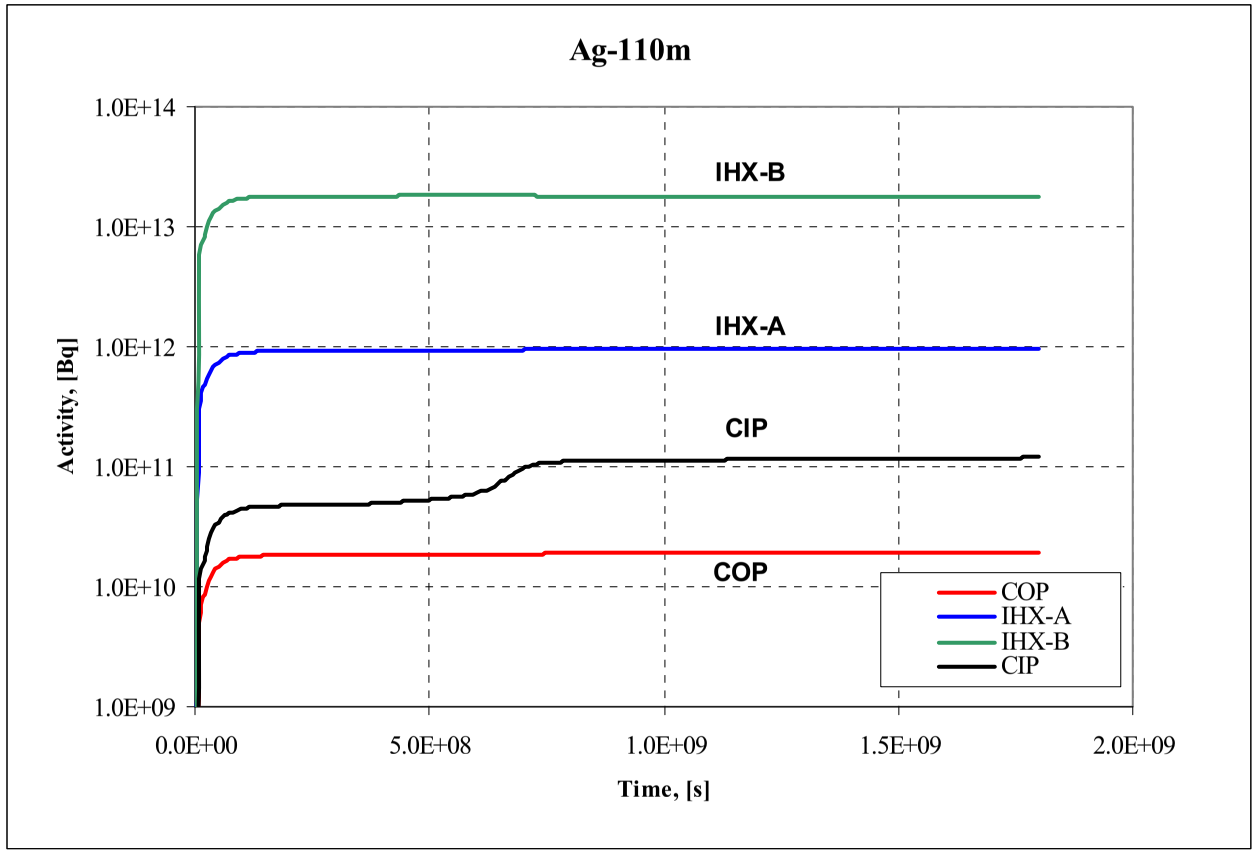

Westinghouse NGNP Team

Transport Analysis Results
Adsorbed Cs-137 Activity

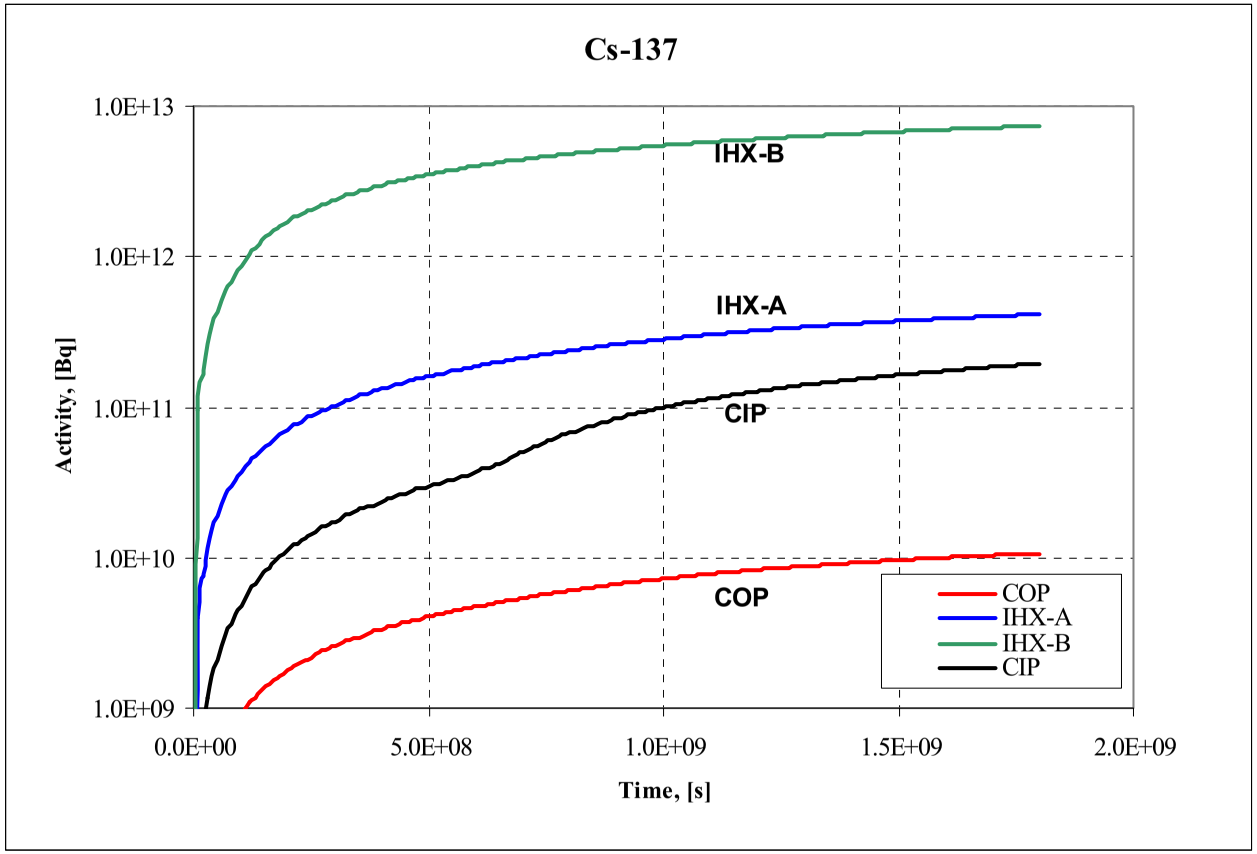

Westinghouse NGNP Team

Transport Analysis
Conclusions

- 87% of the dust generated in core region and FHSS is deposited in the reactor vessel. The remaining graphite dust is deposited in the IHX A and B and on the pipe bends
- Because of the very small flow through the HPS, the effect of the HPS filters on the dust in the PHTS is rather small (only about 8% as much dust is trapped by the filter as is deposited on the PHTS)
- In the present calculation the additional resistance for the heat transfer and for the gas flow caused by the deposited dust was neglected.
- Because the deposition layer in IHX is strongly affected by resuspension of agglomerated particles, the influence of using different size sections for the agglomerated (large) particles) should be investigated

Task 3:Radiation Exposures
Background

- Fission products condensed and attached to dust in PHTS cause potential radiation exposure to workers performing maintenance or inspection work

Radiation Exposures Approach

- Total depositions calculated with SPECTRA code for four regions: CIP, IHX-A, IHX-B and COP
- Calculated nuclide specific total activities (Bq) at 95% level of 60 years accumulation (deposited activity in Bq/cm^2 and circulating activity in Bq/cm^3)
- For both deposited and circulating activity external dose rates calculated with MicroShield code for five relevant locations (dose points)
- Only activity outside the reactor vessel and biological shielding taken into account

Radiation Exposures
Locations of Exposure Points

Elevation view

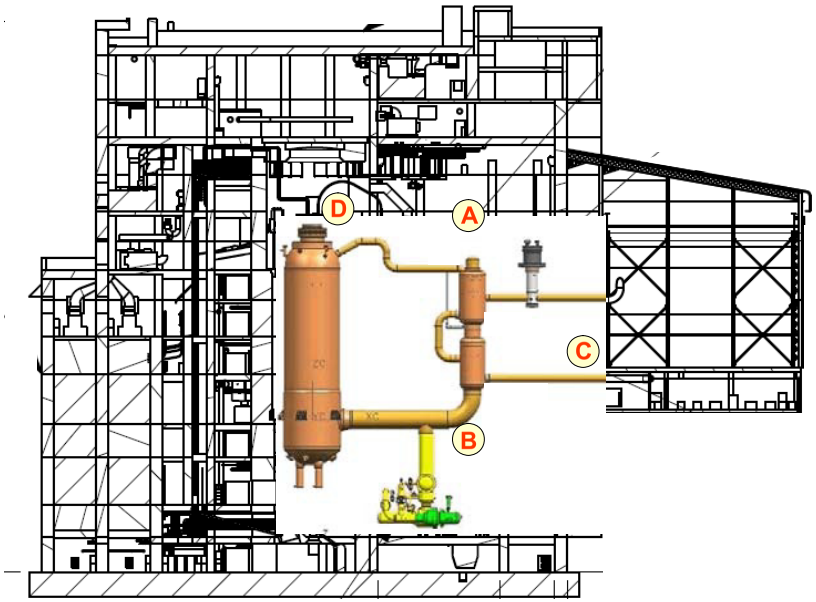

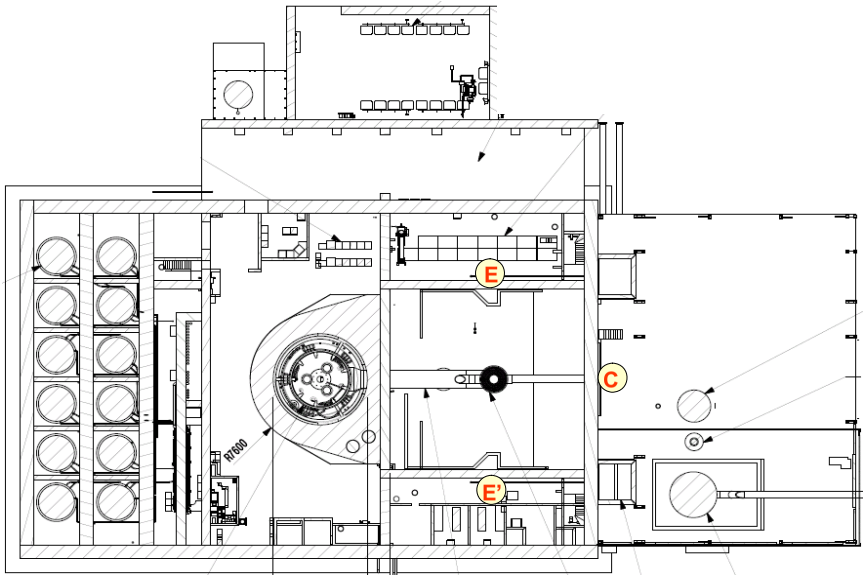

Westinghouse NGNP Team

Radiation Exposures
Calculation Model

Example calculation model, horizontal part COP

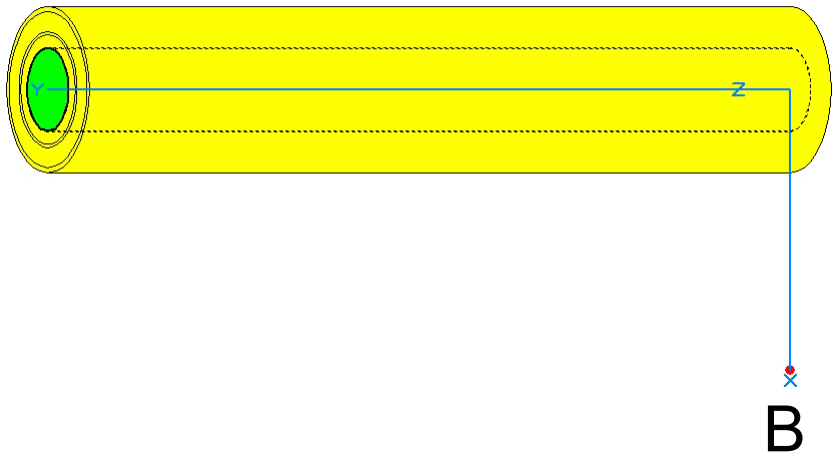

Dimensions:

Length : 1070 cm
Diameter : 103.4 cm

Shielding:

Iron : 0.8 cm, 7.86 g/cm^3
Inconel: 16 cm, 7.95 g/cm^3
Iron : 4 cm, 7.86 g/cm^3
Helium : 25 cm, 0.0012 g/cm^3
Iron : 6.3 cm, 8.86 g/cm^3
Air gap: 250 cm, 0.0012 g/cm^3

Source medium:

Helium: 9 MPa, 0,016 g/cm^3

Radiation Exposures
Dose Rates at Designated Locations

Source		Dose Rates (μSv per hour)				
		A	B	C	D	E
Core Outlet Pipe	Dust MFP GFP		0.15 0.45 14.5			
IHX-A	Dust MFP GFP		0.3 53 0.5	$9.4\ 10^{-9}$ $4.7\ 10^{-5}$ $1.2\ 10^{-6}$		$3.2\ 10^{-6}$ $3.2\ 10^{-3}$ $8.3\ 10^{-5}$
IHX-B	Dust MFP GFP	$8.3\ 10^{-5}$ $1.7\ 10^{-1}$ $1.5\ 10^{-4}$		$5.2\ 10^{-8}$ $6.5\ 10^{-4}$ $2.0\ 10^{-7}$		$1.8\ 10^{-5}$ $4.9\ 10^{-2}$ $1.8\ 10^{-5}$
Core Inlet Pipe	Dust MFP GFP	$4.0\ 10^{-4}$ $3.3\ 10^{-2}$ $3.0\ 10^{-3}$	11.5 96 6.1		880 7290 470	
Total		$2.1\ 10^{-1}$	183	$7.0\ 10^{-4}$	8640	5.210^{-2}

Dose Rates CIP as Function of Distance

Maximum dose rate at location D near Core Inlet Pipe

8.6 mSv/h, dose rate decreases rapidly with distance

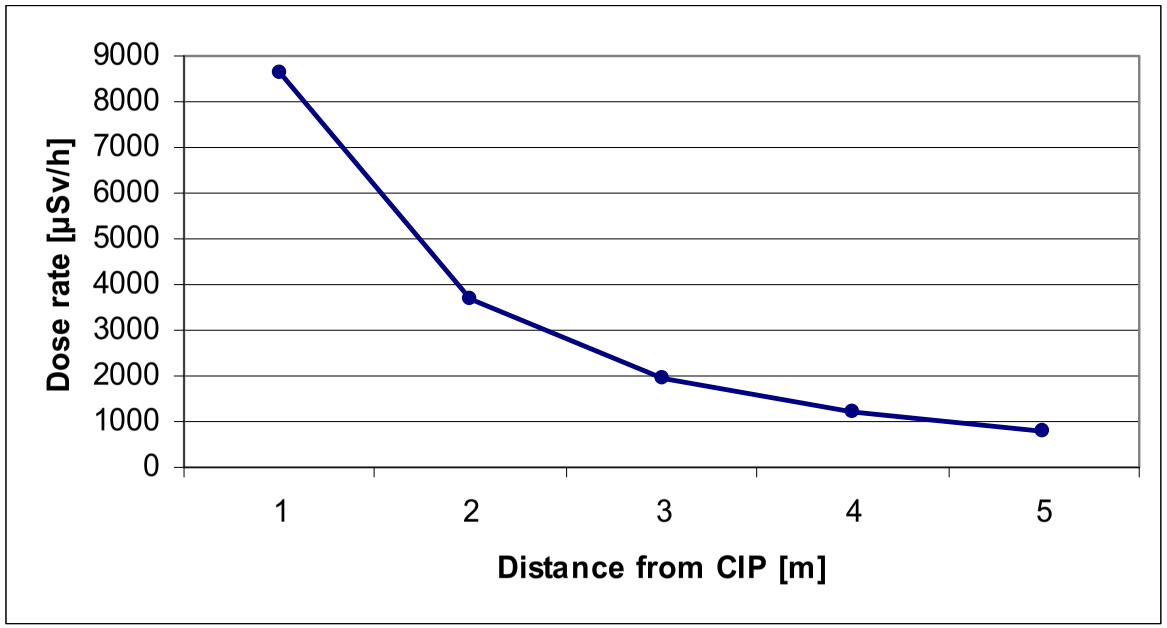

Allowable Worker Time at Locations

Based on maximum allowable exposure of 50 mSv per year is the maximum allowable worker time at designated locations:

- At locations A, C and E (shielding by concrete structures): no restrictions
- At location B (inside heat exchanger hall):
  275 h/a
- At location D (near reactor vessel head):
  6 – 60 h/a depending on distance from core inlet pipe and without additional shielding

Task 4: Permeation of Tritium
Background

- The high temperature in IHX and the properties of selected materials (Incoloy 617 for IHX A and Incoloy 800 for IHX B) results in tritium permeation into the SHTS
- The large area-to-thickness ratio of the IHX heat exchange surface contributes to a large permeation flux into the SHTS
- Tritium permeation is a diffusion-limited process according to Sievert's Law
- Tritium from the SHTS could be transported into power conversion system and/or the hydrogen production system

Tritium Permeation
Literature Research

- **Sievert's Law:**

$$k(t) = \frac{\Phi}{PRF} \cdot \frac{A}{L} \cdot \left(\sqrt{p_{T,PHTS}(t)} - \sqrt{p_{T,SHTS}(t)} \right)$$

- **Hydrogen permeability (Φ) of IHX alloys (Incoloy 800, Inconel 617)**
  - Φ (Inconel 617, IHX A, T= 950 ^{0}C) $8 \cdot 10^{-10}$ mol s^{-1} m^{-1} $Pa^{-0.5}$
  - Φ (Incoloy 800H, IHX B T = 760 ^{0}C) $6 \cdot 10^{-10}$ mol s^{-1} m^{-1} $Pa^{-0.5}$
  - Similar Φ values for other Nickel-based alloys (Hastelloy XR)
  - Slightly lower Φ value for Tritium as compared to Hydrogen

- **Permeation Reduction Factors (PRF)**
  - natural oxide (mainly Cr_2O_3) 10^2-10^3 (may be unstable for IHX A)
  - Al_2O_3 coating ~10^3 (commercial, stable)
  - SiC and TiC/TiN coating 10^4-10^5 (tests on small scale)

Tritium Permeation
Assumptions for Calculation

- Diffusion in helium flow does not limit permeation
- Influence of helium mass flow on permeation neglected
- All tritium available as molecular tritium HT
- Partial pressure in SHTS remains zero
- Only permeation through IHX heat exchange area
- Tritium production at steady state operation=$2.08*10^{-9}$ mol/s
- Leak from PHTS=0.12% /day
- Permeability = IHXA $7.75*10^{-10}$ / IHX B $5.71*10^{-10}$ mol/(m.s.$Pa^{0.5}$)
- Different PRFs for materials

The steady-state tritium concentration is calculated, taking into account rates of production, leakage from the PHTS and permeation into the SHTS for different PRFs

Tritium Permeation Calculation

Calculation scheme

Sievert's Law:

$$k = \frac{\Phi}{PRF} \cdot \frac{A}{L} \cdot \left(\sqrt{p_{T,PHTS}} - \sqrt{p_{T,SHTS}} \right)$$

k	permeation (mol/s)
A/L	area / wall thickness (m)
Φ	permeability (mol/(m.s.Pa$^{0.5}$))
PRF	permeation reduction factor (-)
$p_{T,PHTS}$	tritium partial pressure, primary system (Pa)
$p_{T,SHTS}$	tritium partial pressure, secondary system (Pa)

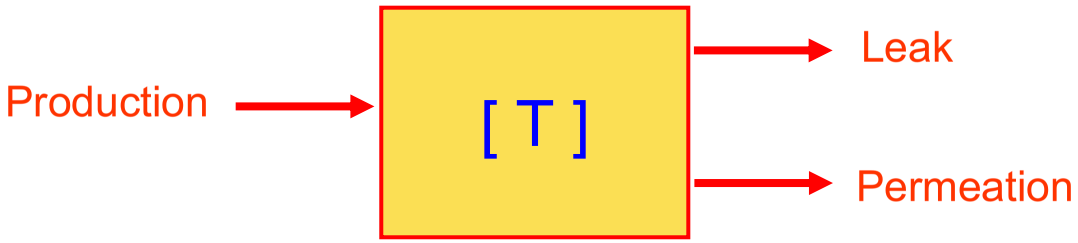

Tritium Permeation
Results of Calculation

PRF = 10^3 commercial available Al_2O_3 coating
PRF = 10^4 - 10^5 experimental tested, commercial not yet available

PRF (-)	T(mol)	*k*(mol/s)	Leak (mol/s)	*k*/Prod. (-)
$1.0*10^{+2}$	$4.1*10^{-8}$	$2.1*10^{-9}$	$5.8*10^{-16}$	1.00
$1.0*10^{+3}$	$4.1*10^{-6}$	$2.1*10^{-9}$	$5.8*10^{-14}$	1.00
$1.0*10^{+5}$	$2.8*10^{-2}$	$1.7*10^{-9}$	$3.8*10^{-10}$	0.82
$1.0*10^{+6}$	$1.2*10^{-1}$	$3.6*10^{-10}$	$1.7*10^{-9}$	0.17
$1.0*10^{+7}$	$1.5*10^{-1}$	$3.9*10^{-11}$	$2.0*10^{-9}$	0.02

Even most advanced SiC or TiC/TiN coatings cannot effectively reduce the permeation of tritium into the SHTS

Tritium Permeation Conclusions

- Large area and small thickness in the heat exchange area of IHX result in very efficient permeation of tritium from PHTS to SHTS
- For the assumed HPS flow rate, during normal operation nearly 100% of the tritium produced in the core region permeates through IHX to SHTS
- Permeation can not significantly be reduced by the application of permeation barriers on the heat exchange area in the IHX

Tritium Permeation Recommendations

Reduction of tritium in SHTS may be achieved by:

- Lowering tritium concentration in PHTS
  - Decrease production of tritium in the core region
  - Increase mass flow of HPS
  - Add oxidants to helium in PHTS
- Direct removal of tritium from SHTS
  - Add purification system to SHTS
  - Add oxidants to coolant in SHTS
- Lower reactor outlet temperature
- Ceramic IHX

Contamination Control
Recommendations: Task 1 - Sources

	What We Learned	Future Directions
Task 1.1 Tritium Source	•H^3 production rate of 7E+6 Bq/s	•Reduce He^3 and Li^6 impurities in reactor
Task 1.2 C-14 Source	•C^{14} activity in coolant is 1.6E+10 Bq	•Limit nitrogen ingress at shutdown
Task 1.3 Fission Products Source	•Sources based on FRG fuel performance •Models are well developed	•Complete tests of demonstration fuel in PBMR development program
Task 1.4 Dust Source	•Particles size based on AVR tests •Production rate of 48 Kg/fpy	•Complete measurements planned in PBMR-DPP

Contamination Control
Recommendations: Task 2 - Transport

	What We Learned	Future Directions
Task 2.1 SPECTRA code	•Code models both dust and RN transport	•Increase groups for dust particle size •Test re-suspension
Task 2.2 Dust Transport	•90% of dust settles in reactor vessel •Local layers of 50μm	•Explore effects on flow resistance and heat transfer
Task 1.3 Fission Products Transport	•Metallic FPs adhere quickly to dust •Small effect of HPS	•Explore uncertainty in Ag^{110} deposition

Contamination Control
Recommendations: Task 3 - Radiation Exposure

	What We Learned	Future Directions
Task 3.0 Radiation Exposure	•Locations for exposure defined •Dose rates quantified	•Identify specific worker activities •Determine times of exposure

Contamination Control
Recommendations: Task 4 - Tritium Permeation

	What We Learned	Future Directions
Task 4.0 Tritium Permeation	•Near 100% of tritium reached SHTS •Current surface treatments provide insufficient holdup	•Examine higher flow rate to both PHTS and SHTS HPS •Consider increased oxidants in SHTS •Lower ROT •Ceramic IHX

Closing Discussion as Needed